JOURNAL OF PETROLOGY | VOLUME 49 | NUMBER 11 | PAGES 2043–2080 | 2008 | doi:10.1093/petrology/egn057

Li, B and Be Contents of Harzburgites from the Dramala Complex (Pindos Ophiolite, Greece): Evidence for a MOR-type Mantle in a Supra-subduction Zone Environment

L. PELLETIER[1]*, F. VILS[1], A. KALT[1] AND K. GMÉLING[2]

[1]INSTITUTE OF GEOLOGY AND HYDROGEOLOGY, UNIVERSITY OF NEUCHATEL, EMILE ARGAND 11, CP158, 2009 NEUCHATEL, SWITZERLAND

[2]INSTITUTE OF ISOTOPES, HUNGARIAN ACADEMY OF SCIENCES, PO BOX 77, 1525 BUDAPEST, HUNGARY

RECEIVED JANUARY 12, 2007; ACCEPTED OCTOBER 14, 2008
ADVANCE ACCESS PUBLICATION DECEMBER 4, 2008

The Pindos ophiolite represents oceanic lithosphere obducted during the Jurassic. The Dramala mantle section mainly consists of highly depleted spinel harzburgite and minor plagioclase-bearing harzburgite. Textural observations and major element compositions of minerals indicate that the harzburgites experienced impregnation by a mafic, depleted melt and subsequent high-temperature (high-T) hydration and cooling (>750°C) forming pargasite and edenitic hornblende. During further cooling (from ≥ 350–400°C to < 100°C), talc + tremolite ± serpentine ± olivine, serpentine + magnetite, and finally plagioclase alteration phases formed. To test the hypothesis of a supra-subduction zone origin for the Dramala mantle, we measured Li, B and Be contents of minerals by secondary ion mass spectrometry. Whole-rock contents were measured using inductively coupled plasma–mass spectrometry and prompt gamma neutron activation analysis. We observe low Li and B contents of primary minerals (olivine, orthopyroxene, clinopyroxene) consistent with values for unmetasomatized mantle minerals; only Li contents of clinopyroxene (up to 3·7 μg/g) are slightly elevated. The bulk Li contents (0·5–1·1 μg/g) are in the upper range of values for unmetasomatized mantle, whereas B contents (<0·04–1·1 μg/g) are variable and slightly elevated compared with the unmetasomatized mantle as a result of serpentinization. Beryllium abundances in all minerals are very low (<0·005 μg/g), except for pargasite, where a maximum Be content of 0·012 μg/g was measured. The selective addition of Li to clinopyroxene can be related to the interaction with a depleted melt, and/or to partitioning of Li into clinopyroxene upon cooling. During high-T hydration and cooling, the fluid calculated to be in equilibrium with the pargasite or edenitic hornblende (based on Li, Be and B) could have been reaction-modified seawater. Low-T hydration may have led to a very minor increase in bulk B content of most samples and to the formation of serpentine with highly variable B contents (0·1–28 μg/g). Low-T hydration decreased the Li content of orthopyroxene, and Li was probably leached from some samples. The lack of correlation between degree of serpentinization and bulk B contents as well as the presence of high- and low-B serpentine can be explained by low fluid–rock ratios, decreasing T during serpentinization and lack of equilibrium as a result of fast obduction–exhumation. The low light-element contents of primary minerals and whole-rock samples clearly argue against a supra-subduction zone (SSZ) origin of the Dramala mantle section, and against the previous hypothesis of hydrous melting of the Pindos mantle above a subduction zone. We therefore conclude that the Dramala harzburgites represent a mid-ocean ridge (MOR)-type mantle, and not an SSZ-type mantle, juxtaposed with MOR-type and SSZ-type oceanic crust, either in a back-arc or in an intra-oceanic subduction zone setting.

KEY WORDS: *light elements; melt impregnation; peridotite; supra-subduction zone ophiolite; MOR-type mantle; lithium; beryllium; boron*

*Corresponding author. Present address: EMPA, Ueberlandstrasse 129, CH-8600 Dübendorf, Switzerland. E-mail: laure.pelletier@empa.ch

INTRODUCTION

Ophiolites and the supra-subduction zone setting

Many researchers believe that most ophiolites formed in supra-subduction zone (SSZ) settings (Miyashiro, 1973; Beccaluva *et al.*, 1984, 2004, 2005; Pearce *et al.*, 1984; Wallin & Metcalf, 1998; Bizimis *et al.*, 2000; Metcalf *et al.*, 2000; Saccani & Photiades, 2004). The interpretation is mainly based on the association of depleted peridotite with island arc tholeiite (IAT) and boninite found in these ophiolites, corresponding to what is observed in present-day forearc environments (Natland & Tarney, 1982; Parkinson & Pearce, 1998). Many of the ophiolites are attributed to pre-arc settings during early initiation of subduction zones (Pearce *et al.*, 1984; Wallin & Metcalf, 1998; Metcalf *et al.*, 2000). Rarely, SSZ ophiolites are assigned to the early stages of back-arc spreading, subsequent to the splitting of an arc (Pearce *et al.*, 1984).

The criteria commonly used to assign an SSZ origin to ophiolite sequences are: (1) mantle structures comparable with those observed at mid-ocean ridges (MORs) (Pearce *et al.*, 1984, and references therein); (2) a depleted mantle sequence, mainly composed of harzburgite (80–90 vol. %), with very low modal clinopyroxene (e.g. Noiret *et al.*, 1981; Pearce *et al.*, 1984; Searle & Cox, 1999; Bizimis *et al.*, 2000), as a result of high degrees of partial melting; (3) the occurrence of very high Cr-numbers in spinel from the harzburgitic mantle (>0·6; Pearce, 2003, and references therein); (4) podiform chromitites associated with dunites and harzburgites (Pearce *et al.*, 1984; Arai & Yurimoto, 1994; Zhou *et al.*, 1996; Arai, 1997a, 1997*b*); (5) chemical characteristics of the igneous crust that range from mid-ocean ridge basalt (MORB) via IAT to boninite (high-Mg andesite), notably an enrichment in Sr, K, Rb, Ba and Th and a lack of enrichment in Ta, Nb, Hf, Zr, Ti, Y and Yb (Pearce *et al.*, 1984, and references therein; Pe-Piper *et al.*, 2004); (6) crustal cumulate sequences with clinopyroxene crystallized before plagioclase (Pearce *et al.*, 1984; Murton, 1989; Gaetani *et al.*, 1994; Beccaluva *et al.*, 2005). All these features were described from present-day arc-related environments (Pearce, 2003, and references therein).

Many studies were focused on the crustal sections of SSZ ophiolites, but data from mantle sections that constrain SSZ signature are scarce. Bizimis *et al.* (2000) studied the Ti and trace element contents of clinopyroxene in the Dramala harzburgites from the Pindos ophiolite, Greece. These clinopyroxenes are characterized by extremely low contents of Ti and heavy rare earth elements (HREE). They show an enrichment in light REE (LREE), and to a lesser extent in middle REE (MREE), Zr and Sr compared with clinopyroxenes from abyssal peridotites (Bodinier & Godard, 2004, and references therein). Bizimis *et al.* (2000) attributed this signature to hydrous melting of MORB-depleted peridotite above a subduction zone, giving the famous 'spoon-shaped' trace-element pattern in clinopyroxene of peridotites from arc-related environments; for example, the Izu–Bonin–Mariana forearc mantle or the Lihir sub-arc mantle (Parkinson & Pearce, 1998; Grégoire *et al.*, 2001; Ohara *et al.*, 2002).

Despite the similarities between ophiolitic mantle and present-day arc-related mantle, the model of an SSZ origin for most ophiolitic mantle is not undisputed. The presence of clinopyroxene-poor harzburgites in the SSZ ophiolites is not conclusive because similar rocks have been described from many present-day MORs: Mid-Atlantic Ridge Ocean Drilling Program (ODP) Leg 209 (Kelemen *et al.*, 2004; Paulick *et al.*, 2006), East Pacific Rise (Hess Deep) ODP Leg 147 (Allan & Dick, 1996; Arai & Matsukage, 1996; Dick & Natland, 1996), Gakkel Ridge (Hellebrand *et al.*, 2002), and Macquarie Island in the South Tasmanian Ocean Basin (Dijkstra & Cawood, 2004). The formation of podiform chromitite can be due to the involvement of water during melting of refractory peridotite (Edwards *et al.*, 2000), but also to melt–rock (moderately depleted harzburgite) reaction where the melt can be of MORB or boninitic composition (Arai & Yurimoto, 1994; Zhou *et al.*, 1996; Arai, 1997*a*, 1997*b*; Arai & Matsukage, 1998). High Cr-number in spinel (>0·6) has been described in the Newfoundland margin spinel harzburgites (Müntener & Manatschal, 2006), showing that high Cr-number in spinel can be an inherited signature. Also, high Cr-number in spinel has been described at two MORs: the East Pacific Rise Hess Deep ODP Leg 147 by Allan & Dick (1996), Arai & Matsukage (1996) and Dick & Natland (1996) with a maximum of 0·57, and at the Mid-Atlantic Ridge ODP Leg 209 by Seyler *et al.* (2007) with a maximum of 0·51.

Moreover, it is becoming increasingly clear that lavas with island-arc chemical signatures may also occur in other tectonic settings. Modern ridges can display lavas with a 'subduction-component' in addition to 'MORB-type' lavas, as a result of mantle heterogeneities (Moores *et al.*, 2000). Klein & Karsten (1995) and Sturm *et al.* (2000) described basalts from the Chile Ridge adjacent to the Chile trench with geochemical characteristics unlike MORB, but with affinities to arc volcanic rocks, created by processes associated with subduction of a spreading center. Moreover, boninite genesis is not restricted to subduction-related settings, but can also be associated with spreading at an MOR (Crawford *et al.*, 1989). Nonnotte *et al.* (2005) showed that addition of seawater to a residual peridotite at shallow depth beneath an MOR [Deep Sea Drilling Project (DSDP) Site 334] can potentially lead to boninitic–andesitic magmas. Benoît *et al.* (1999) demonstrated that in an MOR setting, remelting of a hydrated residual peridotite (after MORB extraction) at low pressure (*P*) by intruding mantle diapirs can yield depleted cumulates with an arc signature, but with an MOR-type

crystallization sequence. Haase *et al.* (2005) also mentioned the presence of Nb- and Ta-depleted andesites at the plume-influenced Pacific–Antarctic MOR, which were formed by crystallization of basalt and assimilation of melts from hydrothermally altered amphibolites. Caution is thus warranted in using the systematics of classical trace elements to identify the provenance of ophiolites (SSZ or MOR). Clearly, to attribute a geodynamic setting to an ophiolite sequence, including its mantle section, it is necessary to examine the entire sequence and to combine geological field data with a geochemical analysis of minerals and bulk-rock samples.

Li, B and Be as indicators of subduction settings

In the last decade, the light elements, particularly B, have proven to be powerful tracers of slab fluids and melts (Benton *et al.*, 2004; Leeman *et al.*, 2004; Paquin *et al.*, 2004; Scambelluri & Philippot, 2004; Tenthorey & Hermann, 2004; Savov *et al.*, 2005, and references therein; Scambelluri *et al.*, 2006, and references therein). There is abundant evidence for a progressive release of Li and B from the oceanic slab during subduction. Fluids enriched in B and Li are liberated from subducting sediment and basaltic crust by dehydration reactions (Moran *et al.*, 1992; Bebout *et al.*, 1993, 1999; Domanik *et al.*, 1993; You *et al.*, 1994, 1995*a*, 1995*b*; Peacock & Hervig, 1999; Chan & Kastner, 2000; Benton *et al.*, 2001). Beryllium can be released by melting (Johnson & Planck, 1999), but also by dehydration during high-P and high-T metamorphism of subducted altered oceanic crust (Marschall *et al.*, 2007). The abundances and isotopic compositions of Li, Be and B in arc lavas imply the presence of mantle sources that are considerably modified by slab-derived components (Tatsumi, 1989; Ishikawa & Nakamura, 1994; Leeman, 1996; Chan *et al.*, 1999, 2002; Rose *et al.*, 2001; Ryan, 2002; Tomascak *et al.*, 2002). Slab signatures of arc lavas show considerable variations in light-element contents and isotope composition (Ishikawa & Nakamura, 1994; Moriguti & Nakamura, 1998; Rosner *et al.*, 2003; Leeman *et al.*, 2004, and references therein), which have been attributed to differences in composition, age and tectonic setting of the subducting plate (Plank & Langmuir, 1993; Rüpke *et al.*, 2002), to depth-controlled release of slab-derived components (Ishikawa & Nakamura, 1994; Moriguti & Nakamura, 1998), to sediment melting and to selective trapping of chemical components in the deep sub-arc mantle (slab–mantle interface) prior to reaching the zone of melt generation (Ayers, 1998; Tomascak *et al.*, 2002; Paquin *et al.*, 2004). Churikova *et al.* (2007) and Portnyagin *et al.* (2007) showed that the mantle source of arc magmas is strongly enriched in B, Be and Li compared with MORB-source mantle (deduced from melt inclusions in olivine from island arc xenoliths). The conclusion of the above-cited studies is that SSZ mantle, for example in the Pindos ophiolite, should be enriched considerably in Li, B, and Be compared with MOR mantle.

Rationale of the study

An SSZ origin has been postulated by many workers for the Pindos ophiolite (Pearce *et al.*, 1984; Jones *et al.*, 1991; Bizimis *et al.*, 2000; Saccani & Photiades, 2004) because of petrographic and geochemical evidence in the crustal section of the ophiolite. The ophiolite is highly dismembered and consists of four units each containing either oceanic mantle or crust. The Dramala Complex (mantle) and the Aspropotamos Complex (crust) have been the subject of several geochemical, structural and petrogenetic studies. In the Aspropotamos Complex, lava affinities are diverse and evolved with time from normal (N)-MORB to IAT, and finally to boninite (Kostopoulos, 1988; Pe-Piper *et al.*, 2004; Beccaluva *et al.*, 2005). Peridotites of the Dramala Complex are highly depleted, and podiform chromite deposits are rare (Jones *et al.*, 1991). The crustal cumulates, which directly overlie the peridotites of the Dramala Complex, show a typical MOR-type cumulate sequence, with the crystallization of plagioclase before clinopyroxene (Kostopoulos, 1988). However, clinopyroxene from the harzburgites shows the 'spoon-shaped' trace-element pattern interpreted as the result of hydrous melting in an SSZ setting (Bizimis *et al.*, 2000).

We carried out a detailed study on textures, and major- and light-element (Li, Be, B) contents of minerals and bulk-rocks of fresh harzburgite and serpentinite from the Dramala Complex, to test the hypothesis of an origin in an SSZ setting of the Pindos mantle rocks. The results show the investigated mantle rocks to be very similar to an MOR-type mantle, modified by melt–rock reaction and impregnation.

GENERAL GEOLOGICAL FRAMEWORK

The Sub-Pelagonian ophiolites include the Pindos, Vourinos and Othris complexes (Greece) and the Albanian ophiolites (Fig. 1). They are aligned in a NNW–SSE direction within the Hellenides (Fig. 1). The Pindos and Vourinos ophiolites are thought to be connected beneath the Tertiary post-orogenic Mesohellenic Trough of the Sub-Pelagonian zone (Makris, 1977; Jones *et al.*, 1991; Fig. 1), and the Pindos ophiolite may be related to the Othris ultramafic rocks along strike to the south (Smith, 1979).

The Sub-Pelagonian ophiolites are related to the evolution of small oceanic basins that developed at the eastern margin of Pangaea, adjacent to the Neo-Tethys, from the Triassic to the Tertiary. In the future southeastern European region, sea-floor spreading began in the Triassic and led to the formation of oceanic lithosphere (Jones & Robertson, 1991; Pe-Piper & Piper, 2002; Robertson, 2002). In the Middle to Late Jurassic, the 'pieces' of future southeastern Europe

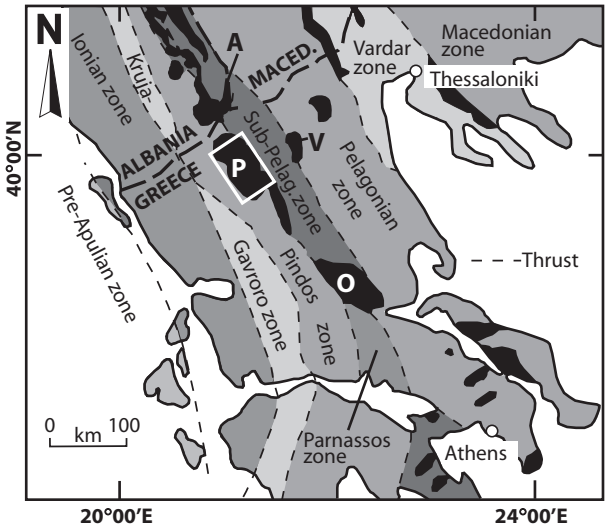

Fig. 1. The Pindos ophiolite within the Hellenides, modified after Robertson & Shallo (2000). The white box represents the area shown in Fig. 2. P, Pindos ophiolite; V, Vourinos ophiolite; O, Othris ophiolite; A, Albanian ophiolites; Maced., Macedonia; Sub-Pelag. zone, Sub-Pelagonian zone.

formed part of several tectonic plates, which are, from NE to SW, the Eurasian continent, the Vardar ocean, the Pelagonian microcontinent, the Pindos ocean, and the Apulian–Adriatic microplate (Stampfli & Borel, 2004).

Two different origins were proposed for the ophiolites in Greece: (1) all the Sub-Pelagonian ophiolites come from the Vardar ocean, and their actual regional distribution is a consequence of post-obduction extensional tectonics (Aubouin, 1959; Dercourt *et al.*, 1986, 1993; Jacobshagen, 1986); (2) the actual regional distribution of the ophiolites reflects their origin in different ocean basins. In this context, the Pindos, Vourinos and Othris ophiolites are assigned to the Pindos basin, located to the west of the Pelagonian microcontinent (Smith & Woodcock, 1976; Robertson *et al.*, 1991). Another debated point is the nature of these small ocean basins. They could be related to a fore-arc environment (Dilek & Flower, 2003), to back-arc spreading (Stampfli *et al.*, 1998), or to a Red Sea-type rifting (Robertson *et al.*, 1991).

In the Late Jurassic the future Sub-Pelagonian ophiolites were obducted onto the passive margin of the Pelagonian microcontinent. Stampfli & Borel (2004) explained the large-scale obduction by ridge failure in the Vardar ocean, induced by continuous rotation of Africa. The obduction onto the Pelagonian microcontinent must have been preceded by intra-oceanic obduction, as the metamorphic soles at the base of the ophiolites are mainly composed of metabasite and metasediment (Jones & Robertson, 1991; Ross & Zimmerman, 1996). The metamorphic soles generally recrystallized under greenschist- to amphibolite-facies conditions and were dated at 169–176 Ma (Pe-Piper & Piper, 2002, and references therein).

According to Robertson & Shallo (2000), the Sub-Pelagonian ophiolites can be subdivided into two groups: (1) the 'Eastern-type' ophiolites, including the Eastern Albanian and the Vourinos ophiolites, are interpreted as SSZ-type ophiolites, which formed above an intra-oceanic subduction zone in the Late Jurassic; (2) the 'Western-type' ophiolites, including the Western Albanian, the Othris and the Pindos ophiolites, which were formed during the Early Jurassic at a slow-spreading ridge system (MOR-type ophiolite); at the onset of subduction, they evolved to SSZ-type ophiolites.

THE PINDOS OPHIOLITE

The northern Pindos mountains are made up of a series of imbricate Mesozoic and Tertiary thrust sheets, which include the Jurassic Pindos ophiolite (Capedri *et al.*, 1980; Jones & Robertson, 1991). Five tectono-stratigraphic units were described by Jones & Robertson (1991): (1) the Pindos Ophiolite Group (Jurassic, Fig. 2) with three subunits, the Dramala Complex (dismembered ultramafic rocks), the Loumnitsa Unit (metamorphic sole), and the Aspropotamos Complex (dismembered intrusive and extrusive rocks); (2) the shallow-water limestones of the Orliakas Group (Late Cretaceous); (3) the Avdella Mélange (Late Triassic–Late Jurassic) with volcanic rocks and sediments of a subduction–accretion complex; (4) the deep-water sediments of the Dio Dendra Group (Late Jurassic–Late Cretaceous); (5) the Pindos Flysch (Late Cretaceous–Tertiary). The following description will focus on the Pindos Ophiolite Group and the Avdella Mélange, which are relevant for this paper.

The Dramala Complex represents oceanic mantle and part of its crustal sequence. It includes tectonized spinel harzburgite and minor plagioclase-bearing harzburgite, websterite, pyroxenite, and ultramafic cumulates (Jones & Robertson, 1991; Ross & Zimmerman, 1996; Pe-Piper & Piper, 2002). All these ultramafic rocks have slightly to highly serpentinized equivalents. Locally, breccias of harzburgite and chert are cemented by ophicalcite, showing that the Dramala mantle was once exposed on the sea floor (Jones *et al.*, 1991). Harzburgite fabrics from the Pindos and Vourinos ophiolite complexes are very similar (Rassios, 1991; Rassios *et al.*, 1994), and the results of magnetic studies suggest a connection underneath the Mesohellenic Trough (Rassios & Moores, 2006), supporting the idea that both ophiolites were derived from the same oceanic lithosphere. The Dramala ultramafic rocks are overlain by crustal cumulates with plagioclase-bearing dunite, troctolite and anorthosite gabbro (Capedri *et al.*, 1982; Rassios, 1991).

The Loumnitsa Unit (metamorphic sole) is located at the base of the Dramala Complex and consists of metasediments and metabasites, with MORB and within-plate basalt (WPB) affinities (Jones & Robertson, 1991). This unit was

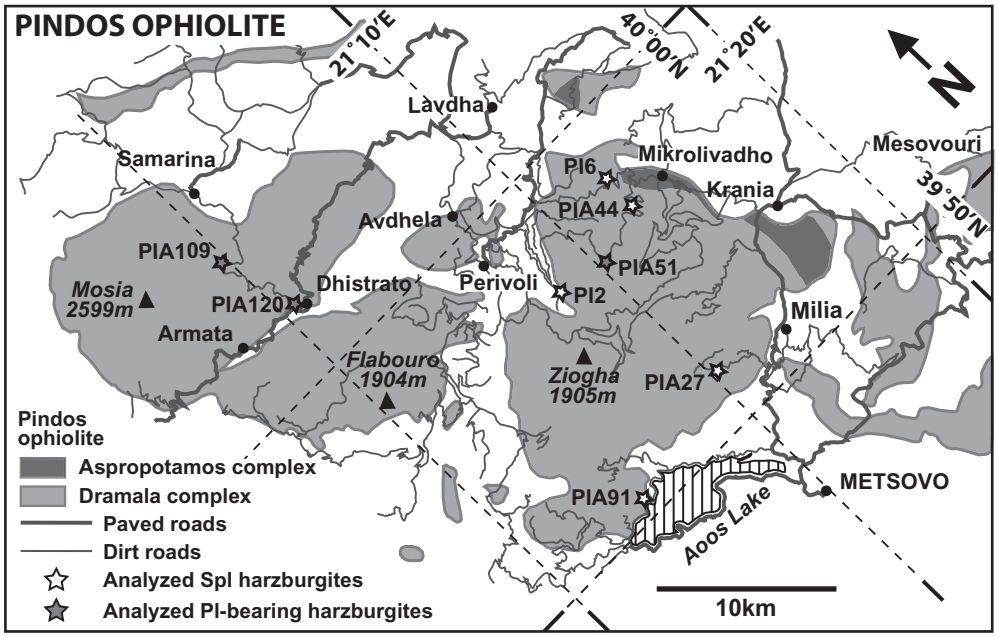

Fig. 2. Simplified map of the Pindos ophiolite, including the Dramala Complex (oceanic mantle) and the Aspropotamos Complex (oceanic crust) and location of the analyzed samples; modified after Jones & Robertson (1991) and Economou-Eliopoulos & Vacondios (1995).

dated using the K–Ar and the Ar–Ar methods on hornblende from different amphibolites, yielding ages between 165 ± 5 and 176 ± 5 Ma (Roddick *et al.*, 1979; Spray & Roddick, 1980; Thuizat *et al.*, 1981; Spray *et al.*, 1984).

The Aspropotamos Complex (Lower to Middle Jurassic) preserves a crustal succession, including ultramafic and mafic cumulates, plagiogranite, sheeted dykes and pillow lavas. Successive phases of lava extrusion show a geochemical trend from high-Ti MORB to MORB–IAT and finally to IAT-boninite-type for the youngest dykes (Capedri *et al.*, 1980; Kostopoulos, 1988; Jones & Robertson, 1991; Jones *et al.*, 1991; Pe-Piper *et al.*, 2004; Saccani & Photiades, 2004; Beccaluva *et al.*, 2005). Capedri *et al.* (1980) described lavas strongly depleted in incompatible elements, which are similar to some rocks of immature island arcs. These geochemical characteristics of the intrusive and extrusive rocks were used to define the Pindos ophiolite as an SSZ-type ophiolite.

The Avdella Mélange represents a subduction–accretion complex and includes volcanic rocks, sediments and metamorphic rocks of the Loumnitsa Unit. Basalts are Triassic and exhibit WPB, WPB to transitional (T)-MORB, and N-MORB signatures. These extrusive rocks were formed at the initial stage of sea-floor spreading (Pe-Piper & Piper, 2002, and references therein).

SAMPLE CHARACTERISTICS

All samples described below were collected from the Dramala Complex, to study the Li, B and Be contents of the mantle and its minerals. The complex is essentially composed of spinel harzburgites. Plagioclase-bearing harzburgites are present in the northwestern and central part of the massif (Fig. 2). The harzburgites show various degrees of serpentinization and deformation. Eight clinopyroxene-bearing spinel harzburgite samples were chosen for this study (Fig. 2). Three of the samples additionally contain plagioclase and are subsequently referred to as plagioclase-bearing harzburgites. Samples with different degrees of serpentinization were chosen to evaluate the impact of this process on the light-element budget. The mineral nomenclature used here is according to Kretz (1983), and serpentine terminology follows those of Wicks & Whittaker (1977) and O'Hanley (1996).

Microstructures range from coarse porphyroclastic to mylonitic (Fig. 3a–f, nomenclature after Mercier & Nicolas, 1975). Most samples have experienced high-T, low-stress plastic deformation leading to the formation of coarse-grained microstructures. Harzburgites preserve primary mantle porphyroclasts, including orthopyroxene with clinopyroxene exsolution lamellae (Opx_1), rare clinopyroxene with orthopyroxene exsolution lamellae (Cpx_1), olivine (Ol_1), and spinel (Spl_1) (Fig. 3a). Neoblasts include orthopyroxene, clinopyroxene, olivine and spinel (Opx_2 and Cpx_2 without exsolution lamellae, Ol_2, Spl_2; Fig. 3a). In the plagioclase-bearing harzburgite, plagioclase is generally associated with a distinct generation of orthopyroxene, clinopyroxene and spinel (Opx_{2i}, Cpx_{2i} and Spl_{2i}; Fig. 3d and e).

Some harzburgites record later, post-kinematic crystallization of anthophyllite, talc, tremolite, and rare

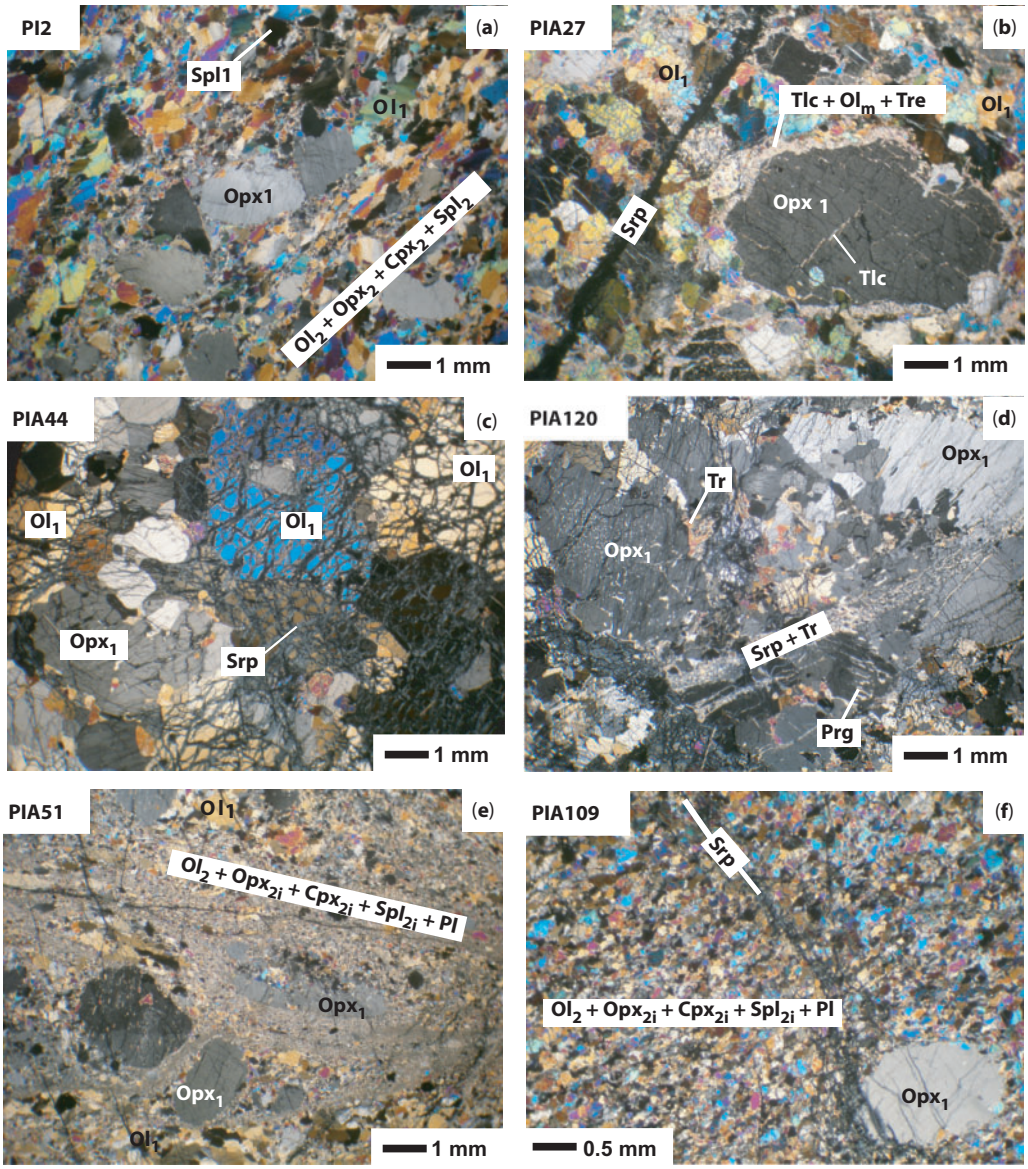

Fig. 3. Textures of the analyzed samples. PI2, PIA27 and PIA44 are spinel harzburgites and PIA51, PIA109 and PIA120 are plagioclase-bearing harzburgites. Mineral abbreviations after Kretz (1983). Suffixes after mineral names represent the generations: 1, primary; 2, secondary; 2i, secondary related to melt infiltration.

metamorphic olivine, Ol_m (Figs 3b, f and 4a, b). Finally, the rocks were serpentinized, with pseudomorphs of serpentine after orthopyroxene (bastite), olivine (mesh texture), and small serpentine veins (Figs 3b, c, e, f and 4a–d).

Spinel harzburgites

Samples PI2 and PIA91 are only weakly serpentinized (<1·7 vol. %), with serpentine crystallized in veins of 10–20 μm width. In thin section, the rocks are deformed and exhibit a porphyroclastic texture (Fig. 3a). Ol_1 (with kink banding), Opx_1 and Spl_1 porphyroclasts have diameters up to 2 mm, whereas Cpx_1 rarely attains 1 mm. Neoblasts are smaller (<0·5 mm). Spl_1 porphyroclasts are usually subhedral, but rare euhedral grains are also present. Rare tremolite (~20 μm) formed at the expense of Cpx_1.

Sample PIA27 has a porphyroclastic texture similar to samples PI2 and PIA91 (Fig. 3b), but contains more hydrated minerals. Cuspate clinopyroxene grains (Cpx_1) crystallized at olivine–orthopyroxene grain boundaries (Fig. 4b) have been replaced by edenitic hornblende. This amphibole also partially or completely replaces clinopyroxene exsolution lamellae within orthopyroxene (Fig. 4a). Anthophyllite and tremolite crystallized at edenitic hornblende rims (Fig. 4b). Fine-grained aggregates of talc and

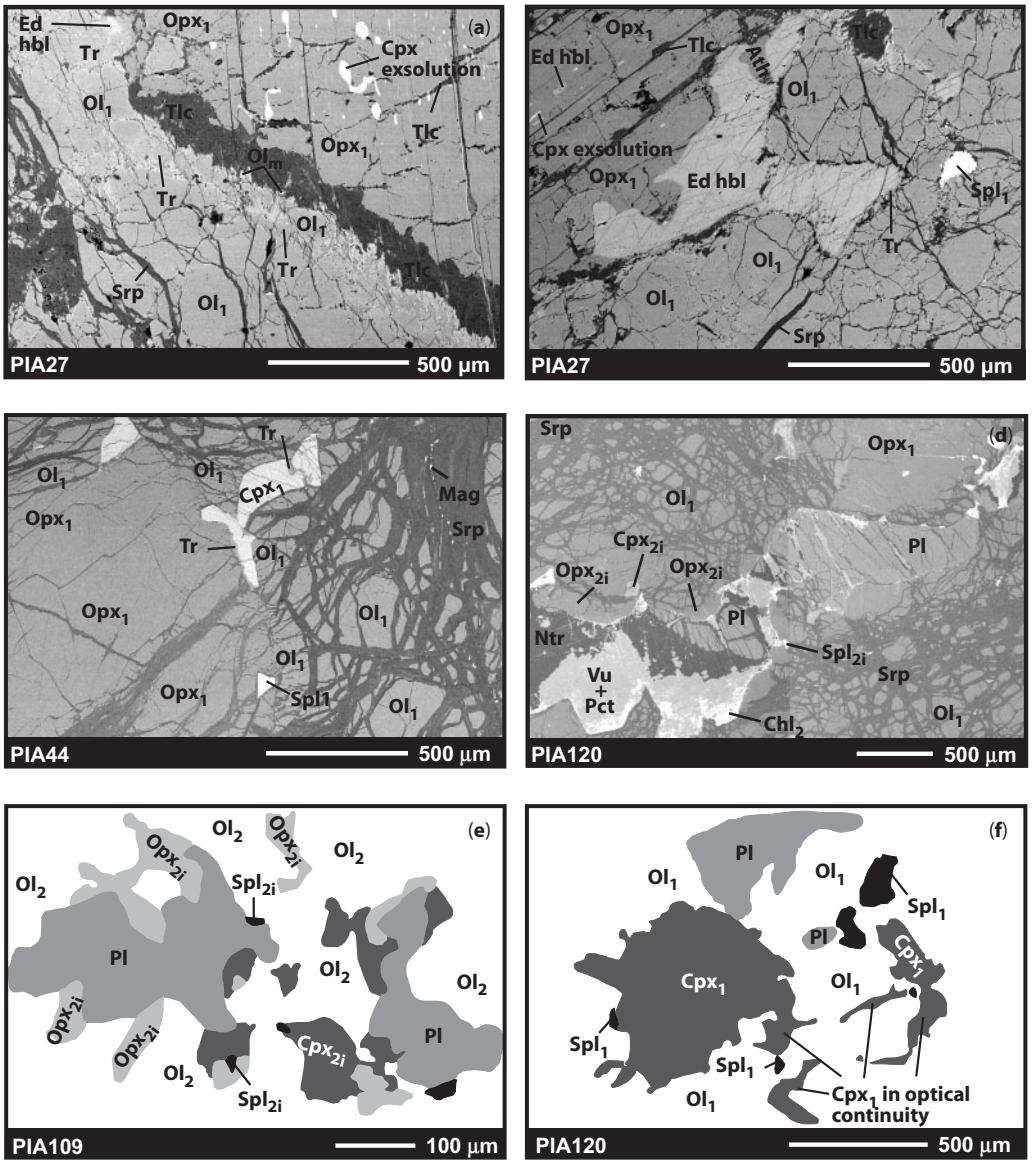

Fig. 4. (a–c) Microtextures related to serpentinization and cooling in the spinel harzburgites. (d–f) Microtextures related to melt infiltration in the plagioclase-bearing harzburgites. Mineral abbreviations after Kretz (1983); Ntr, natrolite; Pct, pectolite; Vu, vuagnatite. Suffixes after mineral names represent the generations: 1, primary; 2, secondary; 2i, secondary related to melt infiltration; m, metamorphic.

olivine (Ol_m) form rims around orthopyroxene. Serpentine is mainly present as mesh textures (Fig. 4a and b) that contain rare magnetite, or in veins (maximum 500 μm width). More rarely, serpentine crystallized as bastite or is associated with talc at orthopyroxene rims. The total percentage of serpentine is 19 vol. %.

PI6 and PIA44 are spinel harzburgites with 47 and 55 vol. % of serpentine, respectively. These rocks show a granoblastic texture, with very rare Ol_1 grains (up to 4 mm, often kinked) and large Opx_1 porphyroclasts (Fig. 3c). Cuspate interstitial grains of Cpx_1 at Opx_1 rims (Fig. 4c) are similar to those in sample PIA27. In some cases, accessory Spl_1 is intergrown with Cpx_1. Hydrous phases include tremolite, which crystallized at clinopyroxene rims (Fig. 4c), and talc, formed at orthopyroxene–olivine contacts. Serpentine forms a mesh texture, rare bastite after orthopyroxene and clinopyroxene, and some veins penetrating clinopyroxene and spinel. Magnetite is concentrated at the margins of the net formed by the mesh texture (Fig. 4c).

Plagioclase-bearing harzburgites

PIA120 is a moderately serpentinized (41 vol. %) plagioclase-bearing harzburgite (Fig. 3f). The earliest minerals

are Ol_1 as well as large grains of Opx_1 (up to 4 mm) and Cpx_1 (up to 400 μm). Some Cpx_1 have corroded margins and occur as clusters of single grains that are in optical continuity (Fig. 4f). Rare, small spinel grains are disseminated in the rock. Plagioclase (up to 1 mm) crystallized as single crystals or in polycrystalline aggregates and dykelets with igneous textures along foliation planes (Fig. 4d and f). Small grains of Opx_{2i}, Cpx_{2i} and Spl_{2i} crystallized at the rims of these aggregates, whereby Opx_{2i} is often found at the contact between olivine and plagioclase (Fig. 4d). Pargasite formed at Opx_1 rims, probably at the expense of clinopyroxene. Metamorphic olivine (Ol_m) crystallized at Opx_1 rims in association with tremolite, diopside and serpentine. Serpentine forms mesh textures and bastite after Opx_1. An association of natrolite ($Na_2Al_2Si_3O_{10}\cdot 2H_2O$), vuagnatite [$CaAlSiO_4(OH)$], pectolite [$NaCa_2(Si_3O_8)(OH)$], and chlorite partially replaced plagioclase (Fig. 4d). Two types of chlorite are present: Chl_1 in association with tremolite, and Chl_2 within the plagioclase aggregates.

PIA51 and PIA109 are weakly serpentinized plagioclase-bearing harzburgites (9 vol. % serpentine). PIA51 is a mylonitized peridotite with ultrafine bands (~20 μm) of plagioclase and Ol_2, Opx_{2i}, Cpx_{2i} and Spl_{2i} (Fig. 3d). Primary mantle relics are Opx_1 and Ol_1 porphyroclasts (up to 3 mm), which are preserved in the less deformed zones. Apparently undeformed plagioclase is subhedral and preferentially concentrated at the margins of the mylonitized zones. PIA109 is a highly recrystallized sample (Figs 3e and 4e). Opx_1 porphyroclasts (up to 4 mm) have corroded rims and float in a matrix of recrystallized Ol_2, Opx_{2i}, Cpx_{2i}, Spl_{2i} and plagioclase (grain size up to 100 μm). Cpx_1 is present as inclusions in the Opx_1 clasts. In sample PIA51, relict Spl_1 grains (up to 1 mm) are preserved. In PIA109, pargasite is present as inclusions in Opx_1 and probably formed at the expense of clinopyroxene. In PIA51, hornblende formed as subhedral grains in the less deformed zones. Tremolite crystallized after clinopyroxene at Opx_1 rims, and talc is sometimes present at Opx_1–Ol_1 grain boundaries. Serpentine forms veins with rare magnetite, and vuagnatite and chlorite partially replaced plagioclase. Rare bastite after Opx_1 and mesh texture are observed.

Nature of the serpentine minerals

The different serpentine polymorphs were determined by C. Groppo on a micro-Raman facility (HORIBA Jobin Yvon HR800) at the University of Torino (Italy), following the procedure described by Groppo *et al.* (2006). All details concerning these analyses will be published in a separate paper. For all serpentine points of samples PIA27, PIA44, PIA109 and PIA120 previously analyzed for Li, B and Be by secondary ion mass spectrometry (SIMS), the polymorphs were determined. Serpentine crystallized in veins is lizardite. In rare cases, when veins were larger, some chrysotile was observed in the center of the veins. Serpentine crystallized in bastite and after olivine is generally lizardite, but some chrysotile can be present. Only in spinel harzburgite PIA27, where serpentine formed after orthopyroxene (no bastite texture), is it chrysotile. In spinel harzburgite PIA44, bastite is in places composed of a fine mixture of lizardite and talc.

INTERPRETATION OF SPECIFIC TEXTURES

Textures related to melt impregnation

In the samples from the Dramala Complex, no plagioclase coronae around primary spinel were observed, indicating that feldspar was not formed by subsolidus decompression reactions (Piccardo *et al.*, 2004*b*). Many plagioclase peridotites are commonly interpreted as resulting from impregnation of spinel peridotites by diffuse porous flow of melt, melt–rock reaction, or fractional crystallization of plagioclase and pyroxenes (Dick, 1989; Rampone *et al.*, 1997; Dijkstra *et al.*, 2001, 2003). The Dramala samples present textural evidence of these processes, which is discussed below.

In plagioclase-bearing harzburgite, millimeter-scale plagioclase dykelets are aligned along the foliation plane defined by flattened olivine and orthopyroxene. In the Othris peridotite, where there is major and trace element evidence of melt impregnation (Dijkstra *et al.*, 2001; Barth *et al.*, 2008), this texture was interpreted as representing cumulate phases of a melt that impregnated the harzburgites. There are also primary clinopyroxene grains (Cpx_1) with irregular outlines caused by embayments of olivine (Fig. 4f), which are in optical continuity and associated with plagioclase. A similar texture was described from abyssal peridotites from the South West Indian Ridge (Seyler *et al.*, 2001) and from the Othris peridotites (Dijkstra *et al.*, 2003), and was interpreted as dissolution of primary clinopyroxene by a pyroxene-undersaturated melt. In the Dramala harzburgites, plagioclase is often associated with secondary clinopyroxene (Cpx_{2i} of Fig. 4d and e), a feature generally interpreted as originating from an infiltrating melt (Pearce *et al.*, 2000; Dijkstra *et al.*, 2001, 2003, and references therein). The ubiquitous presence of this texture in some plagioclase-bearing harzburgites indicates that melt migrated by diffuse porous flow.

In many places in plagioclase-bearing harzburgite, secondary, undeformed orthopyroxene (Opx_{2i}) crystallized at the contact between primary olivine and plagioclase (Fig. 4d). This secondary orthopyroxene replaced olivine along its contact with plagioclase via the reaction olivine + melt = orthopyroxene + plagioclase, as documented in melt-impregnated peridotites of the Lanzo massif (Piemontese Italian Alps) by Piccardo *et al.* (2004*b*) and in the Othris peridotites by Dijkstra *et al.* (2003).

The presence of corroded primary clinopyroxene (Cpx_1) in the sample with plagioclase aggregates, where secondary clinopyroxene (Cpx_{2i}) crystallized at vein rims, may show that there was an evolution of the melt composition over time or that T was decreasing. The incoming melt probably evolved from a pyroxene-undersaturated to a pyroxene-saturated state, as observed by Piccardo *et al.* (2004*b*) in some Alpine–Apennine peridotites and by Dijkstra *et al.* (2003) in the Othris harzburgites. According to Dijkstra *et al.* (2003), increasing saturation of the melt in clinopyroxene and plagioclase could be due to cooling.

Some spinel harzburgites also show evidence of melt impregnation in their textures. Figure 4c shows an interstitial clinopyroxene crystallized at a triple junction between olivine and primary orthopyroxene. These lobed grains show no exsolution lamellae of orthopyroxene. Both the shape and position of this clinopyroxene exclude a primary origin. A similar texture was described from abyssal spinel peridotites (plagioclase-free) by Seyler *et al.* (2001) and was interpreted as clinopyroxene having crystallized from incompletely extracted melts. Piccardo *et al.* (2004*b*) described a similar texture from Alpine–Apennine peridotites. In Fig. 4b, the edenitic hornblende and the other associated retrograde amphiboles (anthophyllite and tremolite) are probably pseudomorphs after this type of clinopyroxene, as they present exactly the same texture.

Textures related to cooling and hydration

In the Dramala harzburgite, earliest cooling and hydration is documented by replacement of clinopyroxene by edenitic hornblende (sample PIA27), suggesting that T was $> 750^{\circ}C$ (Lykins & Jenkins, 1992; Sharma & Jenkins, 1999). As edenitic hornblende and pargasite form pseudomorphs after clinopyroxene crystallized from a melt (sample PIA27; Fig. 4b) and replace clinopyroxene exsolution lamellae in orthopyroxene clasts (samples PIA27, Fig. 4b; PIA109 and PIA120) we consider these amphiboles to have crystallized from a high-T fluid and not from a melt.

Edenitic hornblende was partially replaced during further cooling by anthophyllite and tremolite. Further cooling and hydration are also indicated by coronas of talc ± tremolite ± olivine around orthopyroxene (sample PIA27, PI6, PIA51). In sample PIA27 (Figs 3b and 4a, b), this transformation was penetrative and replaced entire grains. Experiments on peridotite–seawater interaction (Allen & Seyfried, 2003), petrographic studies (Mével, 2003), and observations on serpentinized peridotites at the Mid-Atlantic Ridge ODP Leg 209 (Bach *et al.*, 2004, 2006) suggest that the transformation of pyroxenes to talc (and tremolite) is favoured above 300–400°C, where pyroxenes react faster than olivine. In many Dramala samples, serpentine was formed with talc and may replace the latter, leading to bastite. This phenomenon can be explained by a decrease of silica activity in the fluid as pyroxene transforms to talc (and tremolite). Once the serpentine–talc silica buffer is reached, serpentine and talc co-precipitate (Frost & Beard, 2007). When olivine begins to hydrate, serpentine becomes the most important hydrous mineral.

Serpentine also crystallized in veins, at olivine–orthopyroxene grain boundaries, and at the expense of olivine (mesh texture). These textures are younger than the talc-bearing coronas and the bastite texture. Mesh rims are composed of serpentine, whereas mesh centers show an association of serpentine with a little magnetite. The P–T relations between the serpentine polymorphs are not well known, and the stability fields partially overlap. Thus, they give no precise indication of the serpentinization T (see discussion by Bach *et al.*, 2004). However, it is commonly accepted that the direct transformation of olivine to serpentine preferentially takes place below 250–300°C (Allen & Seyfried, 2003; Mével, 2003; Bach *et al.*, 2004).

In sample PIA120, bulk serpentinization was followed by the alteration of plagioclase (Fig. 4d) to natrolite, vuagnatite, and pectolite. Formation of natrolite after plagioclase during low-T (<100°C) hydrothermal alteration was observed in pillow basalts from the West Philippine Sea Basin (ODP Leg 195, site 1201; D'Antonio & Kristensen, 2005). A post-serpentine alteration is also visible in the mesh centers of some samples, probably caused by the transformation of magnetite into limonite (yellowish color under the microscope).

In conclusion, the Dramala harzburgites record fluid–rock reactions during cooling from approximately $> 750^{\circ}C$ to $< 100^{\circ}C$. Cooling must have proceeded quickly and the fluid–rock ratio was probably low because otherwise the rocks would display higher degrees of serpentinization, and the higher-T hydrous phases (talc, pargasite and edenitic hornblende) would not have been preserved.

ANALYTICAL TECHNIQUES

Major element compositions of minerals were determined by electron microprobe (Cameca SX-50 and Jeol JXA-8200 at the Institute of Geological Sciences of the University of Bern, Cameca SX-51 at the Institute of Mineralogy of the Ruprecht-Karls University of Heidelberg, and Jeol JXA-8200 at the ETH Zürich) equipped with four to five wavelength-dispersive spectrometers. Operating conditions comprise an accelerating voltage of 15 kV and a 20 nA beam current. The spot size was about 3 μm except for hydrous minerals, where a defocused beam was used (amphiboles and talc 5 μm; serpentine 1–10 μm; natrolite 5–10 μm). Natural and synthetic oxides and silicates were used as standards. Approximate detection limits (in wt %) were: (1) for silicates and spinel, SiO_2 (0·02), TiO_2 (0·01), Cr_2O_3 (0·01), FeO (0·07), MnO (0·01), ZnO (0·07), NiO (0·02), CaO (0·01), SrO (0·004), BaO (0·004), Na_2O (0·01), and K_2O (0·01); (2) for silicates, Al_2O_3 (0·01) and MgO (0·01); (3) for spinel,

Al_2O_3 (0·04) and MgO (0·03). Backscattered electron (BSE) images were obtained at the Centre Suisse d'Electronique et de Microtechnique (CSEM, Neuchâtel), with a Philips XL-30 scanning electron microscope, operated at 25 kV.

Light-element compositions were measured *in situ* in minerals using SIMS with a modified Cameca ims 3f ion microprobe (equipped with a primary beam mass filter) at the Institute of Mineralogy of the University of Heidelberg. The protocol established by Marschall & Ludwig (2004) was used for sample preparation and measurements to minimize B surface contamination. SIMS measurements were performed on points previously analyzed by electron microprobe. The primary $^{16}O^-$ ion beam was set to 14 keV and 20 nA. Positive secondary ions were accelerated to 4·5 keV and the energy window was set to 40 eV. The energy filtering technique was applied with an offset of ~75 eV at a mass resolution $m/\triangle m$ between 1018 and 1080. Quantitative results were obtained using relative sensitivity factors with ^{30}Si as reference isotope (Ottolini *et al.*, 1993). Detection limits (the critical value; Currie, 1968) for sample PI2 were calculated at 2·0, 1·4 and 3·7 ng/g (ppb) for Li, Be and B, respectively. For other samples, values were lower at 1·4 for Li, 1·0 for Be and 2·6 ng/g for B. All rock-forming minerals were analyzed, except for spinel and other oxides (for which no standard was available). BSE images of the serpentine matrix showed that serpentine grains are extremely small and could potentially be intergrown with other phases such as brucite, chlorite or magnetite at the micrometer scale, meaning that the SIMS analyses could represent multi-grain analyses.

Lithium and Be whole-rock contents were determined by inductively coupled plasma mass spectrometry (ICP-MS) at the Department of Earth Sciences, University of Bristol. The Pindos harzburgites and two ultramafic rock standards (PCC-1 and UB-N) were dissolved using a HF–HNO_3 multi-acid method on a hotplate. After evaporating the HF, samples were taken up in 2% HNO_3 at a dilution of ~500:1 of the original rock. ICP-MS analyses were performed on a Thermo Electron Element sector field ICP-MS system in pulse-counting mode. Mass calibration was completed using a multi-element solution (10 μg/l of each of Li, B, Na, Sc, Fe, Co, Ga, Y, Rh, In, Ba, Lu, Tl, U in 5% HNO_3). Precision and reproducibility of solution ICP-MS analyses were <12% for Li and <25% for Be. Detection limits were ~37 ng/g for Li and ~3 ng/g for Be. Measured intensities were normalized to solutions of USGS reference material PCC-1 (peridotite), except for Be, where ANRT reference material UB-N (serpentinite) was used. The published value for PCC-1 of 985 ng/g Li (Moriguti *et al.*, 2004) was used to calculate the concentrations of Li. The accepted concentration of Be in UB-N is 200 ng/g (Govindaraju, 1994).

Boron whole-rock contents were measured by prompt gamma neutron activation analysis (PGNAA) at the prompt gamma activation analysis facility of the Budapest Research Reactor (BRR). This method has already been used to analyze B whole-rock contents in geological samples (Gméling *et al.*, 2005; Marschall *et al.*, 2005). PGNAA has a high sensitivity for analyzing whole-rock B concentrations. In contrast to other geoanalytical methods, sample preparation procedures are not needed, and hence contamination problems are eliminated (Anderson & Kasztovszky, 2004). The principle of the PGNAA method is the detection of prompt γ-rays that originate from the (n,γ)-reactions during neutron irradiation (Révay & Belgya, 2004). The detection limit was different in each sample, depending on measurement time and sample weight, but ranges from 10 to 30 ng/g. PGNAA has a precision of 1–2% for B, but of ~5% at concentrations below 1 μg/g. Further information on this analytical technique has been given by Révay *et al.* (2004), Molnár (2004) and Marschall *et al.* (2005).

MAJOR ELEMENT COMPOSITION OF MINERALS

Microprobe analyses were normalized considering Fe as Fe^{2+} in all minerals, except for spinel, where Fe^{2+} and Fe^{3+} were calculated stoichiometrically, and plagioclase, where Fe was considered as Fe^{3+}. Mg-number was calculated as $Mg/(Mg + Fe^{2+})$ for all minerals, including spinel.

Olivine

Ol_1 and Ol_2 compositions are similar and coincide with the mantle olivine array (Takahashi *et al.*, 1987). The Mg-number are between 0·89 and 0·92 and NiO contents are 0·18–0·53 wt % (Table 1, Fig. 5). Olivine from plagioclase-bearing harzburgite shows a greater variation in Ni content and lower Mg-number compared with olivine from spinel harzburgite (Fig. 5). Metamorphic olivine (Ol_m) has lower Mg-number and Ni contents (Table 1, Fig. 5). Ol_1 and Ol_2 of sample PIA44 have Mg-number within the mantle olivine array, but variable NiO contents ranging from 0·05 to 0·45 wt %. This variation may be due to the presence of pentlandite (Fe–Ni sulfide; Filippidis, 1982; Sovatzoglou-Skounakis & Economou-Eliopoulos, 1997; McInnes *et al.*, 2001), which crystallized during serpentinization at olivine rims in sample PIA44.

Spinel

The Cr-number [$= Cr/(Cr + Al)$] of spinel is variable in spinel harzburgites (0·27–0·69; Table 2, Fig. 6a and b). The higher contents reflect the refractory origin of these rocks. The Cr-number of spinel from plagioclase-bearing harzburgites is more restricted, with values between 0·20 and 0·38 (Fig. 6b). Moreover, spinel in plagioclase-bearing harzburgites is enriched in Ti compared with that in

Table 1: Major element composition of olivine (representative analyses)

Rock:	spl harz	spl harz	spl harz	spl harz	spl harz	pl harz	pl harz	pl harz	pl harz
	Ol 1	Ol 1	Ol m	Ol 1	Ol 1	Ol 1	Ol m	Ol 1	Ol 1
Sample:	PI2	PIA27	PIA27	PI6	PIA44	PIA120	PIA120	PIA109	PIA51
Type:	core	core	core	core	core	core	core	core	core
SiO_2	41·0	40·9	40·2	41·1	40·6	40·8	40·0	41·4	41·8
TiO_2	b.d.	b.d.	b.d.	b.d.	b.d.	b.d.	0·11	b.d.	0·01
Cr_2O_3	0·01	b.d.	0·03	0·01	0·05	0·01	0·02	b.d.	0·04
Al_2O_3	b.d.	b.d.	b.d.	0·01	b.d.	0·01	0·03	b.d.	b.d.
FeO	9·31	8·11	12·5	8·57	8·57	10·5	16·6	9·53	9·10
MnO	0·17	0·12	0·28	0·10	0·14	0·18	0·29	0·10	0·17
NiO	0·38	0·28	0·20	0·39	0·18	0·32	0·16	0·37	0·43
MgO	49·8	50·4	46·6	50·6	50·3	48·8	43·2	50·1	49·5
CaO	0·03	0·02	0·01	0·02	0·01	0·02	0·06	0·03	0·01
Na_2O	0·02	0·01	b.d.	0·02	0·02	0·01	0·01	b.d.	b.d.
K_2O	b.d.	b.d.	b.d.	b.d.	b.d.	0·01	0·02	0·02	b.d.
Total	100·7	99·8	99·8	100·9	99·8	100·7	100·5	101·6	101·1
Stoich.	4O	4O	4O	4O	4O	4O	4O	4O	4O
Si	0·995	0·997	1·000	0·992	0·992	0·996	1·009	0·999	1·010
Ti	b.d.	b.d.	b.d.	b.d.	b.d.	b.d.	0·002	b.d.	0·000
Cr	0·000	b.d.	0·001	0·000	0·001	0·000	0·000	b.d.	0·001
Al	b.d.	b.d.	b.d.	0·000	b.d.	0·000	0·001	b.d.	b.d.
Fe^{2+}	0·189	0·165	0·261	0·173	0·175	0·215	0·351	0·192	0·184
Mn	0·004	0·003	0·006	0·002	0·003	0·004	0·006	0·002	0·003
Ni	0·007	0·006	0·004	0·008	0·003	0·006	0·003	0·007	0·008
Mg	1·803	1·831	1·728	1·823	1·831	1·778	1·625	1·799	1·783
Ca	0·001	0·001	0·000	0·001	0·000	0·001	0·002	0·001	0·000
Na	0·001	0·000	b.d.	0·001	0·001	0·000	0·000	b.d.	b.d.
K	b.d.	b.d.	b.d.	b.d.	b.d.	0·000	0·001	0·001	b.d.
Total	3·000	3·003	3·000	3·006	3·008	3·000	2·999	3·000	2·990
Mg-no.	0·905	0·917	0·869	0·913	0·913	0·892	0·822	0·904	0·907

b.d., below detection limit.

spinel harzburgites (except for sample PIA51), and plots in the field of plagioclase-bearing abyssal peridotite as defined by Dick & Bullen (1984) and Dick *et al.* (1984) (Fig. 6b). Spl_1 shows a systematic decrease in Cr_2O_3 (by ~2·50 wt %) and an increase in Al_2O_3 (by ~2·50 wt %) from core to rim. Spl_2 neoblasts have compositions similar to Spl_1 rims in spinel peridotites.

Orthopyroxene

Orthopyroxene porphyroclasts display large intragrain and intergrain compositional variations (Fig. 7a and b). Opx_1 from spinel harzburgites and plagioclase-bearing harzburgites are zoned and show exsolution lamellae of clinopyroxene. They show a rimward decrease in Al_2O_3 and Cr_2O_3 and an increase in SiO_2 (Table 3, Fig. 7a and b). Zoning is more pronounced in plagioclase-bearing harzburgites than in spinel harzburgites (Fig. 7a and b). Al_2O_3 contents range from ~1·00 to 3·25 wt % in the core and from ~0·30 to 3·00 wt % at the rim. Zoning is illustrated in Fig. 7b, where the various samples are defined by their Al_2O_3 and Cr_2O_3 contents. Opx_2 neoblasts have the same composition as Opx_1 porphyroclast rims in both spinel and plagioclase-bearing harzburgites (Fig. 7a and b). Sample PIA44 (serpentinized spinel harzburgite) shows a peculiar pattern, with nearly no variation in its Al_2O_3 content, but a great variability in its Cr_2O_3 content (Fig. 7b). The Mg-number is between 0·90 and 0·92 in all samples.

Clinopyroxene

Cpx_1 porphyroclasts from spinel and plagioclase-bearing harzburgites are zoned and have exsolution lamellae

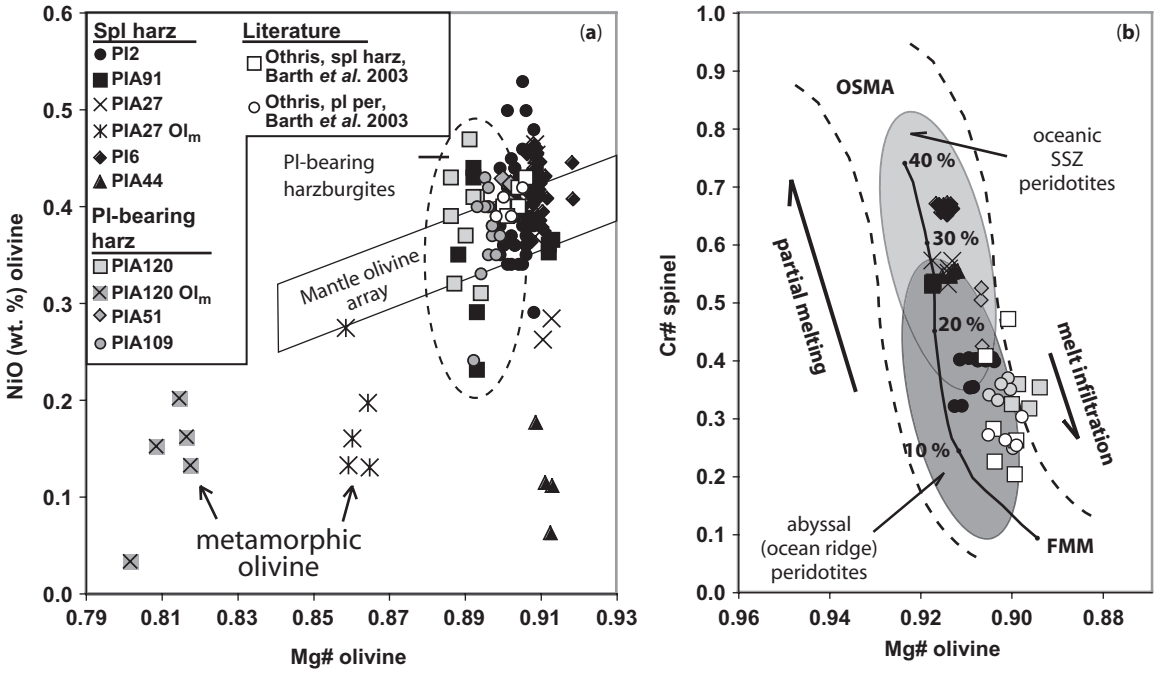

Fig. 5. (a) NiO (wt %) vs Mg-number of olivine. Mantle olivine array after Takahashi *et al.* (1987). Ol_m, metamorphic olivine. (b) Cr-number in spinel vs Mg-number in olivine. Light grey field represents values for oceanic SSZ peridotites (Pearce *et al.*, 2000) and dark grey field those for abyssal ocean ridge peridotites (Dick & Bullen, 1984). OSMA, olivine–spinel mantle array and partial melting trend after Arai (1994); FMM, fertile MORB mantle.

of orthopyroxene. Zoning is more pronounced in the plagioclase-bearing harzburgites. The grains show a rimward decrease in Al_2O_3 and Cr_2O_3 and an increase of Mg-number (Table 4, Fig. 7c and d). Clinopyroxenes (Cpx_1 and Cpx_{2i}) from plagioclase-bearing harzburgite are enriched in TiO_2 (~0·17–0·50 wt %) and Al_2O_3, and show lower Mg-number (~0·91–0·93) compared with those occurring in spinel harzburgite ($TiO_2 < 0·01$–0·15 wt %; Mg-number ~0·92–0·95). Sample PIA51 (plagioclase-bearing harzburgite) shows intermediate values. In spinel harzburgite, Cpx_2 neoblasts show a higher Mg-number and a depletion in TiO_2 and Al_2O_3 compared with Cpx_1 cores (Fig. 7c and d). Cpx_1 rims have the same composition as Cpx_2 neoblasts.

Plagioclase

Plagioclase has An-number [= Ca/(Ca + Na)] between 0·78 and 0·92 (Table 5). Profiles through plagioclase grains in sample PIA120 show a rimward increase in An-number. Barium and Sr contents are below their respective detection limits.

Serpentine

The major element composition of serpentine is controlled by the composition of the mineral it replaces, and not by the type of serpentine polymorph (lizardite or chrysotile; Pelletier *et al.*, in preparation). Serpentine formed after olivine is low in Cr_2O_3, compared with crystals formed after orthopyroxene or clinopyroxene (Table 6). Al_2O_3 and FeO contents are variable, with values of < 0·01–2·40 and ~2·50–8·50 wt %, respectively. Mg-number ranges from ~0·88 to 0·97. In sample PIA27 (serpentinized spinel harzburgite), two types of serpentine are present (Table 6): (1) Fe-rich, Cr- and Al-poor serpentine crystallized in veins and in mesh textures after olivine (Srp_1); (2) Fe-poor, Cr- and Al-rich serpentine associated with talc at orthopyroxene rims (Srp_2).

Talc and chlorite

Talc is nearly stoichiometric, with Mg-number between 0·95 and 0·98 (Table 6). It contains variable amounts of Al_2O_3 (0·35–2·06 wt %). In sample PIA120 (plagioclase-bearing harzburgite) Mg-number are ~0·91 and ~0·34 for Chl_1 and Chl_2, respectively. Chlorite in other samples is Mg-rich with Mg-number between 0·94 and 0·97 (Table 6).

Amphiboles

Two types are present, high-*T* amphiboles (pargasite and edenitic hornblende) and lower-*T* amphiboles (anthophyllite and tremolite). In pargasite, the Mg-number varies between 0·87 and 0·91, and (Na + K) on site A is between 0·75 and 0·94 c.p.f.u. (Table 7). The Mg-number of edenitic hornblende is between 0·92 and 0·99, and (Na + K) on site A ranges from 0·58 to 0·67 c.p.f.u. (Table 7). Lower-*T* anthophyllite crystallized at edenitic hornblende rims

Table 2: Major element composition of spinel (representative analyses)

Rock:	spl harz	spl harz	spl harz	spl harz	spl harz	spl harz	spl harz	spl harz	spl harz	pl harz	pl harz	pl harz	pl harz
	Spl 1	Spl 1	Spl 2	Spl 1	Spl 1	Spl 1	Spl 1	Spl 1	Spl 1	Spl 2i	Spl 2i	Spl 1	Spl 2
Sample:	PI2	PI2	PI2	PIA91	PIA91	PIA27	PIA27	PIA44	PIA44	PIA120	PIA109	PIA51	PIA51
Type:	clast	clast	blast	clast	clast	clast	clast	clast	clast	clast	blast	clast	blast
	core	rim		core	rim	core	rim	core	rim	core		core	
SiO_2	0·02	b.d.	0·08	b.d.	b.d.	0·06	0·10	0·02	0·05	0·03	0·06	0·03	0·04
TiO_2	b.d.	0·03	0·03	0·04	0·03	b.d.	0·03	0·01	0·04	0·26	0·15	0·01	0·02
Cr_2O_3	35·3	31·2	24·0	43·2	37·6	45·7	40·8	44·8	41·8	30·1	28·1	35·4	30·6
Al_2O_3	34·4	37·8	44·7	26·7	31·8	22·8	26·3	24·1	25·4	35·9	36·5	31·8	35·2
Fe_2O_3	0·80	0·53	1·10	1·61	1·55	2·52	1·74	2·69	4·00	3·22	3·89	3·21	3·43
FeO	13·5	12·7	12·3	13·9	13·2	14·1	18·6	14·50	14·6	16·3	15·0	14·5	14·3
MnO	0·08	0·04	0·49	0·80	0·76	0·86	0·87	0·86	0·82	0·05	0·56	0·70	0·65
NiO	0·16	0·13	0·16	0·07	0·08	0·02	b.d.	0·02	0·05	0·17	0·11	0·04	0·14
ZnO	0·18	0·19	0·04	0·17	0·30	b.d.	0·29	0·13	0·07	b.d.	0·20	0·12	0·42
MgO	15·4	16·1	17·2	14·1	15·0	13·4	10·7	13·4	13·5	14·0	14·3	14·2	14·3
CaO	0·01	b.d.	b.d.	0·01	b.d.	0·01	0·01	0·02	0·02	0·03	b.d.	0·01	0·01
Total	99·7	98·8	100·0	100·6	100·4	99·6	99·5	100·6	100·3	100·1	98·8	100·0	99·1
Stoich.	4O	4O	4O	4O	4O	4O	4O	4O	4O	4O	4O	4O	4O
	3 cations	3 cations	3 cations	3 cations	3 cations	3 cations	3 cations	3 cations	3 cations	3 cations	3 cations	3 cations	3 cations
Si	0·001	b.d.	0·002	b.d.	b.d.	0·002	0·002	0·001	0·001	0·001	0·002	0·001	0·001
Ti	b.d.	0·001	0·001	0·001	0·001	b.d.	0·001	0·000	0·001	0·006	0·003	0·000	0·000
Cr	0·807	0·708	0·523	1·021	0·867	1·111	0·997	1·075	1·000	0·690	0·649	0·824	0·707
Al	1·174	1·277	1·449	0·940	1·095	0·827	0·958	0·861	0·904	1·227	1·256	1·103	1·215
Fe^{3+}	0·017	0·012	0·023	0·036	0·034	0·058	0·040	0·062	0·091	0·070	0·085	0·071	0·075
Fe^{2+}	0·326	0·304	0·282	0·348	0·323	0·364	0·479	0·368	0·370	0·396	0·365	0·358	0·350
Mn	0·002	0·001	0·011	0·020	0·019	0·022	0·023	0·022	0·021	0·001	0·014	0·017	0·016
Ni	0·004	0·003	0·004	0·002	0·002	0·001	b.d.	0·000	0·001	0·004	0·003	0·001	0·003
Zn	0·004	0·004	0·001	0·004	0·007	b.d.	0·007	0·003	0·002	b.d.	0·004	0·003	0·009
Mg	0·665	0·690	0·705	0·628	0·652	0·615	0·493	0·607	0·608	0·604	0·619	0·622	0·623
Ca	0·000	b.d.	b.d.	0·000	b.d.	0·000	0·000	0·001	0·001	0·001	b.d.	0·000	0·000
Mg-no.	0·671	0·695	0·714	0·643	0·669	0·628	0·507	0·623	0·621	0·604	0·629	0·635	0·640
Cr-no.	0·408	0·357	0·265	0·521	0·442	0·573	0·510	0·555	0·525	0·360	0·341	0·428	0·368

Fe_2O_3 in spinel calculated assuming perfect stoichiometry. Cr-number calculated as Cr/(Cr + Al). b.d., below detection limit.

during cooling (Fig. 4b) has Mg-number of 0·92–0·93. The Mg-number in tremolite ranges from 0·93 to 0·97.

Li, B AND Be CONTENTS OF ROCK-FORMING MINERALS

The results of light-element analyses are listed in Table 8 and presented in Fig. 8. In primary minerals, clinopyroxene has the highest Li contents, ranging up to 3·7 μg/g (Fig. 8a). Lithium concentrations are 0·5–1·1 μg/g in olivine, and 0·1–1·5 μg/g in orthopyroxene. Lithium zoning is frequent in olivine and pyroxenes, and typically Li decreases from core to rim. Rarely, Li increases rimwards. In orthopyroxene, zoning is in some cases related to the presence of clinopyroxene exsolution lamellae and shows a very complex 'wavy' pattern. The concentration of Li is <0·0014 μg/g in plagioclase (Table 8).

Variable Li contents were measured in serpentine with values from <0·005 to 1·4 μg/g (Fig. 8b, Table 8). Serpentine minerals are too small to be analyzed as single grains (see the section 'Analytical techniques'). Consequently, the results represent multi-grain values for serpentine. Only in the case of sample PIA44 was talc identified within serpentine (see the section 'Nature of

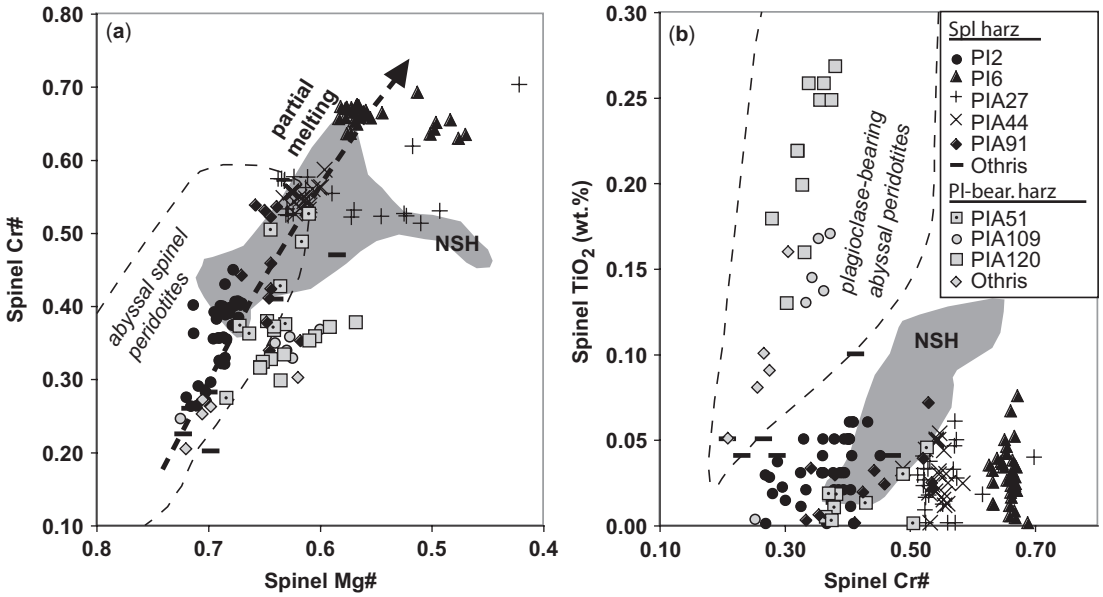

Fig. 6. Spinel composition. (a) Cr-number vs Mg-number, partial melting trend and abyssal spinel peridotite field after Dick & Bullen (1984) and Dick *et al.* (1984). (b) TiO_2 (wt %) vs Cr-number. Abyssal plagioclase-bearing peridotite field after Dick & Bullen (1984) and Dick *et al.* (1984). Newfoundland spinel harzburgite (NSH) field in grey after Müntener & Manatschal (2006). Othris spinel harzburgite and plagioclase-bearing harzburgite after Barth *et al.* (2003) and Dijkstra *et al.* (2003).

the serpentine minerals'). Therefore serpentine (multi-grain) analyses in this sample give higher values for Li (up to 11·2 μg/g; Fig. 8b; Table 8).

Lithium contents in amphiboles are variable (Fig. 8a and b), but edenitic hornblende has higher values (1·9–2·4 μg/g) than other amphiboles (pargasite, anthophyllite and tremolite). The alteration phases chlorite, talc and pectolite have high Li contents, at 2·0–3·3, 0·1–3·8 and 5·1–11·0 μg/g, respectively (Fig. 8b). Natrolite and vuagnatite are poor in Li (<0·4 μg/g; Table 8).

Boron concentrations in all primary minerals are low and range from <0·008 to 0·1, 0·4 and 0·6 μg/g, for olivine, orthopyroxene and clinopyroxene, respectively. Metamorphic olivine, which is present in sample PIA27, has the highest B content (9·1 μg/g; only one grain was large enough to be analyzed). Boron concentrations are highly variable in serpentine (0·1–27·6 μg/g) (Fig. 8d). Contents can vary by one order of magnitude in the same serpentine polymorph in a single sample at the millimeter scale. These contents were measured in pure serpentine and not in a mixture of different phases (see section 'Nature of the serpentine minerals'; Pelletier *et al.*, in preparation). Boron contents of the alteration phases natrolite, vuagnatite and pectolite are low, at <0·26 μg/g (Table 8).

Beryllium contents of all minerals are generally below the detection limit (~1·4 ng/g). Only high-T amphiboles (edenitic hornblende and pargasite) show a maximum value of 0·012 μg/g (Table 8).

Li, B AND Be CONTENTS OF WHOLE-ROCK SAMPLES

Whole-rock data are listed in Table 9. Lithium in harzburgites ranges from 0·5 to 1·1 μg/g. The most serpentinized peridotites show a greater variation in Li contents. Boron contents range from <0·04 to 1·1 μg/g, and Be contents are below the detection limit (<3 ng/g) in all the samples.

DISCUSSION

In the previous sections we showed that the spinel and plagioclase-bearing harzburgites experienced deformation, melt infiltration, hydration and cooling. These processes could all potentially have modified the Li, B and Be content of the primary Dramala mantle. As the role of deformation cannot be assessed, we will only discuss the impact of the other processes on the light-element systematics.

Compositional effects of melt impregnation

Major element composition of minerals

Low modal clinopyroxene (Table 9), and the compositions of olivine and spinel (Figs 5 and 6) show that the Pindos harzburgites were highly refractory before melt impregnation. They experienced extraction of at least 15% partial melt as illustrated in Fig. 5b (Saccani & Photiades, 2004). Plagioclase-bearing harzburgites are less depleted than spinel harzburgites, which is consistent with the fact that they were refertilized by mafic melts to a greater extent.

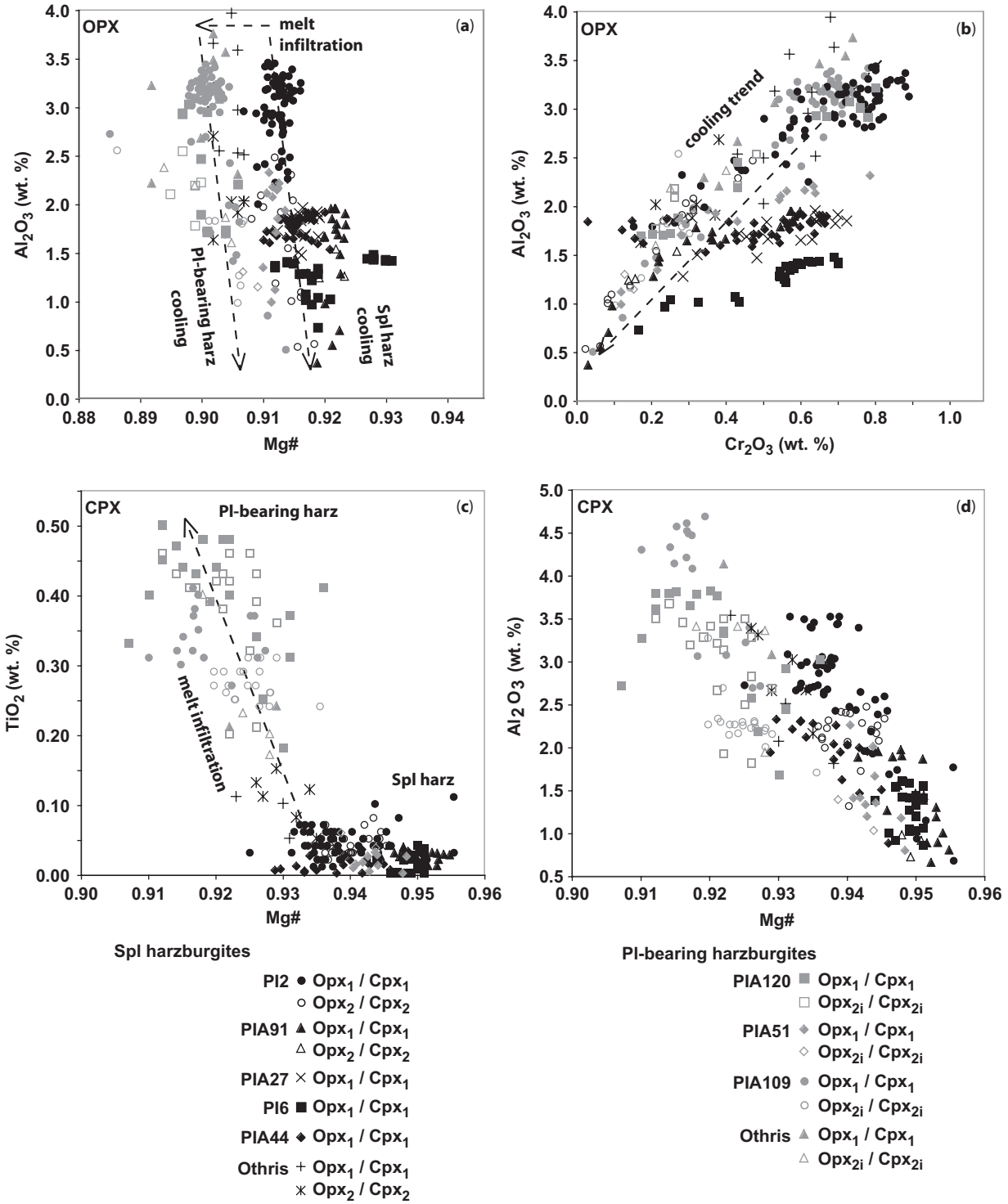

Fig. 7. Pyroxene composition. (a) Al_2O_3 (wt %) vs Mg-number in orthopyroxene, showing different interpreted cooling trends of spinel and plagioclase-bearing harzburgites and the shift in their Mg-number as a result of melt infiltration. (b) Al_2O_3 (wt %) vs Cr_2O_3 (wt %) in orthopyroxene, showing the interpreted cooling trend of the spinel harzburgites. (c) TiO_2 (wt %) vs Mg-number in clinopyroxene, showing the enrichment in TiO_2 of the plagioclase-bearing harzburgites as a result of melt infiltration. (d) Al_2O_3 (wt %) vs Mg-number in clinopyroxene, showing the enrichment in Al_2O_3 and the lower Mg-number of the plagioclase-bearing harzburgites as a result of melt infiltration. Othris data after Barth *et al.* (2003) and Dijkstra *et al.* (2003).

Table 3: Major element composition of orthopyroxene (representative analyses)

Rock:	spl harz	spl harz	spl harz	spl harz	spl harz	spl harz	spl harz	spl harz	spl harz	pl harz	pl harz	pl harz	pl harz	pl harz
	Opx 1	Opx 1	Opx 2	Opx 1	Opx 1	Opx 2	Opx 1	Opx 1	Opx 1	Opx 1	Opx 1	Opx 2i	Opx 1	Opx 2i
Sample:	PI2	PI2	PI2	PIA91	PIA91	PIA91	PIA27	PIA44	PIA44	PIA120	PIA120	PIA120	PIA109	PIA109
Type:	clast	clast	blast	clast	clast	blast	clast	clast	clast	clast	clast	blast	clast	blast
	core	rim		core	rim		core	core	rim	core	rim	vein	core	
SiO_2	56·2	56·4	57·1	57·0	57·9	57·9	56·3	56·4	58·0	55·5	56·0	55·6	55·6	57·3
TiO_2	0·04	b.d.	0·03	0·02	b.d.	0·01	0·01	b.d.	0·03	0·16	0·17	0·14	0·09	0·11
Cr_2O_3	0·79	0·20	0·26	0·39	0·03	0·14	0·70	0·63	0·43	0·69	0·43	0·48	0·71	0·24
Al_2O_3	3·03	1·80	1·85	1·69	0·37	1·26	1·92	1·84	1·65	2·59	2·20	2·54	4·02	1·83
FeO	5·76	5·68	6·25	5·45	5·56	5·45	5·40	5·84	5·84	6·30	6·26	6·80	6·49	6·41
MnO	0·16	0·10	0·13	0·19	0·17	0·15	0·07	0·03	0·11	0·12	0·21	0·11	0·15	0·14
NiO	0·06	0·11	0·07	0·13	0·16	0·08	b.d.	0·14	0·06	0·03	0·08	0·07	0·07	0·08
MgO	34·1	34·4	34·7	34·5	35·3	34·8	34·3	34·4	34·8	33·1	33·9	33·2	33·7	35·1
CaO	0·68	0·46	0·41	0·72	0·25	0·27	0·86	0·75	0·58	1·73	0·93	0·81	0·05	0·47
Na_2O	0·02	b.d.	b.d.	0·02	0·02	b.d.	0·01	b.d.	0·01	0·01	b.d.	0·01	0·04	b.d.
K_2O	0·02	0·01	b.d.	b.d.	b.d.	b.d.	0·01	b.d.	b.d.	b.d.	b.d.	0·02	b.d.	0·01
Total	100·9	99·2	100·8	100·1	99·8	100·1	99·6	100·0	101·5	100·2	100·1	99·8	100·9	101·7
Stoich.	6O	6O	6O	6O	6O	6O	6O	6O	6O	6O	6O	6O	6O	6O
Si	1·923	1·958	1·954	1·961	1·992	1·983	1·947	1·946	1·967	1·923	1·936	1·932	1·905	1·947
Ti	0·001	b.d.	0·001	0·001	b.d.	0·000	0·000	b.d.	0·001	0·004	0·004	0·004	0·002	0·003
Cr	0·021	0·006	0·007	0·011	0·001	0·004	0·019	0·017	0·011	0·019	0·012	0·013	0·019	0·006
Al	0·122	0·074	0·075	0·068	0·015	0·051	0·078	0·075	0·066	0·106	0·090	0·104	0·162	0·073
Fe^{2+}	0·165	0·165	0·179	0·157	0·160	0·156	0·156	0·169	0·166	0·183	0·181	0·197	0·186	0·182
Mn	0·005	0·003	0·004	0·005	0·005	0·004	0·002	0·001	0·003	0·004	0·006	0·003	0·004	0·004
Ni	0·002	0·003	0·002	0·003	0·004	0·002	b.d.	0·004	0·002	0·001	0·002	0·002	0·002	0·002
Mg	1·740	1·778	1·769	1·765	1·813	1·779	1·769	1·769	1·756	1·708	1·745	1·719	1·719	1·775
Ca	0·025	0·017	0·015	0·027	0·009	0·010	0·032	0·028	0·021	0·064	0·034	0·030	0·002	0·017
Na	0·001	b.d.	b.d.	0·001	0·001	b.d.	0·000	b.d.	0·001	0·001	b.d.	0·001	0·003	b.d.
K	0·001	0·001	b.d.	b.d.	b.d.	b.d.	0·000	b.d.	b.d.	b.d.	b.d.	0·001	b.d.	0·000
Total	4·005	4·003	4·005	3·999	4·000	3·989	4·005	4·008	3·994	4·011	4·009	4·007	4·004	4·010
Mg-no.	0·913	0·915	0·908	0·918	0·919	0·919	0·919	0·913	0·914	0·903	0·906	0·897	0·902	0·907
Cr-no.	0·149	0·069	0·086	0·135	0·049	0·069	0·197	0·186	0·148	0·152	0·117	0·112	0·105	0·079

Cr-number calculated as Cr/(Cr + Al). b.d., below detection limit.

The spinel composition is highly sensitive to melt percolation and impregnation. Spinel in plagioclase-bearing harzburgites has lower Mg-number and higher TiO_2 contents than spinel in spinel harzburgites (Fig. 6a and b). Comparable Ti enrichment in spinel was reported from impregnated depleted abyssal peridotites (Dick & Bullen, 1984; Allan & Dick, 1996) and from plagioclase-bearing harzburgites from Othris (Dijkstra *et al.*, 2001; Barth *et al.*, 2003). In Fig. 6a, some spinels do not follow the partial melting trend defined by Dick & Bullen (1984) and Dick *et al.* (1984). The shift in Mg-number could be due to chemical modification during serpentinization, which can play an important role if grains are small.

Spinel harzburgite exhibits Cr-number of spinel ranging between 0·3 and 0·65 (Fig. 5b), similar to spinel harzburgite from Hess Deep (0·1–0·5; Dick & Natland, 1996). Cr-number values are generally lower than those published for spinel harzburgites in forearc environments (0·5–0·8: Arai, 1997*b*). The observed variation could be due to the interaction of spinel with percolating melt. For the Luobusa ophiolite, Tibet, Zhou *et al.* (1996) showed that harzburgites close to dunite bodies are characterized by higher Cr-number in spinel and lower modal orthopyroxene. These two features are observed in sample PI6, which has the highest Cr-number in spinel (0·67) and the lowest modal orthopyroxene (~3%, Table 9). However, these

Table 4: Major element composition of clinopyroxene (representative analyses)

Rock:	spl harz	spl harz	spl harz	spl harz	spl harz	spl harz	spl harz	spl harz	spl harz	pl harz	pl harz	pl harz	pl harz	pl harz	pl harz	pl harz
	Cpx 1	Cpx 1	Cpx 2	Cpx 1	Cpx 1	Cpx 1	Cpx 1	Cpx 1	Cpx 1	Cpx 1	Cpx 1	Cpx 2i	Cpx 1	Cpx 1	Cpx 2i	Cpx 2
Sample:	PI2	PI2	PI2	PIA91	PIA91	PIA27	PIA27	PIA44	PIA44	PIA120	PIA120	PIA120	PIA109	PIA109	PIA109	PIA51
Type:	clast	clast	blast	clast	clast	in opx	in opx	ass opx	ass opx	clast	clast	blast	clast	clast	blast	blast
	core	rim		core	rim	exsol	exsol	core	core	core	rim	vein	core	core		
SiO_2	53·2	55·5	54·7	54·0	54·3	54·0	53·8	53·3	53·6	51·3	53·2	51·1	53·4	52·9	53·4	54·7
TiO_2	0·06	0·03	0·01	0·02	0·01	b.d.	b.d.	0·03	0·03	0·51	0·38	0·60	0·29	0·31	0·33	0·03
Cr_2O_3	1·22	0·29	0·18	0·68	0·21	1·23	1·40	0·76	0·67	1·36	0·67	1·54	0·45	0·83	0·52	0·52
Al_2O_3	3·53	0·68	0·92	1·85	0·88	2·11	2·24	1·99	1·59	4·07	2·77	4·45	2·16	2·67	2·43	1·63
FeO	2·20	1·49	1·90	1·79	1·62	1·96	1·99	1·93	1·71	2·68	2·55	2·52	2·51	2·44	2·64	1·80
MnO	0·01	0·09	0·07	0·04	0·05	0·08	b.d.	b.d.	0·02	0·09	0·15	0·05	0·05	0·09	0·12	0·09
NiO	0·06	0·05	0·03	0·10	0·08	0·07	0·11	0·07	0·07	0·02	0·03	0·03	0·06	0·02	b.d.	0·03
MgO	16·8	18·0	18·1	17·5	17·9	17·4	17·4	17·5	17·8	15·9	17·2	15·7	17·5	17·2	17·0	17·0
CaO	23·8	25·0	24·8	23·9	24·2	23·0	23·0	24·7	24·7	23·1	23·3	23·4	23·6	23·4	23·4	24·6
Na_2O	0·05	0·02	0·02	0·03	0·02	0·31	0·34	0·03	0·05	0·48	0·42	0·47	0·32	0·33	0·39	0·04
K_2O	0·01	b.d.	0·02	0·01	b.d.	0·01	b.d.	b.d.	b.d.	0·01	b.d.	b.d.	b.d.	0·01	b.d.	b.d.
Total	100·9	101·1	100·8	99·9	99·3	100·1	100·3	100·2	100·3	99·4	100·7	99·8	100·3	100·2	100·2	100·4
Stoich.	6O	6O	6O	6O	6O	6O	6O	6O	6O	6O	6O	6O	6O	6O	6O	6O
Si	1·915	1·987	1·971	1·958	1·981	1·956	1·946	1·935	1·945	1·883	1·924	1·871	1·937	1·922	1·937	1·973
Ti	0·002	0·001	0·000	0·001	0·000	b.d.	b.d.	0·001	0·001	0·014	0·010	0·016	0·008	0·008	0·009	0·001
Cr	0·035	0·008	0·005	0·020	0·006	0·035	0·040	0·022	0·019	0·040	0·019	0·045	0·013	0·024	0·015	0·015
Al	0·150	0·029	0·039	0·079	0·038	0·090	0·095	0·085	0·068	0·176	0·118	0·192	0·092	0·114	0·104	0·069
Fe^{2+}	0·066	0·045	0·057	0·054	0·049	0·059	0·060	0·058	0·052	0·083	0·077	0·077	0·076	0·074	0·080	0·054
Mn	0·000	0·003	0·002	0·001	0·001	0·002	b.d.	b.d.	0·001	0·003	0·005	0·002	0·002	0·003	0·004	0·003
Ni	0·002	0·001	0·001	0·003	0·002	0·002	0·003	0·002	0·002	0·001	0·001	0·001	0·002	0·001	b.d.	0·001
Mg	0·903	0·961	0·973	0·944	0·972	0·940	0·939	0·946	0·960	0·871	0·926	0·858	0·944	0·931	0·920	0·914
Ca	0·917	0·960	0·957	0·930	0·947	0·893	0·891	0·960	0·961	0·907	0·902	0·916	0·917	0·912	0·901	0·952
Na	0·003	0·002	0·002	0·002	0·001	0·022	0·024	0·002	0·003	0·034	0·030	0·033	0·022	0·023	0·027	0·003
K	0·000	b.d.	0·001	0·000	b.d.	0·000	b.d.	b.d.	b.d.	0·000	b.d.	b.d.	b.d.	0·000	b.d.	b.d.
Total	3·993	3·995	4·008	3·993	3·998	3·995	3·999	4·012	4·012	4·012	4·012	4·011	4·013	4·012	4·008	3·985
Mg-no.	0·932	0·955	0·944	0·946	0·952	0·941	0·940	0·942	0·949	0·913	0·923	0·918	0·925	0·926	0·920	0·944
Cr-no.	0·188	0·224	0·118	0·198	0·137	0·281	0·296	0·204	0·220	0·184	0·139	0·188	0·124	0·172	0·126	0·176

Cr-number calculated as Cr/(Cr + Al). b.d., below detection limit.

observations should be considered with caution as this sample is highly serpentinized (~46 vol. %).

Ti-rich clinopyroxene is enriched in Al_2O_3, has Na_2O values between 0·26 and 0·50 wt %, and has lower Mg-number compared with clinopyroxene from spinel harzburgite (Fig. 7c and d). These features were described in abyssal plagioclase-bearing peridotites (Allan & Dick, 1996) and in plagioclase-bearing harzburgites from Othris (Dijkstra *et al.*, 2001; Barth *et al.*, 2003).

The composition of Cpx_{2i} from the plagioclase-bearing harzburgites corresponds to the most depleted end of MOR cumulate compositions (Fig. 9). Anorthite contents of plagioclase range from 0·81 to 0·91 (Table 5, Fig. 9), which suggests that the melt was low in Na_2O. The crystallization of secondary orthopyroxene (Opx_{2i}) indicates that the melt should have been relatively rich in silica. Clinopyroxene and plagioclase also have compositions similar to depleted cumulates crystallized in impregnated peridotites of the Monte Maggiore unit (Corsica; Rampone *et al.*, 1997).

From all these chemical observations we conclude that the melt reacting with some of the Dramala harzburgites was depleted to ultra-depleted (i.e. melt produced by low-*P* partial melting of a refractory peridotite; Bloomer *et al.* 1989; Natland, 1989; Ross & Elthon, 1993; Sobolev & Shimizu, 1993; Dijkstra *et al.*, 2001; Arai & Takemoto,

Table 5: Major element composition of plagioclase (representative analyses)

Rock:	pl harz	pl harz	pl harz
	Pl	Pl	Pl
Sample:	PIA109	PIA120	PIA120
Location:	matrix	vein	vein
		core	rim
SiO_2	44·8	46·8	46·2
Al_2O_3	34·8	34·8	35·0
Fe_2O_3	0·33	0·03	0·11
CaO	18·4	16·8	17·2
Na_2O	0·98	2·08	1·74
K_2O	b.d.	0·02	0·01
Total	99·3	100·4	100·3
Stoich.	8O	8O	8O
	5 cations	5 cations	5 cations
Si	2·079	2·130	2·113
Al	1·904	1·866	1·887
Fe^{3+}	0·012	0·001	0·004
Ca	0·917	0·818	0·842
Na	0·088	0·184	0·154
K	b.d.	0·001	0·000
An-no.	0·912	0·817	0·845

An-number calculated as Ca/(Ca + Na). Ba and Sr are below the detection limit. b.d., below detection limit.

2007), or that the melt became depleted as a result of melt–rock reactions during percolation (Piccardo *et al.*, 2004*a*).

Impact on Li, B and Be systematics

Bulk-rock Li contents of all samples (0·5–1·1 μg/g) are close to the depleted mantle value (0·7 μg/g) of Salters & Stracke (2004). There is no difference between the Li contents of the primary mantle minerals in plagioclase-bearing harzburgites and in spinel harzburgites. In both, clinopyroxene is enriched in Li compared with clinopyroxene from unmetasomatized mantle and shows a similar range of values (Fig. 10a). Lithium contents of olivine and orthopyroxene are comparable with, or slightly lower than, those of unmetasomatized mantle minerals (Fig. 10a and b). Values for Li in olivine are constant between 0·5 and 1·1 μg/g, which could be due to the extremely refractory character of the harzburgites prior to the infiltration event.

The $^{opx/cpx}D_{Li}$ and $^{ol/cpx}D_{Li}$ of Pindos harzburgites are not those of equilibrated peridotites (Fig. 10a and b; Eggins *et al.*, 1998; Seitz & Woodland, 2000; Kaliwoda, 2004; Ottolini *et al.*, 2004; Kaeser *et al.*, 2007). According to Seitz & Woodland (2000), Li enrichment in clinopyroxene can be related to metasomatism by mafic silicate melt or hydrous fluid. As there is textural evidence of melt infiltration in the Dramala harzburgites, we consider that Li metasomatism could be, at least in part, related to melt impregnation. Moreover, a similar Li metasomatism was observed in the Mid-Atlantic Ridge ODP Leg 209 (Site 1274A) harzburgite (Vils *et al.*, 2008), where melt metasomatism was described by Seyler *et al.* (2007). The preferential input of Li into clinopyroxene during impregnation of peridotites by mafic silicate melts was also observed by Eggins *et al.* (1998), Ottolini *et al.* (2004) and Woodland *et al.* (2004) (Fig. 10a).

Bulk-rock B contents cannot be unequivocally related to melt infiltration, as they were potentially modified by serpentinization. Measured B abundances in primary minerals tend to be comparable with, or even slightly lower than, values for unmetasomatized mantle (Table 8, Fig. 8c). From the bulk-rock B content of sample PIA109 (0·1 μg/g), where serpentinization was limited (see Table 9), we consider that no (or only little) B was added to the bulk-rock during the melt infiltration event. Measured bulk-rock Be contents are two orders of magnitude lower than values for depleted or primitive mantle (Table 9), and Be contents of primary minerals are generally below detection limits (Table 8). The preferential input of Li compared with B or Be can be explained by higher mineral–melt partition coefficients for Li as compared with B or Be for olivine, orthopyroxene and clinopyroxene (Brenan *et al.*, 1998a). According to these observations, the impregnating melt must have been poor in Li, B and Be, in agreement with the postulated (ultra-)depleted character (see above).

In principle, the enrichment of clinopyroxene in Li could alternatively be explained by preferential partitioning of Li into clinopyroxene upon cooling, as observed during high-*T* experiments (Coogan *et al.*, 2005) and as suggested for clinopyroxene phenocrysts from Hawaiian basalts (Jeffcoate *et al.*, 2007).

In our samples, no systematic increase of Li was observed at clinopyroxene rims, which could point to a diffusive enrichment of clinopyroxene during initial cooling. In the Dramala samples, Li usually decreases rimward in olivine, orthopyroxene and clinopyroxene. This pattern most probably reflects late cooling during serpentinization, with some Li loss from primary minerals to serpentine, talc, tremolite and chlorite (Fig. 10a and b). In conclusion, diffusive repartitioning during initial high-*T* cooling may have contributed to Li enrichment in clinopyroxene.

High-*T* hydration—impact on Li, B and Be systematics

As noted in the previous section, the B contents of whole-rock samples and minerals are similar to those of unmetasomatized mantle, and Be contents are considerably lower (Table 9). Lithium contents of primary minerals are also comparable with their respective values for

Table 6: Major element composition of serpentine, talc and chlorite (representative analyses)

	Serpentine										Talc		Chlorite		
Rock:	spl harz	spl harz	spl harz	spl harz	spl harz	spl harz	spl harz	pl harz	pl harz	pl harz	spl harz	pl harz	spl harz	pl harz	pl harz
	Srp 1	Srp 1	Srp 2	Srp 1	Srp 1	Srp 1	Srp 1	Srp 1	Srp 1	Srp 1	Tlc	Tlc	Chl 1	Chl 1	Chl 2
Sample:	PI2	PIA27	PIA27	PIA44	PIA44	PIA44	PI6	PIA120	PIA109	PIA51	PIA27	PIA51	PI6	PIA120	PIA120
Texture:	vein	mesh after ol	bastite after opx	mesh after ol	bastite after opx	bastite after cpx	mesh after ol	mesh after ol	mesh after ol	mesh after ol					
SiO_2	41·9	38·8	40·9	39·8	39·4	42·5	42·6	42·4	40·9	41·7	60·5	61·5	33·3	31·0	24·4
TiO_2	0·01	b.d.	0·01	b.d.	0·02	0·01	0·01	0·03	0·01	b.d.	0·01	0·02	b.d.	0·03	0·03
Cr_2O_3	0·02	b.d.	0·34	0·03	0·48	0·58	0·01	0·03	0·03	0·01	0·54	0·15	2·56	0·01	0·05
Al_2O_3	0·34	0·01	0·48	0·32	1·66	0·63	0·20	0·54	0·53	0·47	2·06	1·08	13·3	20·1	20·2
FeO	5·42	4·89	2·78	6·51	7·98	7·72	6·19	3·56	4·95	5·39	1·50	2·07	3·64	5·53	32·9
MnO	0·14	0·20	0·09	0·11	0·16	0·04	0·17	0·08	0·12	0·12	0·02	0·02	0·03	0·02	0·66
NiO	0·11	0·08	0·07	0·05	0·05	b.d.	0·21	0·09	0·08	0·10	0·09	0·09	0·14	0·11	0·14
MgO	36·3	37·1	38·3	35·8	34·3	35·8	38·7	38·7	38·0	37·2	30·9	30·3	35·0	30·6	9·37
CaO	0·04	0·02	0·06	0·45	0·42	0·14	0·55	0·19	0·19	0·31	0·01	0·04	b.d.	0·04	0·27
Na_2O	0·04	0·02	0·03	0·07	0·08	0·02	0·56	0·05	0·05	0·01	0·09	0·35	0·04	0·06	0·18
K_2O	0·02	0·01	b.d.	0·01	0·04	b.d.	0·01	b.d.	0·04	0·02	0·01	0·01	b.d.	0·02	0·01
H_2O											4·71	4·70	12·7	12·7	10·9
Total	84·3	81·1	83·1	83·2	84·6	87·4	89·2	85·6	84·8	85·4	100·4	100·3	100·9	100·3	99·0
Stoich.	9O	9O	9O	9O	9O	9O	9O	9O	9O	9O	12O 2OH	12O 2OH	18O 8OH	18O 8OH	18O 8OH
Si	2·045	1·978	2·005	1·993	1·958	2·025	1·988	2·021	1·989	2·017	3·850	3·922	3·137	2·936	2·685
Ti	0·000	b.d.	0·000	b.d.	0·001	0·001	0·000	0·001	0·000	b.d.	0·001	0·001	b.d.	0·002	0·003
Cr	0·001	b.d.	0·013	0·001	0·019	0·022	0·000	0·001	0·001	0·000	0·027	0·008	0·191	0·001	0·005
Al	0·020	0·000	0·028	0·019	0·097	0·036	0·011	0·030	0·030	0·027	0·155	0·081	1·480	2·238	2·615
Fe^{2+}	0·221	0·208	0·114	0·273	0·332	0·308	0·242	0·142	0·202	0·218	0·080	0·110	0·287	0·437	3·030
Mn	0·006	0·009	0·004	0·005	0·007	0·002	0·007	0·003	0·005	0·005	0·001	0·001	0·002	0·002	0·062
Ni	0·004	0·003	0·003	0·002	0·002	b.d.	0·008	0·004	0·003	0·004	0·005	0·005	0·011	0·009	0·013
Mg	2·642	2·820	2·801	2·677	2·541	2·545	2·694	2·748	2·751	2·681	2·934	2·880	4·917	4·309	1·539
Ca	0·002	0·001	0·003	0·024	0·022	0·007	0·028	0·010	0·010	0·016	0·001	0·003	b.d.	0·004	0·031
Na	0·004	0·002	0·003	0·007	0·008	0·002	0·050	0·005	0·005	0·001	0·012	0·043	0·008	0·011	0·039
K	0·001	0·000	b.d.	0·000	0·003	b.d.	0·000	b.d.	0·003	0·001	0·001	0·000	b.d.	0·003	0·002
H											2·000	2·000	8·000	8·000	8·000
Total	4·947	5·023	4·975	5·000	4·989	4·946	5·030	4·965	4·999	4·971	7·065	7·055	10·032	9·950	10·022
Mg-no.	0·923	0·931	0·961	0·907	0·885	0·892	0·918	0·951	0·932	0·925	0·974	0·963	0·945	0·908	0·337

b.d., below detection limit.

unmetasomatized mantle (Fig. 8); only clinopyroxene could have been enriched in Li by metasomatism induced by a mafic melt (see previous section). Therefore, high-T hydration cannot have added significant amounts of light elements to rocks and minerals. Its effect seems to be limited to the formation of edenitic hornblende and pargasite, which have lower Li and B and higher Be contents than clinopyroxene. This is in line with amphibole–fluid partition coefficients for Be, which are generally higher than those for B and Li (Brenan *et al.*, 1998*b*).

The crystallization of hornblende and tremolite after clinopyroxene was described from the Zabargad peridotites by Agrinier *et al.* (1993), and interpreted as resulting from interaction of a seawater-derived fluid with peridotite. For peridotites from the Voltri massif (NW Italy), Hoogerduijn Strating *et al.* (1993) explained pargasite growth at the expense of clinopyroxene as caused by a fluid related to a melt infiltration event. We calculated the partition coefficients for Li, Be and B between amphibole and fluid at high T from diopside–pargasite pairs in sample

Table 7: Major element composition of amphiboles (representative analyses)

Rock:	spl harz	spl harz	spl harz	spl harz	pl harz	pl harz	pl harz
	Tr	Ed hbl	Tr	Ath	Prg	Tr	Prg
Sample:	PIA91	PIA27	PIA27	PIA27	PIA120	PIA120	PIA109
Type:	core	core	core	core	core	core	core
SiO_2	56·3	47·2	56·9	56·5	44·2	57·1	44·2
TiO_2	0·06	0·11	0·03	b.d.	2·21	0·10	1·74
Cr_2O_3	0·34	1·94	0·54	0·25	1·75	0·29	1·52
Al_2O_3	3·74	11·4	2·91	1·34	13·0	1·26	12·5
Fe_2O_3	n.c.	n.c.	n.c.	n.c.	n.c.	n.c.	n.c.
FeO	1·58	2·83	1·92	4·70	3·73	2·72	4·20
MnO	0·01	b.d.	0·04	0·08	0·12	0·15	0·08
NiO	0·09	0·13	0·05	0·10	0·14	0·06	0·09
MgO	22·2	19·3	22·8	33·8	17·6	22·8	18·4
CaO	13·2	12·2	12·3	0·45	12·3	13·1	12·1
Na_2O	0·49	2·02	0·78	0·02	2·73	0·36	3·18
K_2O	0·03	0·41	0·01	0·01	b.d.	0·02	0·01
H_2O	2·19	2·13	2·19	2·23	2·11	2·19	2·11
Total	100·2	99·7	100·4	99·5	100·0	100·1	100·1
Si	7·700	6·639	7·791	7·617	6·290	7·828	6·283
Ti	0·007	0·011	0·003	b.d.	0·237	0·010	0·187
Cr	0·037	0·216	0·059	0·026	0·196	0·032	0·171
Al	0·602	1·899	0·469	0·212	2·186	0·204	2·095
Fe^{3+}	n.c.	n.c.	n.c.	n.c.	n.c.	n.c.	n.c.
Fe^{2+}	0·181	0·333	0·219	0·530	0·443	0·312	0·499
Mn	0·002	b.d.	0·004	0·009	0·015	0·018	0·009
Ni	0·010	0·015	0·006	0·011	0·016	0·007	0·010
Mg	4·533	4·040	4·649	6·788	3·737	4·669	3·898
Ca	1·929	1·846	1·800	0·064	1·880	1·921	1·849
Na	0·129	0·552	0·207	0·006	0·753	0·097	0·876
K	0·004	0·074	0·002	0·001	0·001	0·004	0·003
H	2·000	2·000	2·000	2·000	2·000	2·000	2·000
Total	15·134	15·626	15·209	15·267	15·753	15·100	15·879
Mg-no.	0·962	0·924	0·955	0·928	0·894	0·937	0·886
(Na + K)A	0·134	0·626	0·209	0·008	0·753	0·100	0·879

(Na + K)A, Na + K on site A; n.c., not calculated; b.d., below detection limit. Data obtained by normalization with 23 oxygens and 15 cations + Na + K, except for anthophyllite: normalization with 23 oxygens and considering $Fe^{3+} = 0$.

PIA120 [using diopside–fluid partition coefficients from Brenan *et al.* (1998*b*)], to deduce the composition of the fluid in equilibrium with pargasite and edenitic hornblende in the Dramala harzburgites. The fluid composition, calculated for pargasite (samples PIA109 and PIA120) and edenitic hornblende (sample PIA27), was similar for the three samples, and is in the range of 1·4–5·8 μg/g Li, 0·0008–0·0075 μg/g Be, and 0·05–1·21 μg/g B. This composition would be in agreement with an evolved seawater-derived fluid for Li, Be and B (seawater composition: Li ~0·18 μg/g, Be ~0·0002 ng/g and B ~4·4 μg/g; Noakes & Hood, 1961; Li, 1982; Measures & Edmond, 1982), assuming that such a fluid had reacted at high T with mafic and/or ultramafic rocks before interacting with the studied samples. High-T alteration of oceanic basalts would have enriched the fluid in Li and B (Thompson & Melson, 1970; Seyfried *et al.*, 1984), whereas serpentinization and/or low-T weathering of basalts could have decreased its B content (Thompson & Melson, 1970; Bonatti *et al.*, 1984; Boschi *et al.*, 2008). Measures & Edmond (1983) showed that Be is strongly enriched in ridge crest hydrothermal solutions, with values 400–1600 times higher than seawater. As edenitic

Table 8: Li, Be and B contents of rock-forming minerals (representative analyses)

Sample	N	Mineral	Li (μg/g)	2σ	Be (μg/g)	2σ	B (μg/g)	2σ
		Olivine						
PI2	13	Ol 1	0·73	0·03	0·002	0·002	0·11	0·02
		Ol 1	0·98	0·07	<0·0014		<0·0037	
		Ol 1	0·82	0·03	<0·0014		0·04	0·02
		Ol 1	0·62	0·05	<0·0014		0·016	0·009
PIA27	3	Ol 1	0·79	0·04	<0·0010		0·07	0·02
		Ol 1	0·95	0·05	<0·0010		0·03	0·01
		Ol 1	0·72	0·04	<0·0010		0·09	0·02
PIA27	1	Ol m	0·76	0·05	<0·0010		9	3
PI6	4	Ol 1	0·56	0·03	<0·0010		0·02	0·02
		Ol 1	0·65	0·04	<0·0010		0·03	0·01
		Ol 1	0·83	0·02	<0·0010		0·01	0·01
		Ol 1	0·86	0·04	<0·0010		0·01	0·01
PIA44	8	Ol 1	0·87	0·03	<0·0010		0·014	0·007
		Ol 1	0·51	0·02	<0·0010		0·026	0·006
		Ol 1	0·94	0·03	<0·0010		0·011	0·006
		Ol 1	0·67	0·04	<0·0010		0·009	0·005
PIA120	2	Ol 1	1·05	0·02	0·001	0·001	0·014	0·006
		Ol 1	0·97	0·02	<0·0010		0·007	0·003
PIA109	2	Ol 1	0·94	0·03	<0·0010		0·010	0·005
		Ol 1	0·72	0·02	<0·0010		0·022	0·008
		Amphibole						
PIA27	3	Ed hbl	2·4	0·1	0·002	0·001	0·08	0·01
		Ed hbl	2·1	0·2	<0·0010		0·06	0·02
	1	Ath	0·7	0·1	0·002	0·001	0·40	0·06
	2	Tr	0·03	0·01	<0·0010		1·17	0·06
		Tr	0·08	0·02	<0·0010		1·5	0·2
PI6	3	Tr	1·6	0·3	<0·0010		2·8	0·1
		Tr	0·09	0·02	0·001	0·001	1·7	0·1
		Tr	0·06	0·03	0·001	0·001	1·19	0·07
PIA120	3	Prg	0·6	0·1	0·003	0·001	<0·0026	
		Prg	1·1	0·1	0·004	0·001	0·02	0·01
		Prg	0·62	0·05	0·004	0·001	0·03	0·01
PIA109	2	Prg	1·7	0·1	0·012	0·003	0·04	0·01
		Prg	0·9	0·1	<0·0010		0·05	0·02
		Orthopyroxene						
PI2	25	Opx 1	1·14	0·07	<0·0014		0·07	0·01
		Opx 1	0·9	0·1	<0·0014		0·05	0·01
		Opx 1	0·70	0·09	<0·0014		0·02	0·01
		Opx 1	0·85	0·08	<0·0014		<0·0037	
	2	Opx 2	0·88	0·09	<0·0014		0·06	0·03
		Opx 2	0·7	0·1	<0·0014		0·39	0·05
PIA27	6	Opx 1	0·10	0·02	<0·0010		0·04	0·01
		Opx 1	0·20	0·03	<0·0010		0·03	0·01
		Opx 1	0·34	0·02	<0·0010		0·04	0·01
		Opx 1	0·45	0·07	<0·0010		0·17	0·03
PI6	4	Opx 1	0·10	0·03	0·001	0·001	0·02	0·01
		Opx 1	0·29	0·04	<0·0010		0·03	0·01
		Opx 1	0·29	0·07	<0·0010		0·02	0·01

(continued)

Table 8: Continued

Sample	N	Mineral	Li (μg/g)	2σ	Be (μg/g)	2σ	B (μg/g)	2σ
PIA44	7	Opx 1	0·62	0·05	<0·0010		0·01	0·01
		Opx 1	0·69	0·06	<0·0010		0·01	0·01
		Opx 1	0·64	0·08	<0·0010		0·018	0·005
		Opx 1	0·55	0·03	<0·0010		0·02	0·01
PIA120	4	Opx 1	0·44	0·03	<0·0010		0·009	0·003
		Opx 1	0·66	0·05	<0·0010		0·010	0·004
		Opx 1	0·61	0·04	0·001	0·001	<0·0026	
		Opx 1	0·20	0·03	<0·0010		0·02	0·01
	2	Opx 2i	0·26	0·04	<0·0010		<0·0026	
		Opx 2i	0·26	0·02	<0·0010		0·03	0·01
PIA109	9	Opx 1	0·88	0·07	0·002	0·001	0·007	0·004
		Opx 1	0·64	0·05	0·002	0·001	0·009	0·005
		Opx 1	1·49	0·04	0·002	0·001	<0·0026	
		Opx 1	1·30	0·06	0·001	0·001	<0·0026	
	4	Opx 2i	0·64	0·04	0·002	0·001	0·008	0·003
		Opx 2i	0·94	0·04	0·001	0·001	0·011	0·004
		Opx 2i	0·81	0·05	<0·0010		0·007	0·004
		Opx 2i	0·68	0·04	0·001	0·001	<0·0026	
		Plagioclase						
PIA109	2	Pl	<0·0014		0·007	0·002	<0·0026	
		Pl	<0·0014		0·005	0·002	0·015	0·006
		Clinopyroxene						
PI2	7	Cpx 1	3·3	0·2	<0·0014		<0·0037	
		Cpx 1	3·0	0·2	<0·0014		<0·0037	
		Cpx 1	2·5	0·1	<0·0014		0·58	0·07
		Cpx 1	1·5	0·1	<0·0014		0·12	0·03
	2	Cpx 2	3·2	0·2	<0·0014		<0·0037	
		Cpx 2	2·2	0·2	0·002	0·001	0·19	0·03
PIA27	2	Cpx exsol	0·47	0·04	<0·0010		0·25	0·03
		Cpx exsol	0·4	0·1	<0·0010		0·26	0·03
PI6	5	Cpx 1	0·6	0·1	0·003	0·002	0·020	0·009
		Cpx 1	0·8	0·1	<0·0010		0·02	0·01
		Cpx 1	0·11	0·03	<0·0010		0·01	0·01
		Cpx 1	1·8	0·1	<0·0010		0·023	0·009
PIA44	8	Cpx 1	2·4	0·1	<0·0010		0·015	0·008
		Cpx 1	3·0	0·2	0·001	0·001	0·02	0·01
		Cpx 1	2·7	0·1	<0·0010		0·03	0·01
		Cpx 1	3·7	0·2	<0·0010		0·05	0·01
PIA120	2	Cpx 1	1·7	0·1	0·004	0·005	<0·0026	
	2	Cpx 1	0·20	0·02	<0·0010		0·008	0·006
	2	Cpx 2i	1·5	0·1	0·003	0·002	0·03	0·01
	2	Cpx 2i	0·77	0·05	0·005	0·003	0·008	0·003
PIA109	2	Cpx 1	3·3	0·1	<0·0010		<0·0026	
	2	Cpx 1	3·7	0·1	0·004	0·002	<0·0026	
	2	Cpx 2i	2·8	0·1	0·004	0·001	0·06	0·01
	2	Cpx 2i	3·0	0·1	0·003	0·001	0·037	0·008

(continued)

Table 8: Continued

Sample	N	Mineral	Li (μg/g)	2σ	Be (μg/g)	2σ	B (μg/g)	2σ
		Alteration Phases After Plagioclase						
PIA120	2	Chl 2	2·0	0·1	<0·0010		0·07	0·01
		Chl 2	3·3	0·2	<0·0010		0·27	0·05
	3	Ntr	0·01	0·01	<0·0010		0·007	0·003
		Ntr	0·1	0·1	<0·0010		0·010	0·004
		Ntr	0·01	0·01	<0·0010		0·009	0·005
	3	Vua	0·03	0·01	0·002	0·001	0·26	0·04
		Vua	0·4	0·1	0·001	0·001	0·22	0·03
		Vua	0·2	0·1	0·002	0·001	0·23	0·03
PI6	2	Pct	5·1	0·3	<0·0010		0·10	0·03
		Pct	11·0	0·5	<0·0010		0·8	0·3
		Serpentine						
PIA27	3	Srp 1 (ol)	0·05	0·03	0·001	0·001	22	1
		Srp 1 (ol)	0·07	0·03	<0·0010		28	1
		Srp 1 (ol)	0·27	0·03	<0·0010		11·0	0·1
	3	Srp 2 (opx)	0·27	0·02	<0·0010		6	1
		Srp 2 (opx)	0·32	0·06	0·001	0·001	4·6	0·4
		Srp 2 (opx)	0·23	0·03	0·001	0·001	9	1
PI6	1	Srp (ol)	0·32	0·06	<0·0010		5	1
	3	Srp (opx)	0·08	0·02	<0·0010		3	1
		Srp (opx)	0·48	0·05	<0·0010		0·8	0·3
		Srp (opx)	0·20	0·04	<0·0010		0·6	0·2
PIA44	3	Srp (ol)	0·09	0·02	<0·0010		0·12	0·04
		Srp (ol)	0·19	0·03	<0·0010		0·07	0·02
		Srp (ol)	0·09	0·01	<0·0010		0·09	0·04
	2	Srp (opx)	(9·0)	0·5	0·001	0·001	(0·53)	0·03
		Srp (opx)	(3·2)	0·3	<0·0010		(1·0)	0·1
PIA120	3	Srp (ol)	0·78	0·05	<0·0010		0·41	0·03
		Srp (ol)	<0·0014		<0·0010		0·57	0·03
		Srp (ol)	<0·0014		<0·0010		0·8	0·1
PIA109	4	Srp (ol)	0·14	0·02	<0·0010		9	2
		Srp (ol)	0·13	0·02	<0·0010		10	1
		Srp (ol)	0·12	0·02	<0·0010		4	1
		Srp (ol)	0·16	0·02	<0·0010		24	5
		Talc						
PIA27	3	Tlc	0·15	0·03	<0·0010		4·0	0·6
		Tlc	0·12	0·03	<0·0010		0·7	0·1
		Tlc	0·10	0·02	<0·0010		0·8	0·1
PI6	2	Tlc	3·8	0·4	<0·0010		1·5	0·5
		Tlc	2·9	0·2	<0·0010		0·9	0·2

n, total number of analyses. Data in parentheses represent mixtures of serpentine with talc (see comment in text).

hornblende and pargasite form above 750°C (Lykins & Jenkins, 1992; Sharma & Jenkins, 1999), it is likely that seawater passed through mafic rocks and other peridotites and was heated before reacting with the Dramala mantle section.

Low-*T* hydration—impact on Li, B and Be systematics

Talc, anthophyllite, tremolite, serpentine, magnetite, and the plagioclase alteration phases natrolite, vuagnatite, pectolite and chlorite are considered low-*T* hydrous

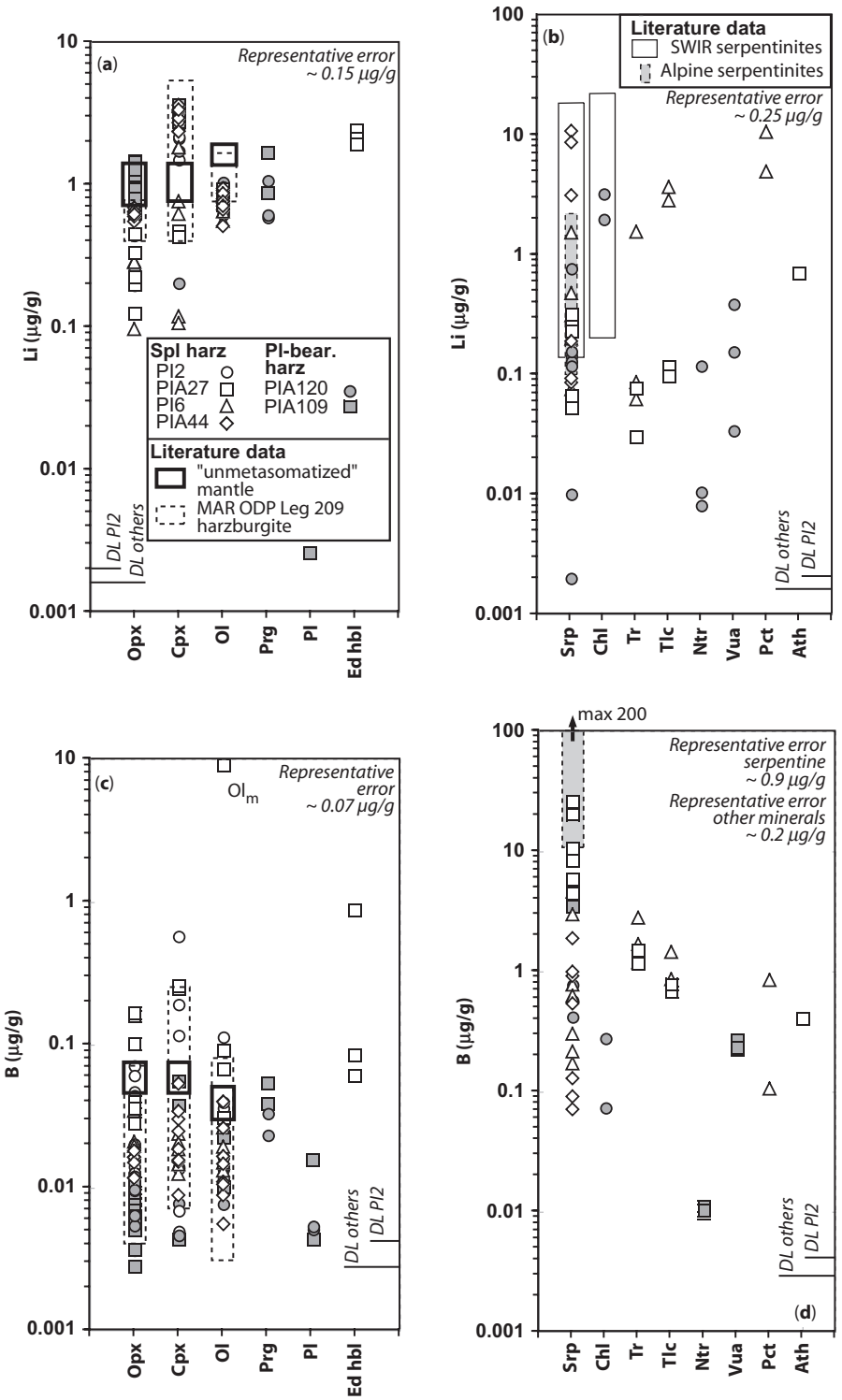

Fig. 8. (a) Li contents of primary mantle minerals and of high-*T* amphiboles. (b) Li contents of minerals related to serpentinization and retrogression. Li contents higher than 1·0 µg/g in serpentine are probably due to a mixture of different phases (see text). (c) B contents of primary mantle minerals and of high-*T* amphiboles. Ol_m, metamorphic olivine. (d) B contents of minerals related to serpentinization and cooling (excepted for Ol_m). 'Unmetasomatized' mantle data after Ottolini *et al.* (2004), Mid-Atlantic Ridge (MAR) ODP Leg 209 serpentinites after Vils *et al.* (2008), SWIR serpentinites after Decitre *et al.* (2002), and Alpine serpentinites after Scambelluri *et al.* (2004). Some values are below the detection limit (DL) for Li in plagioclase and serpentine, and for B in orthopyroxene, clinopyroxene, olivine, pargasite, plagioclase and natrolite.

Table 9: Whole-rock data

Present Study										
Sample	Ol (%)	Cpx (%)	Opx (%)	Spl (%)	Pl (%)	Srp (%)	Other (%)		Li (μg/g)	Be (μg/g)	B (μg/g)
Spl Harzburgites									ICP-MS	ICP-MS	PGNAA
Pl2	79.6	3.7	13.8	1.2		1.7			0.9	< 0.003	< 0.05
PIA91	78.0	3.9	16.0	1.9		0.0	0.2	Tr	1.0	< 0.003	
PIA27	64.5	0.2	6.6	1.0		19.1	8.6	Ed hbl, Tr, Ath, Tlc, Chl	0.6	< 0.003	1.1
Pl6	46.3	0.8	3.0	0.7		46.9	2.3	Tr, Tlc, Pct	0.5	< 0.003	0.1
PIA44	36.8	1.0	5.0	1.6		55.4	0.2	Tr	0.8	< 0.003	< 0.04
Pl-bearing Harzburgites											
PIA120	35.7	1.9	5.0	0.3	2.0	41.1	14.0	Prg, Tr, Chl, Ntr, Vua, Pct	1.0	< 0.003	0.7
PIA51	66.1	4.7	18.2	1.9	0.2	8.5	0.4	Tr, Tlc, Chl, Vua	0.9	< 0.003	
PIA109	63.5	4.2	19.5	0.6	3.0	8.9	0.3	Prg, Tr	1.1	< 0.003	0.1

Literature data											
Paper	Data	Rock types	Li (μg/g) av.	Li (μg/g) max.	Li (μg/g) min.	Be (μg/g) av.	Be (μg/g) max.	Be (μg/g) min.	B (μg/g) av.	B (μg/g) max.	B (μg/g) min.
Unmetasomatized Mantle											
Lyubetskaya & Korenaga (2007)	CAL	Primitive mantle	1.6			0.054			0.17		
McDonough & Sun (1995)	CAL	Primitive mantle	1.6			0.068			0.30		
Chaussidon & Jambon (1994)	CAL	Primitive mantle							0.25	0.35	0.15
Ottolini *et al*. (2004)	ANAL	Spl peridotites of Massif Central and Dreiser Weiher		1.80	1.60					0.10	0.07
Chaussidon & Libourel (1993)	EXP	Depleted mantle								0.30	0.05
Chaussidon & Marty (1995)	CAL	Depleted mantle								0.02	0.01
Salters & Stracke (2004)	CAL	Depleted mantle	0.7			0.025			0.06		
Abyssal Peridotites											
Thompson & Melson (1970)	ANAL	Dredged serpentinized peridotites, Vema FZ + MAR								100	70
Bonatti *et al*. (1984)	ANAL	Dredged serpentinized peridotites, Vema + Romanche FZ, Atlantic							61	85	20
Spivack & Edmond (1987)	ANAL	Dredged serpentinized peridotites, Vema FZ, Atlantic							64	81	50
Decitre *et al*. (2002)	ANAL	Dredged fresh and serpentinized peridotites, SWIR	3.5	8.2	0.6						

(continued)

Table 9: Continued

Literature data Paper	Data	Rock types	Li (μg/g) av.	Li (μg/g) max.	Li (μg/g) min.	Be (μg/g) av.	Be (μg/g) max.	Be (μg/g) min.	B (μg/g) av.	B (μg/g) max.	B (μg/g) min.
Niu (2004)	ANAL	Dredged abyssal peridotites, see details in the paper	6.0	13.7	0.6	0.044	0.212	0.001			
Paulick *et al*. (2006)	ANAL	Drilled serpentinized spl harzburgites, ODP Leg 209 MAR	*	7.0	<0.003						
Boschi *et al*. (2008)	ANAL	Drilled serpentinized spl harzburgites, Atlantis Massif (30°N) MAR							66.6	90.6	34.0
Vils *et al*. (2008)	ANAL	Drilled serpentinized spl harzburgites, ODP Leg 209 MAR	0.7	3.4	0.1	0.0015	0.0080	0.0002	45.1	65.0	10.4
Forearc Peridotites											
Parkinson & Pearce (1998)	ANAL	Drilled serpentinized harzburgites, ODP Leg 125 IBMF	4.1	12.8	1.1						
Benton *et al*. (2001, 2004)	ANAL	Drilled serpentinized peridotite clasts, MF, Conical Seamount	5.9	18.9	1.6				24.3	57.5	6.8
Zanetti *et al*. (2006)	ANAL	Drilled serpentinized peridotites, ODP Leg 125 + 195 IBMF	4.7	12	1.6	0.11	0.16	0.07			
Savov *et al*. (2005)	ANAL	Serpentinized peridotites, MF, Conical Seamount	4.6	18.9	0.5				15.4	58.0	0.4
Wei *et al*. (2005)	ANAL	Serpentine muds, South Chamorro Seamount, MF							58.7	79.0	39.4
Peridotites Interpreted as Modified by Slab Fluids											
Scambelluri *et al*. (2004)	CAL	Serpentinized peridotite, Northern Apennine and Erro Tobbio	1.3						47.0		
Paquin *et al*. (2004)	CAL	Alpe Arami ultra-high pressure garnet peridotites				0.011			0.1		
Brooker *et al*. (2004)	ANAL	Metasomatized (hydrous fluid) spl lherzolites, Zabargad	3.2	4.1	2.5	0.063	0.213	0.012			
Ottolini *et al*. (2004)	ANAL	Metasomatized spl peridotites, Balmuccia and Zabargad	1.5	1.9	1.1				0.16	0.32	0.04
Scambelluri *et al*. (2006)	ANAL	Ulten spl peridotites and grt-amph peridotites		4.2	1.9		0.13	0.01			
Ophiolitic Peridotites											
Marchesi *et al*. (2006)	ANAL	Mayari-Baracoa MOR- and transitional MOR-IAT-peridotites (Cuba)	0.35	0.70	0.23						
Li & Lee (2006)	ANAL	Feather River Ophiolite (California, USA)	0.95	3.09	0.23	0.03	0.06	0.01			
Agranier *et al*. (2007)	ANAL	Feather River Ophiolite (California, USA)	0.99	3.09	0.08				10.2	15.6	6.4

*Only three values including one below detection limit.
ANAL, analyzed; EXP, determined experimentally; CAL, calculated; av., average; max., maximum, min., minimum; FZ, fracture zone; MAR, Mid-Atlantic Ridge; SWIR, South West Indian Ridge; IBMF, Izu–Bonin–Mariana forearc; MF, Mariana forearc.

JOURNAL OF PETROLOGY | VOLUME 49 | NUMBER 11 | NOVEMBER 2008

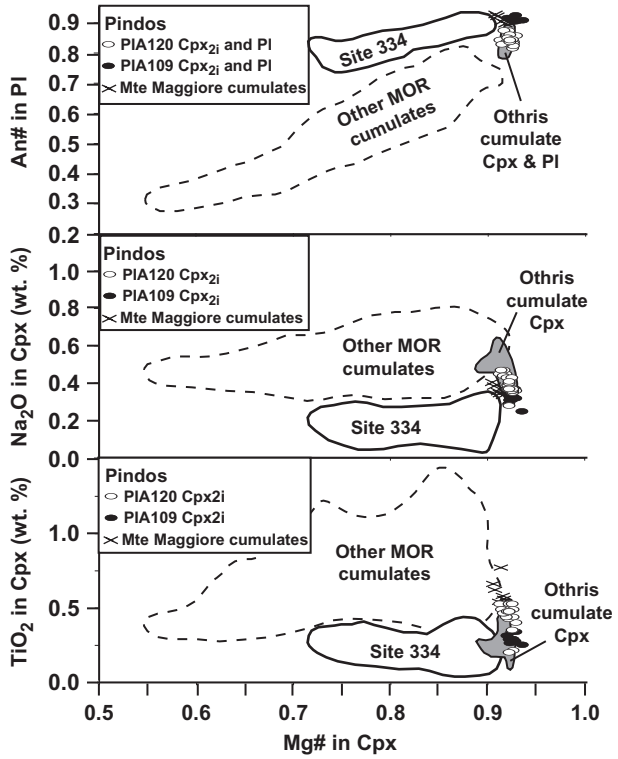

Fig. 9. Mineral compositions of melt-related (cumulate) minerals from the Pindos plagioclase-bearing harzburgites compared with cumulate phases in oceanic rocks. Othris cumulates (grey field) from Dijkstra *et al.* (2001), Site 334 and other MOR cumulates fields from Ross & Elthon (1993), depleted cumulates of the Monte Maggiore (Corsica, France) ophiolitic peridotites from Rampone *et al.* (1997). Diagram modified from Ross & Elthon (1993, fig. 1).

phases here. Textural observations and comparison with literature data on orthopyroxene and olivine hydration show that the crystallization sequence with decreasing T is talc + tremolite ± serpentine ± olivine at $T \geq 350$–400°C, followed by serpentine + magnetite at $T < 250$°C, followed by the plagioclase alteration phases down to $T < 100$°C.

Considering the high Li contents of talc and the high B contents of metamorphic olivine compared with the primary minerals (Table 8), formation of these minerals by hydration of pyroxene at $T \geq 350$–400°C should have increased the bulk Li and B contents of the samples. However, the modes of talc and metamorphic olivine are very low, probably because cooling proceeded rapidly and fluid–rock ratios were low.

Serpentine is the major hydrous phase and can represent up to 55 vol. % of the rock. It is the major carrier of B with up to 28 μg/g (Fig. 8, Table 8). Its Be contents are <3 ng/g. The Li contents are generally lower than 1 μg/g (similar to the Li content of olivine), but can be higher (up to 9 μg/g), if serpentine is intergrown with talc (Fig. 8, Table 8; Pelletier *et al.*, in preparation). Thus, serpentinization of the Dramala mantle by reaction with external fluid should have essentially increased the B whole-rock contents. However, this is not what we observe. Measured B whole-rock concentrations (<0·04–1·1 μg/g) are only slightly higher than those in the depleted mantle (0·06 μg/g), and 1–2 orders of magnitude lower than values for drilled (10·4–90·6 μg/g; see Table 9) or dredged (20–100 μg/g; see Table 9) abyssal peridotites. Also, there is no positive correlation between the degree of serpentinization and the B contents, because the B contents of serpentine are highly variable (0·1–28 μg/g).

The bulk Li concentrations (0·5–1·1 μg/g) in the samples from Dramala are close to those of depleted mantle (0·7 μg/g), and generally lower than those in drilled (<0·003–7·0 μg/g) or dredged (0·6–13·7 μg/g) abyssal peridotites. The bulk Li contents of the serpentinized harzburgites are generally low compared with Dramala harzburgites with low degrees of serpentinization, except for sample PIA120, which is characterized by the presence of abundant Li-rich chlorite (Table 8). Lithium contents of orthopyroxene from serpentinized harzburgites (>20 vol. % serpentinization-related minerals in Table 9) are low (<0·7 μg/g; Table 8), compared with Li contents of orthopyroxene from partially serpentinized harzburgites (0·7–1·5 μg/g; Table 8). We therefore conclude that some Li loss could have occurred during serpentinization.

Fluid–rock ratio, fluid composition, T, and time are most probably responsible for the non-systematic behaviour of B (and to a lesser degree Li) during low-T hydration. Changes in pH may also have played a role, but they cannot be assessed.

(1) *Fluid–rock ratio and fluid composition.* Fluid–rock ratio was probably low, as suggested by the fairly low degree of serpentinization in the Dramala mantle compared with drilled and dredged oceanic samples. Low fluid–rock ratios induce local differences in fluid composition and disequilibrium, as indicated by variable B contents of serpentine. Agranier *et al.* (2007) reported low B (5–15 μg/g) and Li (0·3–3·1 μg/g) concentrations in serpentinized harzburgites from the Feather River ophiolite related to serpentinization at low water–rock ratio. Feather River ophiolite serpentinized harzburgites are also characterized by a lack of correlation between their bulk-rock B content and their loss on ignition. Furthermore, during serpentinization, the Dramala mantle may have been covered by an igneous crust and was not exposed to seawater but to evolved fluids with highly variable compositions, which had interacted with the mafic crust before (Smith *et al.*, 1995; Decitre *et al.*, 2002).

(2) *Temperature and time.* When depleted mantle rocks (B ~0·06 μg/g; Salters & Stracke, 2004) react with seawater (B ~4·44 μg/g; Li, 1982) at low T and

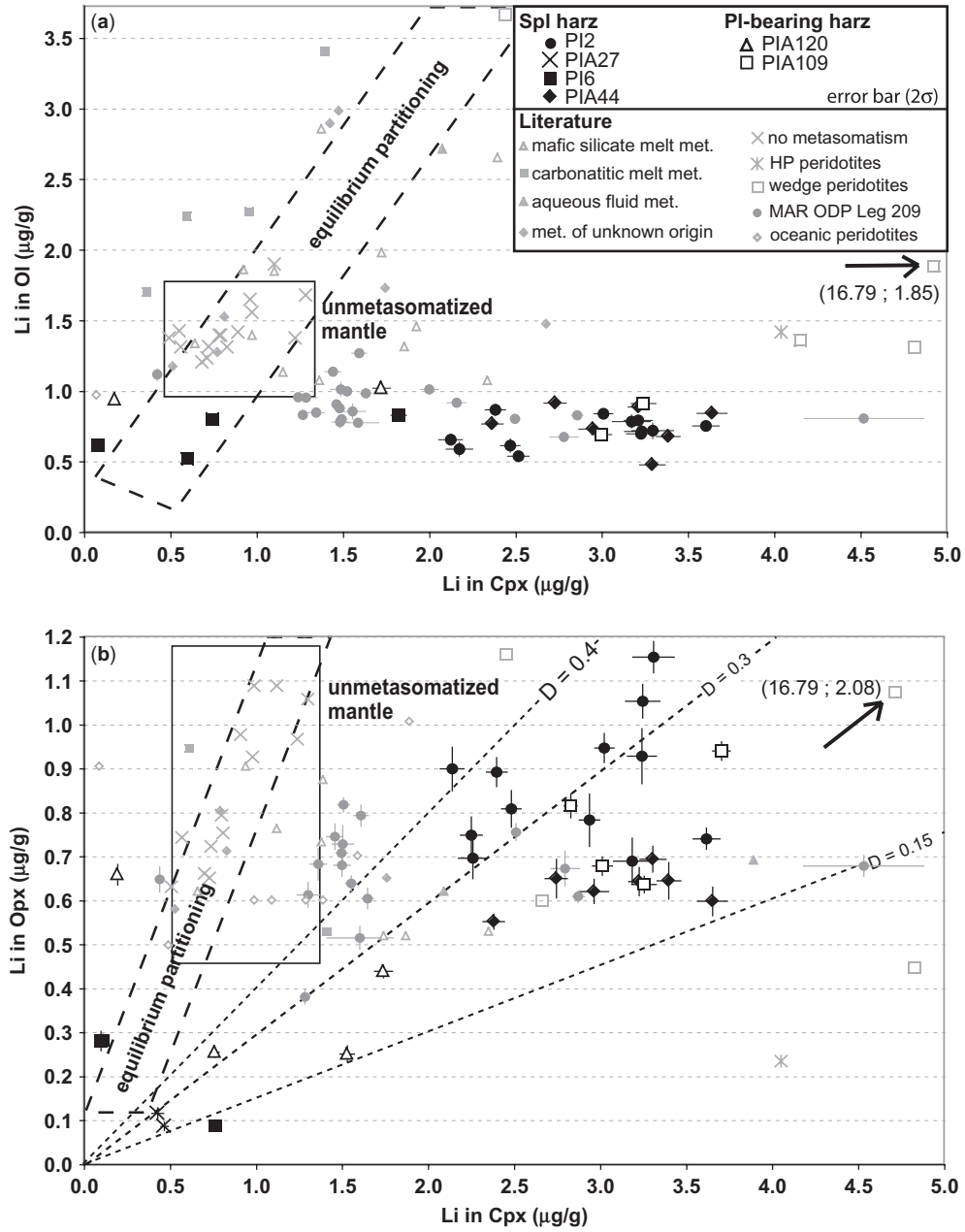

Fig. 10. Li–Li diagrams modified after Seitz & Woodland (2000) showing Li abundances in coexisting (a) clinopyroxene and olivine and (b) clinopyroxene and orthopyroxene from the Pindos spinel and plagioclase-bearing harzburgites. For sample PIA27, results represent clinopyroxene exsolution lamellae in orthopyroxene. Equilibrium partitioning field after Seitz & Woodland (2000), and unmetasomatized mantle box after Ottolini *et al.* (2004). Mid-Atlantic Ridge ODP Leg 209 serpentinites are shown for comparison (Vils *et al.*, 2008). Literature data: Eggins *et al.* (1998); Seitz & Woodland (2000); Decitre *et al.* (2002); Kaliwoda (2004); Ottolini *et al.* (2004); Paquin *et al.* (2004); Scambelluri *et al.* (2004); Wagner & Deloule (2004); Woodland *et al.* (2004); Scambelluri *et al.* (2006); Kaeser *et al.* (2007). met., metasomatism.

equilibrium conditions (Thompson & Melson, 1970; Seitz & Hart, 1973; Seyfried & Dibble, 1980; Bonatti *et al.*, 1984; Spivack & Edmond, 1987), they become enriched in B. Seyfried & Dibble (1980) showed experimentally that B uptake in serpentine is favoured at low T (<300°C).

Serpentinization in the Dramala harzburgite most probably began above 350–400°C. In abyssal environments, known high-T fluids (>350°C) such as those of the Logatchev and Rainbow hydrothermal fields (Mid-Atlantic Ridge) have a pH ~3 (Douville *et al.*, 2002; Schmidt *et al.*, 2006). It is possible that such fluids reacted

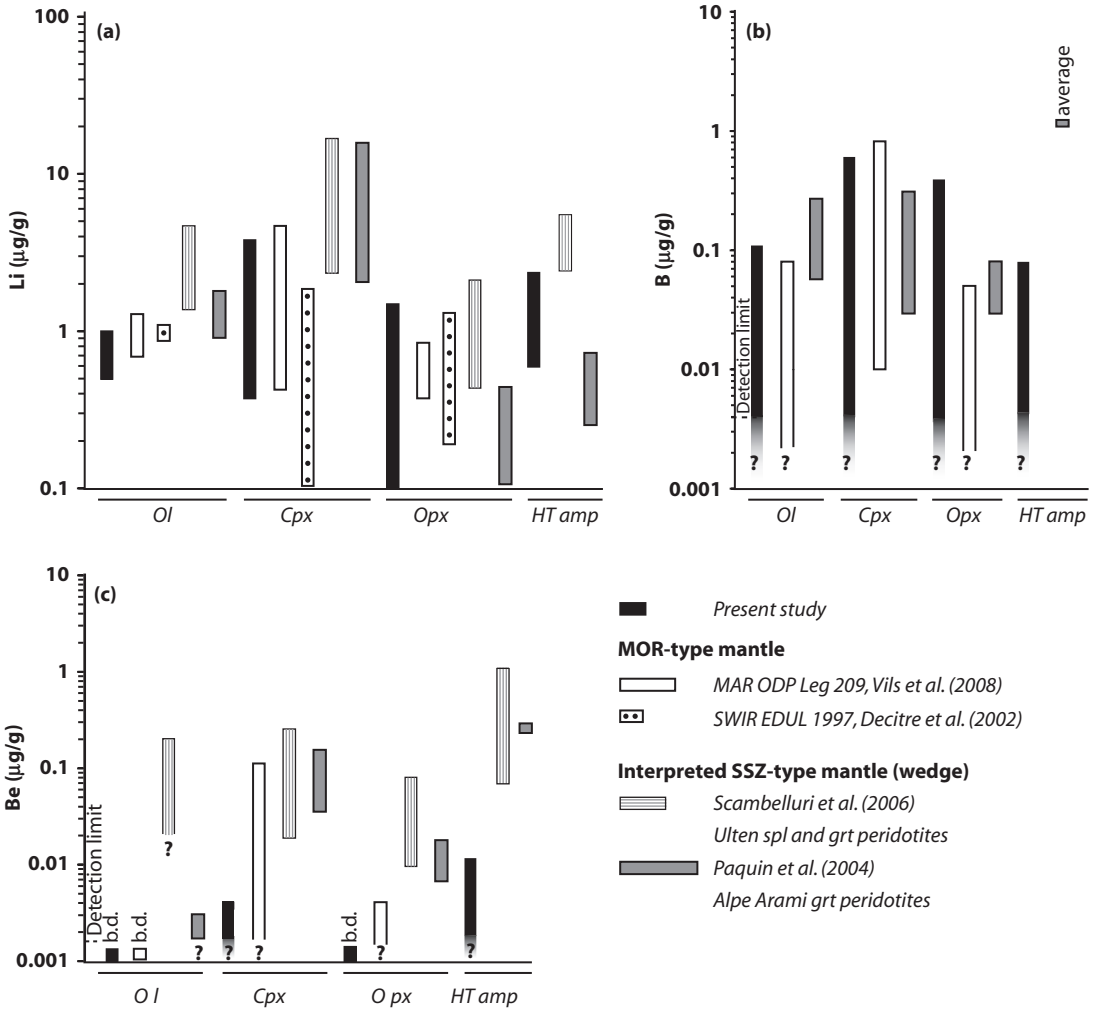

Fig. 11. (a) Li, (b) B and (c) Be contents of olivine, clinopyroxene, orthopyroxene and high-*T* amphiboles from the Pindos mantle and from MOR-type mantle and SSZ-type mantle. b.d., below detection limit.

with the Dramala mantle and produced low-B serpentine. Then, serpentinization in the Dramala harzburgite continued down to low *T* and formed serpentine with higher B contents. As cooling probably proceeded quickly, serpentine could not re-equilibrate with seawater. This would explain the presence of high- and low-B serpentine. This hypothesis is in agreement with Boschi *et al.* (2008), who showed that processes related to low-*T* marine weathering do not change the B content of serpentinites.

The very late formation of the plagioclase alteration phases should lead to an increase in Li contents as a result of the high abundances of this element in chlorite and pectolite. However, the modes of these phases are generally low (except for sample PIA120) so that the Li whole-rock budget is probably not modified significantly.

IMPLICATIONS FOR THE ORIGIN OF THE PINDOS OPHIOLITE

The Dramala harzburgites: MOR- rather than SSZ-type mantle

Bizimis *et al.* (2000) interpreted the Pindos harzburgites as SSZ mantle wedge peridotites, modified by subduction-related hydrous melting. This interpretation is based on the spoon-shaped REE patterns of some Dramala harzburgites and clinopyroxenes. Saccani & Photiades (2004) proposed, on the basis of the composition of the associated lavas of the Aspropotamos Complex, a possible SSZ origin for the Pindos harzburgites (Fig. 2), which include IATs and boninites, in addition to N-MORB. The high Cr-number of spinel in some samples of the Dramala Complex (>0·6; Fig. 5a and b; see also Economou-Eliopoulos & Vacondios, 1995) could be added to the

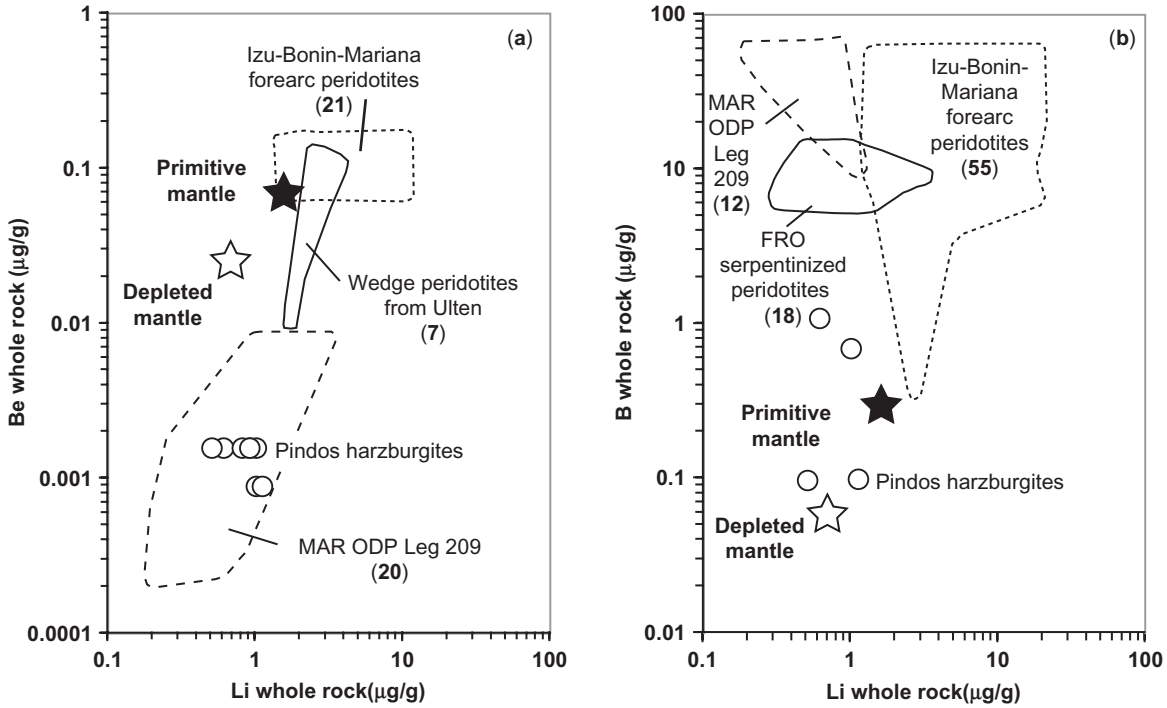

Fig. 12. (a) Be vs Li diagram showing whole-rock estimates from Pindos harzburgites. Detection limit values of the ICP-MS were plotted for Be as indicative in the Pindos harzburgites, as all results are below the detection limit. (b) B vs Li diagram of whole-rock estimates from the Pindos harzburgites. Mid-Atlantic Ridge ODP Leg 209 peridotites of Vils *et al.* (2008), Ulten wedge peridotites from Scambelluri *et al.* (2006), Feather River ophiolite (FRO) serpentinized peridotites from Agranier *et al.* (2007) and Izu–Bonin–Mariana forearc peridotites of Benton *et al.* (2001, 2004), Savov *et al.* (2005) and Zanetti *et al.* (2006) are shown for comparison. Depleted mantle after Salters & Stracke (2004) and Primitive Mantle after McDonough & Sun (1995). Bold numbers in parentheses represent the number of samples analyzed. For Vils *et al.* (2008), Be data were calculated and Li data were measured.

previous arguments, but as noted in the Introduction, none of these characteristics are distinctive of melting of the mantle in an SSZ setting. In addition, the lavas with IAT and boninite characteristics come from the Aspropotamos Complex, which is only in tectonic contact with the Dramala Complex.

The Dramala harzburgites display some textures that are typical of MOR-type mantle; for example, the presence of macroscopic plagioclase aggregates and dykelets (Fig. 4d; Girardeau & Francheteau, 1993), and primary clinopyroxene grains with embayments filled by olivine, which are in optical continuity and associated with plagioclase (Fig. 4f; Seyler *et al.*, 2001). High-T amphibole occurs occasionally in the Pindos peridotites. These amphiboles have very low Be contents (<0·02 µg/g) compared with high-T amphiboles of SSZ-type peridotites (0·24–1·10 µg/g; Fig. 11c), and were probably formed during the interaction between Pindos harzburgite and a seawater-derived fluid, but certainly not with a subduction-related fluid (see below).

In Fig. 11, the Li, Be and B contents of the primary mantle minerals and high-T amphiboles of the Dramala harzburgites are compared with values for minerals from MOR-type peridotite and peridotite interpreted as related to SSZ-type settings. This comparison is problematic because there are no Li, B and Be mineral data for modern SSZ environments (Izu–Bonin–Mariana forearc), but only whole-rock data (Table 9). Mineral data have to be taken from alpine-type peridotites that are interpreted as SSZ-related (Table 9). The light-element contents of these minerals may have been modified during their emplacement into continental crust. Comparison between Dramala harzburgites and SSZ-attributed Alpine peridotites (Paquin *et al.*, 2004; Scambelluri *et al.*, 2006) reveals many differences. Clinopyroxene and olivine from the SSZ-related samples are enriched in Li compared with the Dramala clinopyroxene. An enrichment in B in olivine and high-T amphiboles of these peridotites is also characteristic. The most striking feature is the much higher Be content of clinopyroxene, orthopyroxene and high-T amphibole in minerals from SSZ-attributed Alpine peridotites compared with Dramala. It is important to note that the measured Li, Be and B contents of all minerals from the Dramala harzburgites are similar to the data from ODP Leg 209

sites 1272A and 1274A (Mid-Atlantic Ridge; Vils *et al.*, 2008) and from the South West Indian Ridge (SWIR; Decitre *et al.*, 2002), which represent MOR-type mantle.

Concerning whole-rock data, Li, B and Be values are available for mantle from modern SSZ settings (Table 9). From Fig. 12 and Table 9, it can be deduced that peridotites from the Mariana and Izu–Bonin forearcs have Li contents that are 4–10 times higher than those of the Dramala mantle rocks, B contents are 2–3 orders of magnitude higher, and Be contents are at least 100 times higher. The bulk Be contents presented by Brooker *et al.* (2004) and Scambelluri *et al.* (2006) for Ulten and Zabargad wedge peridotites are also at least one order of magnitude higher than those of the Dramala samples. Li and Be whole-rock contents for Dramala harzburgites are similar to those obtained by Vils *et al.* (2008) for ODP Leg 209 of the Mid-Atlantic Ridge. The B contents are much lower than published values for drilled serpentinized peridotites along the Mid-Atlantic Ridge (11–91 μg/g; Boschi *et al.*, 2008; Vils *et al.*, in preparation), but this is probably due to higher T and/or lower water–rock ratio during serpentinization (Fig. 12b).

In conclusion, the Dramala mantle shows many similarities to MOR-type mantle and many discrepancies compared with SSZ-type mantle. From the published data it seems that modern SSZ-related mantle is characterized by high contents of Li, Be and B. There is no difference in concentration level between drilled samples and those collected otherwise (Table 9). This means that alteration processes, such as formation of clay minerals, do not play an important role, and that the elevated light-element contents must be earlier features. Models predict that in SSZ settings, the mantle melts at relatively low T as a result of influx of fluids released from a subducting slab (Davies & Stevenson, 1992, and references therein). These fluids are rich in B and Li, but also in Be (Marschall *et al.*, 2007, Li 100–200 μg/g, B 50–1200 μg/g, Be 0·4–0·9 μg/g) and will enrich the mantle minerals in these elements. Moreover, as the geothermal gradient is lower than in MOR settings, serpentinization will probably take place at lower T compared with MOR settings. Serpentine will thus be high in B and Li and add to the budget. It could be argued that with slow-spreading ridges, serpentinization continues down to low T on the ocean floor and serpentine attains equilibrium with seawater. This is probably true for modern MOR settings, but not necessarily for the Greek ophiolites. For Pindos and Vourinos ophiolites radiometric dating shows that crystallization of co-magmatic zircon in plagiogranite and gabbro (169–173 Ma; Liati *et al.*, 2004) is virtually contemporaneous with formation of their metamorphic soles (169–176 Ma; Pe-Piper & Piper, 2002, and references therein). This means that the ophiolite mantle sections were hot and cooled quickly while being emplaced.

Tectonic setting of formation of the Pindos ophiolite

The Pindos ophiolite is a highly dismembered ophiolite, and there is no *in situ* contact between mantle harzburgite (Dramala Complex) and the mafic rocks of the Aspropotamos Complex (oceanic crust; Jones & Robertson, 1991). However, in some localities there are *in situ* contacts between the Dramala mantle and some MOR-type cumulates (Jones & Robertson, 1991). In the Aspropotamos Complex, the crustal section shows successive phases of lava extrusion with a geochemical trend from high-Ti MORB to N-MORB–IAT and finally to IAT-boninite-type for the youngest dykes (Capedri *et al.*, 1980; Kostopoulos, 1988; Jones & Robertson, 1991; Jones *et al.*, 1991; Pe-Piper *et al.*, 2004; Beccaluva *et al.*, 2005).

Lithium, Be and B contents of minerals and whole-rock samples from the Dramala harzburgite as well as textural and chemical evidence suggest that these rocks never interacted with subduction-related fluids or melts. Consequently, the Dramala mantle and the Aspropotamos crust apparently represent contrasting tectonic settings.

To resolve assemblage and evolution of the Pindos ophiolite is beyond the scope of this paper, because an integrated structural, sedimentological, petrological and geochemical approach would be required. Any proposed scenario must take into account (1) the juxtaposition of MOR-type mantle associated with (some) SSZ-type extrusive rocks; (2) the occurrence of some ophicalcite in the Dramala mantle (Jones *et al.*, 1991), showing that it was once exposed on the ocean floor; (3) the fact that the crustal section on top of the mantle is largely absent, which suggests that the Dramala mantle probably evolved in a slow-spreading environment; (4) coincidence of the ages of plagiogranites, gabbros and metamorphic soles generally, indicating that oceanic spreading and thrusting were quasi-simultaneous. In addition, the Mesovouri mantle, cropping out in the southeastern part of the Pindos ophiolite (see Fig. 2), towards the Vourinos ophiolite, seems to be similar to the latter in terms of textures (A. Dijkstra, personal communication; no geochemical data available). As the Vourinos ophiolite is commonly interpreted as SSZ-related, this could mean that the Dramala MOR-type mantle is juxtaposed with SSZ-type mantle, but at present this hypothesis remains speculative. Taking into account the evidence cited above, two alternative tectonic settings of formation for the Pindos ophiolite can be proposed, as follows.

(1) The Dramala mantle was formed in a back-arc setting, simultaneously with the Aspropotamos plutonic and extrusive rocks, which formed in a forearc environment (and perhaps the Mesovouri mantle). These units were later tectonically juxtaposed. Hawkins (2003) deduced from the observation of present-day SSZ oceanic lithosphere that crustal contraction would juxtapose arc, back-arc and forearc crust. Therefore, rocks from different

settings can be present in the same SSZ ophiolite. The volcanic arc between the back-arc and forearc basins was probably a nascent arc. The presence of an MOR-type cumulate sequence at the top of the Dramala peridotite (Capedri *et al.*, 1982; Rassios, 1991) is consistent with the fact that most extrusive rocks present in back-arc environments have MORB character (Hawkins, 2003). Present-day equivalents would be the Lau Basin–Tonga Trench region of southwestern Pacific and the Mariana Trough–Mariana Trench region of the northwestern Pacific (Flower & Dilek, 2003).

(2) The Dramala mantle was formed at a slow-spreading MOR, perhaps covered by a thin MOR-type crust, and was emplaced above an intra-oceanic subduction zone close to or directly at the ridge shortly after its formation (Boudier *et al.*, 1988; Barth *et al.*, 2008). During this stage, IATs and boninites erupted in a forearc setting, as proposed by Dilek & Flower (2003) and Flower & Dilek (2003). This could explain the presence of subduction-related lavas in association with MORB. However, it is difficult to imagine how the mantle preserved its MOR signature despite the passage of slab-derived fluids or melts. As proposed by Barth *et al.* (2008), this would require that fluid flow from the slab is very localized.

SUMMARY AND CONCLUSIONS

Spinel harzburgite and plagioclase harzburgite of the Dramala Complex record textural and chemical evidence of melt impregnation, hydration and cooling. The light-element contents (Li, B, Be) of whole-rock samples and minerals are generally low, close to values for depleted mantle.

Prior to melt impregnation, hydration and cooling, the Dramala harzburgites represented depleted spinel-bearing oceanic mantle characterized by extraction of more than 15% partial melt and very low light-element contents.

Infiltration of a mafic melt and its reaction with the primary minerals led to the formation of plagioclase and secondary pyroxenes, and probably to a Li enrichment of clinopyroxene.

Hydration and cooling at high T formed amphibole but probably left the light-element contents of bulk and primary minerals unchanged. The fluid calculated to be in equilibrium with the amphiboles could have been reaction-modified seawater.

Serpentinization led to a moderate increase in bulk B in most samples and to a decrease in Li in some samples. The B and Be contents of all pre-existing minerals remained unchanged, whereas the Li content of orthopyroxene decreased. The non-systematic behaviour of B in whole-rock samples and serpentine may be explained by low fluid–rock ratios, decreasing T and lack of equilibrium as a result of fast exhumation.

Geochemically, the Dramala mantle shows many similarities to MOR-type mantle and many discrepancies compared with SSZ-type mantle. In particular, the low light-element contents of minerals and whole-rock samples argue against any interaction with subduction-related fluids. The Dramala mantle and the tectonically juxtaposed Aspropotamos crust, comprising IATs and boninites, must hence have been formed in contrasting tectonic settings.

Conclusions as to how the Dramala mantle and Aspropotamos crust were assembled are beyond the scope of this paper. We tend to favour a model where the Dramala mantle was formed in a back-arc setting, simultaneously with the Aspropotamos plutonic and extrusive rocks, which formed in a forearc environment. These units were later tectonically juxtaposed.

ACKNOWLEDGEMENTS

We thank E. Gnos, A. Berger, T. Ludwig and H.-P. Meyer for analytical support, and A. Dijkstra, O. Müntener and G. Suhr for comments and discussions. We thank H. Marschall for the whole-rock analyses carried out at the University of Bristol. This work was financially supported by grants of the Swiss National Science Foundation (200020-112149) to A.K. We acknowledge financial support by the Swiss NSF grant 200021-103479/1 and by the Canton of Bern for the electron microprobe at the Institute of Geological Sciences, University of Bern. We also acknowledge the financial support in Hungary (GVOP-3.2.1-2004-04-0268/3.0 and NAP VENEUS05 Contract No. OMFB 00184/2006). We thank S. Arai, M. Barth and H. Marschall for constructive reviews and R. Gieré for editorial handling.

REFERENCES

Agranier, A., Lee, C.-T. A., Li, Z.-X. A. & Leeman, W. P. (2007). Fluid mobile element budgets in serpentinized oceanic lithospheric mantle: Insights from B, As, Li, Pb, PGEs and Os isotopes in the Feather River Ophiolite, California. *Chemical Geology* doi:10.1016/j.chemgeo.2007.08.008.

Agrinier, P., Mével, C., Bosch, D. & Javoy, M. (1993). Metasomatic hydrous fluids in amphibole peridotites from Zabargad Island (Red Sea). *Earth and Planetary Science Letters* **120**, 187–205.

Allan, J. F. & Dick, H. J. B. (1996). Cr-rich spinel as a tracer for melt migration and melt–wall rock interaction in the mantle: Hess Deep, leg 147. In: Gillis, M. C., Allan, K. M. & Meyer, P. S. (eds) *Proceedings of the Ocean Drilling Program, Scientific Results, 147.* College Station, TX: Ocean Drilling Program, pp. 157–172.

Allen, D. E. & Seyfried, W. E. J. (2003). Compositional controls on vent fluids from ultramafic-hosted hydrothermal systems at mid-ocean ridges: An experimental study at 400°C, 500 bars. *Geochimica et Cosmochimica Acta* **67**, 1531–1542.

Anderson, D. L. & Kasztovszky, (2004). Application of PGAA with neutron beam. In: Molnár, G. L. (ed.) *Handbook of Prompt Gamma Activation Analysis with Neutron Beams*. Berlin: Springer, pp. 148–152.

Arai, S. (1994). Characterization of spinel peridotites by olivine spinel compositional relationships—Review and interpretation. *Chemical Geology* **113**, 191–204.

Arai, S. (1997*a*). Control of wall-rock composition on the formation of podiform chromitites as a result of magma/peridotite interaction. *Resource Geology* **47**, 177–187.

Arai, S. (1997*b*). Origin of podiform chromitites. *Journal of Asian Earth Sciences* **15**, 303–310.

Arai, S. & Matsukage, K. (1996). Petrology of the gabbro–troctolite–peridotite complex from Hess Deep, Equatorial Pacific: Implications for mantle–melt interaction within the oceanic lithosphere. In: Gillis, M. C., Allan, K. M. & Meyer, P. S. (eds) *Proceedings of the Ocean Drilling Program, Scientific Results, 147.* College Station, TX: Ocean Drilling Program, pp. 135–155.

Arai, S. & Matsukage, K. (1998). Petrology of a chromitite micropod from Hess Deep, equatorial Pacific: a comparison between abyssal and alpine-type podiform chromitites. *Lithos* **43**, 1–14.

Arai, S. & Takemoto, Y. (2007). Mantle wehrlite from Hess Deep as a crystal cumulate from an ultra-depleted primary melt in East Pacific Rise. *Geophysical Research Letters* **34**, L08302, doi:10.10292006GL029198.

Arai, S. & Yurimoto, H. (1994). Podiform chromitites of the Tari-Misaka ultramafic complex, southwestern Japan, as mantle–melt interaction products. *Economic Geology* **89**, 1279–1288.

Aubouin, J. (1959). Contribution à l'étude géologique de la Grèce Septentrionale. *Annales Géologiques des Pays Helléniques* **10**, 1–483.

Ayers, J. (1998). Trace element modeling of aqueous fluid–peridotite interaction in the mantle wedge of subduction zones. *Contributions to Mineralogy and Petrology* **132**, 390–404.

Bach, W., Garrido, C. J., Paulick, H., Harvey, J. & Rosner, M. (2004). Seawater–peridotite interactions: First insights from ODP Leg 209, MAR 15°N. *Geochemistry, Geophysics, Geosystems* **5**, 2004GC000744.

Bach, W., Paulick, H., Garrido, C. J., Ildefonse, B., Meurer, W. P. & Humphris, S. E. (2006). Unraveling the sequence of serpentinization reactions: petrography, mineral chemistry, and petrophysics of serpentinites from MAR 15°N (ODP Leg 209, Site 1274). *Geophysical Research Letters* **33**, doi:10.1029/2006GL025681.

Barth, M. G., Mason, P. R. D., Davies, G. R., Dijkstra, A. H. & Drury, M. R. (2003). Geochemistry of the Othris Ophiolite, Greece: Evidence for refertilization? *Journal of Petrology* **44**, 1759–1785.

Barth, M. G., Mason, P. R. D., Davies, G. R. & Drury, M. R. (2008). The Othris ophiolite, Greece: A snapshot of subduction initiation at a mid-ocean ridge. *Lithos* **100**, 234–254.

Bebout, G. E., Ryan, J. G. & Leeman, W. P. (1993). B–Be systematics in subduction-related metamorphic rocks: Characterization of the subducted component. *Geochimica et Cosmochimica Acta* **57**, 2227–2237.

Bebout, G. E., Ryan, J. G., Leeman, W. P. & Bebout, A. E. (1999). Fractionation of trace elements by subduction-zone metamorphism—effect of convergent-margin thermal evolution. *Earth and Planetary Science Letters* **171**, 63–81.

Beccaluva, L., Ohnenstetter, D., Ohnenstetter, M. & Paupy, A. (1984). Two magmatic series with island arc affinities within the Vourinos ophiolite. *Contributions to Mineralogy and Petrology* **85**, 253–271.

Beccaluva, L., Coltorti, M., Giunta, G. & Siena, F. (2004). Tethyan vs Cordilleran ophiolites: a reappraisal of distinctive tectono-magmatic features of supra-subduction complexes in relation to the subduction mode. *Tectonophysics* **393**, 163–174.

Beccaluva, L., Coltorti, M., Saccani, E. & Siena, F. (2005). Magma generation and crustal accretion as evidenced by supra-subduction ophiolites of the Albanide–Hellenide Subpelagonian zone. *Island Arc* **14**, 551–563.

Benoît, M., Ceuleneer, G. & Polve, M. (1999). The remelting of hydrothermally altered peridotite at mid-ocean ridges by intruding mantle diapirs. *Nature* **402**, 514–518.

Benton, L. D., Ryan, J. G. & Tera, F. (2001). Boron isotope systematics of slab fluids as inferred from a serpentine seamount, Mariana forearc. *Earth and Planetary Science Letters* **187**, 273–282.

Benton, L. D., Ryan, J. G. & Savov, I. P. (2004). Lithium abundance and isotope systematics of forearc serpentinites, Conical Seamount, Mariana forearc: Insights into the mechanics of slab–mantle exchange during subduction. *Geochemistry, Geophysics, Geosystems* **5**, 2004GC000708.

Bizimis, M., Salters, V. J. M. & Bonatti, E. (2000). Trace and REE content of clinopyroxenes from supra-subduction zone peridotites. Implications for melting and enrichment processes in island arcs. *Chemical Geology* **165**, 67–85.

Bloomer, S. H., Natland, J. H. & Fischer, R. L. (1989). Mineral relationships in gabbroic rocks from fracture zones of Indian Ocean ridges: evidence for extensive fractionation, parental diversity, and boundary-layer recrystallization. In: Saunders, A. D. & Norry, M. J. (eds) *Magmatism in the Ocean Basins. Geological Societ,f London, Special Publications* **42**, 107–124.

Bodinier, J.-L. & Godard, M. (2004). Orogenic, ophiolitic, and abyssal peridotites. In: Carlson, R. W., Holland, H. D. & Turekian, K. K. (eds) *Treatise on Geochemistry, Volume 2: The Mantle and Core.* Oxford: Elsevier, pp. 103–170.

Bonatti, E., Lawrence, J. R. & Morandi, N. (1984). Serpentinization of oceanic peridotites: temperature dependence of mineralogy and boron content. *Earth and Planetary Science Letters* **70**, 88–94.

Boschi, C., Dini, A., Früh-Green, G. L. & Kelley, D. S. (2008). Isotopic and element exchange during serpentinization and metasomatism at the Atlantis Massif (MAR 30°N): Insights from B and Sr isotope data. *Geochimica et Cosmochimica Acta* doi:10.1016/j.gca.2008.01.013.

Boudier, F., Ceuleneer, G. & Nicolas, A. (1988). Shear zones, thrusts and related magmatism in the Oman ophiolite—initiation of thrusting on an oceanic ridge. *Tectonophysics* **151**, 275–296.

Brenan, J. M., Neroda, E., Lundstrom, C. C., Shaw, H. F., Ryerson, F. J. & Phinney, D. L. (1998*a*). Behaviour of boron, beryllium, and lithium during melting and crystallization: Constraints from mineral–melt partitioning experiments. *Geochimica et Cosmochimica Acta* **62**, 2129–2141.

Brenan, J. M., Ryerson, F. J. & Shaw, H. F. (1998*b*). The role of aqueous fluids in the slab-to-mantle transfer of boron, beryllium, and lithium during subduction: Experiments and models. *Geochimica et Cosmochimica Acta* **62**, 3337–3347.

Brooker, R. A., James, R. H. & Blundy, J. D. (2004). Trace elements and Li isotope systematics in Zabargad peridotites: evidence of ancient subduction processes in the Red Sea mantle. *Chemical Geology* **212**, 179–204.

Capedri, S., Venturelli, G., Bocchi, G., Dostal, J., Garuti, G. & Rossi, A. (1980). The geochemistry and petrogenesis of an ophiolitic sequence from Pindos, Greece. *Contributions to Mineralogy and Petrology* **74**, 189–200.

Capedri, S., Venturelli, G. & Toscani, L. (1982). Petrology of an ophiolitic cumulate sequence from Pindos, Greece. *Geological Journal* **17**, 223–242.

Chan, L.-H. & Kastner, M. (2000). Lithium isotopic compositions of pore fluids and sediments in the Costa Rica subduction zone: implications for fluid processes and sediment contribution to the arc volcanoes. *Earth and Planetary Science Letters* **183**, 275–290.

Chan, L. H., Leeman, W. P. & You, C. F. (1999). Lithium isotopic composition of Central American Volcanic Arc lavas: implications for modification of subarc mantle by slab-derived fluids. *Chemical Geology* **160**, 255–280.

Chan, L.-H., Leeman, W. P. & You, C.-F. (2002). Lithium isotopic composition of Central American volcanic arc lavas: implications for modification of subarc mantle by slab-derived fluids: correction. *Chemical Geology* **182**, 293–300.

Chaussidon, M. & Jambon, A. (1994). Boron content and isotopic composition of oceanic basalts: Geochemical and cosmochemical implications. *Earth and Planetary Science Letters* **121**, 277–291.

Chaussidon, M. & Libourel, G. (1993). Boron partitioning in the upper mantle: An experimental and ion probe study. *Geochimica et Cosmochimica Acta* **57**, 5053–5062.

Chaussidon, M. & Marty, B. (1995). Primitive boron isotope composition of the mantle. *Science* **269**, 383–386.

Churikova, T., Wörner, G., Mironov, N. & Kronz, A. (2007). Volatile (S, Cl and F) and fluid mobile trace element compositions in melt inclusions: implications for variable fluid sources across the Kamchatka arc. *Contributions to Mineralogy and Petrology* **154**, 217–239.

Coogan, L. A., Kasemann, S. & Chakraborty, S. (2005). Rates of hydrothermal cooling of new oceanic upper crust derived from lithium-geospeedometry. *Earth and Planetary Science Letters* **240**, 415–424.

Crawford, A. J., Falloon, T. J. & Green, D. H. (1989). Classification, petrogenesis and tectonic setting of boninites. In: Crawford, A. J. (ed.) *Boninites and Related Rocks*. London: Unwin Hyman, pp. 1–49.

Currie, L. A. (1968). Limits for qualitative detection and quantitative determination. *Analytical Chemistry* **40**, 586–593.

D'Antonio, M. & Kristensen, M. B. (2005). Hydrothermal alteration of oceanic crust in the West Philippine Sea Basin (Ocean Drilling Program Leg 195, Site 1201): inferences from a mineral chemistry investigation. *Mineralogy and Petrology* **83**, 87–112.

Davies, J. H. & Stevenson, D. J. (1992). Physical model of source region of subduction zone volcanics. *Journal of Geophysical Research—Solid Earth* **97**, 2037–2070.

Decitre, S., Deloule, E., Reisberg, L., James, R., Agrinier, P. & Mével, C. (2002). Behavior of Li and its isotopes during serpentinization of oceanic peridotites. *Geochemistry, Geophysics, Geosystems* **3**, 2001GC000178.

Dercourt, J., Zonenshain, L. P., Ricou, L. E., *et al*. (1986). Geological evolution of the Tethys belt from the Atlantic to the Pamirs since the Lias. *Tectonophysics* **123**, 241–315.

Dercourt, J., Ricou, L. F. & Vrielynck, B. (1993). *Atlas of Tethys Palaeoenvironmental Maps*. Paris: Gauthier-Villars.

Dick, H. J. B. (1989). Abyssal peridotites, very slow spreading ridges and ocean ridge magmatism. In: Saunders, A. D. & Norry, M. J. (eds) *Magmatism in the Ocean Basins. Geological Society, London, Special Publications* **42**, 107–124.

Dick, H. J. B. & Bullen, T. (1984). Chromian spinel as a petrogenetic indicator in abyssal and alpine-type peridotites and spatially associated lavas. *Contributions to Mineralogy and Petrology* **86**, 54–76.

Dick, H. J. B. & Natland, J. H. (1996). Late stage melt evolution and transport in the shallow mantle beneath the East Pacific Rise. In: Gillis, M. C., Allan, K. M. & Meyer, P. S. (eds) *Proceedings of the Ocean Drilling Program, Scientific Results, 147*. College Station, TX: Ocean Drilling Program, pp. 103–134.

Dick, H. J. B., Fisher, R. L. & Bryan, W. B. (1984). Mineralogical variability of the uppermost mantle along mid-ocean ridges. *Earth and Planetary Science Letters* **69**, 88–106.

Dijkstra, A. H. & Cawood, P. A. (2004). Base-up growth of ocean crust by multiple phases of magmatism: field evidence from Macquarie Island. *Journal of the Geological Society, London* **161**, 739–742.

Dijkstra, A. H., Drury, M. R. & Vissers, R. L. M. (2001). Structural petrology of plagioclase peridotites in the West Othris Mountains (Greece): melt impregnation in mantle lithosphere. *Journal of Petrology* **42**, 5–24.

Dijkstra, A. H., Barth, M. G., Drury, M. R., Mason, P. R. D. & Vissers, R. L. M. (2003). Diffuse porous melt flow and melt–rock reaction in the mantle lithosphere at a slow-spreading ridge: A structural petrology and LA-ICP-MS study of the Othris Peridotite Massif (Greece). *Geochemistry, Geophysics, Geosystems* **4**, 2001GC000278.

Dilek, Y. & Flower, M. F. J. (2003). Arc–trench rollback and forearc accretion: 2. A model template for ophiolites in Albania, Cyprus, and Oman. In: Dilek, Y. & Robinson, P. T. (eds) *Ophiolites in Earth History. Geological Society, London, Special Publications* **218**, 43–68.

Domanik, K. J., Hervig, R. L. & Peacock, S. M. (1993). Beryllium and boron in subduction zone minerals: an ion microprobe study. *Geochimica et Cosmochimica Acta* **57**, 4997–5010.

Douville, E., Charlou, J. L., Oelkers, E. H., Bianvenu, P., Jove Colon, C. F., Donval, J. P., Fouquet, Y., Prieur, D. & Appriou, P. (2002). The Rainbow vent fluids (36°14′N, MAR): The influence of ultramafic rocks and phase separation on trace metal contents on Mid-Atlantic ridge hydrothermal fluids. *Chemical Geology* **184**, 37–48.

Economou-Eliopoulos, M. & Vacondios, I. (1995). Geochemistry of chromitites and host rocks from the Pindos ophiolite complex, northwestern Greece. *Chemical Geology* **122**, 99–108.

Edwards, S. J., Pearce, J. A. & Freeman, J. (2000). New insights concerning the influence of water during the formation of podiform chromitite. In: Dilek, Y., Moores, E. M., Elthon, D. & Nicolas, A. (eds) *Ophiolites and Oceanic Crust: New Insights from Field Studies and Ocean Drilling Program. Geological Society of America, Special Papers* **349**, 139–147.

Eggins, S. M., Rudnick, R. L. & McDonough, W. F. (1998). The composition of peridotites and their minerals: a laser-ablation ICP-MS study. *Earth and Planetary Science Letters* **154**, 53–71.

Filippidis, A. (1982). Experimental study of the serpentinization of Mg–Fe–Ni olivine in the presence of sulfur. *Canadian Mineralogist* **20**, 567–574.

Flower, M. F. J. & Dilek, Y. (2003). Arc–trench rollback and forearc accretion: 1. A collision-induced mantle flow model for Tethyan ophiolites. In: Dilek, Y. & Robinson, P. T. (eds) *Ophiolites in Earth History. Geological Society, London, Special Publications* **218**, 21–41.

Frost, B. R. & Beard, J. S. (2007). On silica activity and serpentinization. *Journal of Petrology* **48**, 1351–1368.

Gaetani, G. A., Grove, G. L. & Bryan, W. B. (1994). Experimental phase relations of basaltic andesite from Hole 839B under hydrous and anhydrous conditions. In: Hawkins, J., Parson, L. & Allan, J. (eds) *Proceedings of the Ocean Drilling Program, Scientific Results, 135*. College Station, TX: Ocean Drilling Program, pp. 557–563.

Girardeau, J. & Francheteau, J. (1993). Plagioclase-wehrlites and peridotites on the East Pacific Rise (Hess Deep) and the Mid-Atlantic Ridge (DSDP Site 334): evidence for magma percolation in the oceanic upper mantle. *Earth and Planetary Science Letters* **115**, 137–149.

Gméling, K., Harangi, Sz. & Kasztovszky, Zs. (2005). Boron and chlorine concentration of volcanic rocks: an application of prompt gamma activation analysis. *Journal of Radioanalytical and Nuclear Chemistry* **265**, 201–212.

Govindaraju, K. (1994). 1994 compilation of working values and sample description for 383 geostandards. *Geostandards Newsletter* **18**, 1–158.

Grégoire, M., McInnes, B. I. A. & O'Reilly, S. Y. (2001). Hydrous metasomatism of oceanic sub-arc mantle, Lihir, Papua New Guinea, Part 2. Trace element characteristics of slab-derived fluids. *Lithos* **59**, 91–108.

Groppo, C., Rinaudo, C., Cairo, S., Gastaldi, D. & Compagnoni, R. (2006). Micro-Raman spectroscopy for a quick and reliable identification of serpentine minerals from ultramafics. *European Journal of Mineralogy* **18**, 319–329.

Haase, K. M., Stroncik, N. A., Hekinian, R. & Stoffers, P. (2005). Nb-depleted andesites from the Pacific–Antarctic Rise as analogs for early continental crust. *Geology* **33**, 921–924.

Hawkins, J. W. (2003). Geology of supra-subduction zones—Implications for the origin of ophiolites. *Geological Society of America, Special Papers* **373**, Ophiolite concept and the evolution of geological thought. 227–268.

Hellebrand, E., Snow, J. E. & Mühe, R. (2002). Mantle melting beneath Gakkel Ridge (Arctic Ocean): abyssal peridotite spinel compositions. *Chemical Geology* **182**, 227–235.

Hoogerduijn Strating, E. H., Rampone, E., Piccardo, G. B., Drury, M. R. & Vissers, R. L. M. (1993). Subsolidus emplacement of mantle peridotites during incipient oceanic rifting and opening of the Mesozoic Tethys (Voltri Massif, NW Italy). *Journal of Petrology* **34**, 901–927.

Ishikawa, T. & Nakamura, E. (1994). Origin of the slab component in arc lavas from across-arc variation of B and Pb isotopes. *Nature* **370**, 205–208.

Jacobshagen, V. (1986). *Geologie von Griechenland.* Berlin: Borntraeger.

Jeffcoate, A. B., Elliott, T., Kasemann, S. A., Ionov, D., Cooper, K. & Brooker, R. (2007). Li isotope fractionation in peridotites and mafic melts. *Geochimica et Cosmochimica Acta* **71**, 202–218.

Johnson, M. C. & Planck, T. (1999). Dehydration and melting experiments constrain the fate of subducted sediments. *Geochemistry, Geophysics, Geosystems* **1**, 1999GC000014.

Jones, G. & Robertson, A. H. F. (1991). Tectono-stratigraphy and evolution of the Mesozoic Pindos ophiolite and related units, northwestern Greece. *Journal of the Geological Society, London* **148**, 267–288.

Jones, G., Robertson, A. H. F. & Cann, J. R. (1991). Genesis and Emplacement of the suprasubduction zone Pindos Ophiolite, northwertern Greece. In: Peters, T., Nicolas, A. & Coleman, S. (eds) *Ophiolite Genesis and Evolution of the Oceanic Lithosphere.* Sultanate of Oman: Ministry of Petroleum and Minerals, pp. 771–799.

Kaeser, B., Kalt, A. & Ludwig, T. (2007). Li, Be and B abundances in minerals of peridotite xenoliths from Marsabit (Kenya): disequilibrium processes and implications for subduction zone signatures. *Geochemistry, Geophysics, Geosystems* doi:10.1029/2006GC001555.

Kaliwoda, M. (2004). Mantel-Xenolithe des Harrat Uwayrid (Saudi-Arabien): Archive der stofflichen une thermischen Entwicklung des lithosphärischen Erdmantels im Bereich eines passiven Kontinentalrandes. PhD thesis. Ruprecht-Karls-Universität, Heidelberg, 365 pp.

Kelemen, P. B., Kikawa, E., Miller, D. J. *et al.* (2004). Leg 209 Preliminary Report. Drilling Mantle Peridotite along the Mid-Atlantic Ridge from 14° to 16°N. In: Peters, L. L. (ed.) *Proceedings of the Ocean Drilling Program, Part A: Initial Reports, 209.* College Station, TX: Ocean Drilling Program, pp. 1–160.

Klein, E. M. & Karsten, J. L. (1995). Ocean-ridge basalts with convergent-margin geochemical affinities from the Chile Ridge. *Nature* **374**, 52–57.

Kostopoulos, D. (1988). Geochemistry and tectonic setting of the Pindos ophiolite, northwestern Greece. PhD thesis. University of Newcastle upon Tyne, 498 pp.

Kretz, R. (1983). Symbols for rock-forming minerals. *American Mineralogist* **68**, 277–279.

Leeman, W. P. (1996). Boron and other fluid-mobile elements in volcanic arc lavas: implications for subduction processes. In: Bebout, G. E., Scholl, D., Kirby, S. & Platt, J. P. (eds) *Subduction Y Top to Bottom. Geophysical Monograph, American Geophysical Union* **96**, 269–276.

Leeman, W. P., Tonarini, S., Chan, L.-H. & Borg, L. E. (2004). Boron and lithium isotopic variations in a hot subduction zone—the southern Washington Cascades. *Chemical Geology* **212**, 101–124.

Li, Y.-H. (1982). A brief discussion on the mean oceanic residence time of elements. *Geochimica et Cosmochimica Acta* **46**, 2671–2675.

Li, Z.-X. A. & Lee, C.-T. A. (2006). Geochemical investigation of serpentinized oceanic lithospheric mantle in the Feather River Ophiolite, California: Implications for the recycling rate of water by subduction. *Chemical Geology* **235**, 161–185.

Liati, A., Gebauer, D. & Fanning, C. M. (2004). The age of ophiolitic rocks of the Hellenides (Vourinos, Pindos, Crete): first U–Pb ion microprobe (SHRIMP) zircon ages. *Chemical Geology* **207**, 171–188.

Lykins, R. W. & Jenkins, D. M. (1992). Experimental determination of pargasite stability relations in the presence of orthopyroxene. *Contributions to Mineralogy and Petrology* **112**, 405–413.

Lyubetskaya, T. & Korenaga, J. (2007). Chemical composition of Earth's primitive mantle and its variance: 1. Method and results. *Journal of Geophysical Research* **112**, 1–21.

Makris, J. (1977). Geophysical investigations of the Hellenides. *Hamburger Geophysikalische Einzelschriften* **34**, 1–124.

Marchesi, C., Garrido, C. J., Godard, M., Proenza, J. A., Gervilla, F. & Blanco-Moreno, J. (2006). Petrogenesis of highly depleted peridotites and gabbroic rocks from the Mayari–Baracoa Ophiolitic Belt (eastern Cuba). *Contributions to Mineralogy and Petrology* **151**, 717–736.

Marschall, H. R. & Ludwig, T. (2004). The low-boron contest: minimising surface contamination and analysing boron concentrations at the ng/g-level by secondary ion mass spectrometry. *Mineralogy and Petrology* **81**, 265–278.

Marschall, H. R., Kasztovszky, Z., Gméling, K. & Altherr, R. (2005). Chemical analysis of high-pressure metamorphic rocks by PGNAA: Comparison with results from XRF and solution ICP-MS. *Journal of Radioanalytical and Nuclear Chemistry* **265**, 339–348.

Marschall, H. R., Altherr, R. & Rüpke, L. (2007). Squeezing out the slab—modelling the release of Li, Be and B during progressive high-pressure metamorphism. *Chemical Geology* **239**, 323–335.

McDonough, W. F. & Sun, S.-S. (1995). The composition of the Earth. *Chemical Geology* **120**, 223–253.

McInnes, B. I. A., Grégoire, M., Binns, R. A., Herzig, P. M. & Hannington, M. D. (2001). Hydrous metasomatism of oceanic sub-arc mantle, Lihir, Papua New Guinea: petrology and geochemistry of fluid-metasomatised mantle wedge xenoliths. *Earth and Planetary Science Letters* **188**, 169–183.

Measures, C. I. & Edmond, J. M. (1982). Beryllium in the water column of the Central North Pacific. *Nature* **297**, 51–53.

Measures, C. I. & Edmond, J. M. (1983). The geochemical cycle of ^{9}Be: a reconnaissance. *Earth and Planetary Science Letters* **66**, 101–110.

Mercier, J. C. C. & Nicolas, A. (1975). Textures and fabrics of upper-mantle peridotites as illustrated by xenoliths from basalts. *Journal of the Geological Society, London* **148**, 267–288.

Metcalf, R. V., Wallin, E. T., Willse, K. R. & Muller, E. R. (2000). Geology and geochemistry of the ophiolitic Trinity terrane, California: Evidence of middle Paleozoic depleted supra-subduction zone magmatism in a proto-arc setting. In: Dilek, Y., Moores, E. M., Elthon, D. & Nicolas, A. (eds) *Ophiolites and Oceanic Crust: New Insights from Field Studies and the Ocean Drilling Program. Geological Society of America, Special Papers* **349**, 403–418.

Mével, C. (2003). Serpentinization of abyssal peridotites at mid-ocean ridges. *Comptes Rendus, Géoscience* **335**, 825–852.

Miyashiro, A. (1973). The Troodos ophiolitic complex was probably formed in an island arc. *Earth and Planetary Science Letters* **19**, 218–224.

Molnár, G. L. (ed.) (2004). *Handbook of Prompt Gamma Activation Analysis with Neutron Beams*. Berlin: Springer.

Moores, E. M., Kellogg, L. H. & Dilek, Y. (2000). Tethyan ophiolites, mantle convection, and tectonic 'historical contingency': A resolution of the 'ophiolite conundrum'. In: Dilek, Y., Moores, E. M., Elthon, D. & Nicolas, A. (eds) *Ophiolies and Oceanic Crust: New Insights from Field Studies and Ocean Drilling Program. Geological Society of America, Special Papers* **349**, 3–12.

Moran, A. E., Sisson, V. B. & Leeman, W. P. (1992). Boron depletion during progressive metamorphism: implications for subduction processes. *Earth and Planetary Science Letters* **111**, 331–349.

Moriguti, T. & Nakamura, E. (1998). Across-arc variation of Li isotopes in lavas and implications for crust/mantle recycling at subduction zones. *Earth and Planetary Science Letters* **163**, 167–174.

Moriguti, T., Makishima, A. & Nakamura, E. (2004). Determination of lithium contents in silicates by isotope dilution ICP-MS and its evaluation by isotope dilution thermal ionisation mass spectrometry. *Geostandards and Geoanalytical Research* **28**, 371–382.

Müntener, O. & Manatschal, G. (2006). High degrees of melt extraction recorded by spinel harzburgite of the Newfoundland margin: The role of inheritance and consequences for the evolution of the southern North Atlantic. *Earth and Planetary Science Letters* **252**, 437–452.

Murton, B. J. (1989). Tectonic controls on boninite genesis. In: Saunders, A. D. & Norry, M. J. (eds) *Magmatism in the Ocean Basins. Geological Society, London, Special Publications* **42**, 347–377.

Natland, J. H. (1989). Partial melting of a lithologically heterogeneous mantle: inferences from crystallization histories of magnesian abyssal tholeiites from the Siqueiros Fracture Zone. In: Saunders, A. D. & Norry, M. J. (eds) *Magmatism in the Ocean Basins. Geological Society, London, Special Publications* **42**, 41–70.

Natland, J. H. & Tarney, J. (1982). Petrologic evolution of the Mariana arc and back-arc basin system—A synthesis of drilling results in the South Philippine Sea. In: *Initial Reports of the Deep-Sea Drilling Project, 60*. Washington, DC: US Government Printing Office, pp. 877–908.

Niu, Y. (2004). Bulk-rock major and trace element compositions of abyssal peridotites: Implications for mantle melting, melt extraction and post-melting processes beneath mid-ocean ridges. *Journal of Petrology* **45**, 2423–2458.

Noakes, J. E. & Hood, D. W. (1961). Boron–boric acid complexes in sea-water. *Deep-Sea Research* **8**, 121–129.

Noiret, G., Montigny, R. & Allègre, C. J. (1981). Is the Vourinos Complex an island arc ophiolite? *Earth and Planetary Science Letters* **56**, 375–386.

Nonnotte, P., Ceuleneer, G. & Benoît, M. (2005). Genesis of andesitic–boninitic magmas at mid-ocean ridges by melting of hydrated peridotites: Geochemical evidence from DSDP Site 334 gabbronorites. *Earth and Planetary Science Letters* **236**, 632–653.

O'Hanley, D. S. (1996). *Serpentinites: Record of Tectonic and Petrological History*. Oxford: Oxford University Press.

Ohara, Y., Stern, R. J., Ishii, T., Yurimoto, H. & Yamazaki, T. (2002). Peridotites from the Mariana Trough: first look at the mantle beneath an active back-arc basin. *Contributions to Mineralogy and Petrology* **143**, 1–18.

Ottolini, L., Bottazzi, P. & Vannucci, R. (1993). Quantification of lithium, beryllium, and boron in silicates by secondary ion mass spectrometry using conventional energy filtering. *Analytical Chemistry* **65**, 1960–1968.

Ottolini, L., Le Fèvre, B. & Vannucci, R. (2004). Direct assessment of mantle boron and lithium contents and distribution by SIMS analyses of peridotite minerals. *Earth and Planetary Science Letters* **228**, 19–36.

Paquin, J., Altherr, R. & Ludwig, T. (2004). Li–Be–B systematics in the ultrahigh-pressure garnet peridotite from Alpe Arami (Central Swiss Alps): implications for slab-to-mantle wedge transfer. *Earth and Planetary Science Letters* **218**, 507–519.

Parkinson, I. J. & Pearce, J. A. (1998). Peridotites from the Izu–Bonin–Mariana forearc (ODP Leg 125): Evidence for mantle melting and melt–mantle interaction in a supra-subduction zone setting. *Journal of Petrology* **39**, 1577–1618.

Paulick, H., Bach, W., Godard, M., De Hoog, J. C. M., Suhr, G. & Harvey, J. (2006). Geochemistry of abyssal peridotites (Mid-Atlantic Ridge, 15°20′N, ODP Leg 209): Implications for fluid/rock interactions in slow spreading environments. *Chemical Geology* **234**, 179–210.

Peacock, S. M. & Hervig, R. L. (1999). Boron isotopic composition of subduction-zone metamorphic rocks. *Chemical Geology* **160**, 281–290.

Pearce, J. A. (2003). Supra-subduction zone ophiolites: The search for modern analogues. In: *Geological Society of America, Special Papers* **373**, 269–293.

Pearce, J. A., Lippard, S. J. & Roberts, S. (1984). Characteristics and tectonic significance of supra-subduction zone ophiolites. In: Kokelaar, B. P. & Howells, M. F. (eds) *Marginal Basin Geology. Geological Society, London, Special Publications* **16**, 77–89.

Pearce, J. A., Barker, P. F., Edwards, S. J., Parkinson, I. J. & Leat, P. T. (2000). Geochemistry and tectonic significance of peridotites from the South Sandwich arc–basin system, South Atlantic. *Contributions to Mineralogy and Petrology* **139**, 36–53.

Pe-Piper, G. & Piper, D. J. W. (2002). *The Igneous Rocks of Greece. The Anatomy of an Orogen*. Berlin: Borntraeger.

Pe-Piper, G., Tsikouras, B. & Hatzipanagiotou, K. (2004). Evolution of boninites and island-arc tholeiites in the Pindos Ophiolite, Greece. *Geological Magazine* **141**, 455–469.

Piccardo, G. B., Müntener, O. & Zanetti, A. (2004*a*). Alpine–Apennine ophiolitic peridotites: new concepts on their composition and evolution. *Ofioliti* **29**, 63–74.

Piccardo, G. B., Müntener, O., Zanetti, A., Romairone, A., Bruzzone, S., Poggi, E. & Spagnolo, G. (2004*b*). The Lanzo South peridotite: melt/peridotite interaction in the mantle lithosphere of the Jurassic Ligurian Tethys. *Ofioliti* **29**, 37–62.

Plank, T. & Langmuir, C. H. (1993). Tracing trace elements from sediment input to volcanic output at subduction zones. *Nature* **362**, 739–743.

Portnyagin, M., Hoernle, K., Plechov, P., Mironov, N. & Khubunaya, S. (2007). Constraints on mantle melting and composition and nature of slab components in volcanic arcs from volatiles (H_2O, S, Cl, F) and trace elements in melt inclusions from the Kamchatka Arc. *Earth and Planetary Science Letters* **255**, 53–69.

Rampone, E., Piccardo, G. B., Vannucci, R. & Bottazzi, P. (1997). Chemistry and origin of trapped melts in ophiolitic peridotites. *Geochimica et Cosmochimica Acta* **61**, 4557–4569.

Rassios, A. (1991). Internal structure and pseudostratigraphy of the Dramala peridotite massif Pindos Mountains, Greece. *Bulletin of the Geological Society of Greece* **25**, 293–305.

Rassios, A. H. E. & Moores, E. M. (2006). Heterogeneous mantle complex, crustal processes, and obduction kinematics in a unified Pindos–Vourinos ophiolitic slab (northern Greece). In: Robertson, A. H. F. & Mountrakis, D. (eds). *Tectonic Development of the Eastern Mediterranean Region. Geological Society, London, Special Publications* **260**, 237–266.

Rassios, A., Grivas, E., Konstantopoulou, G. & Vakondios, I. (1994). The geometry and structures forming around the ductile–brittle transition in the Vourinos–Pindos–Othrys oceanic slab. *Bulletin of the Geological Society of Greece* **30**, 109–121.

Révay, Zs. & Belgya, T. (2004). Principles of PGAA method. In: Molnár, G. L. (ed.) *Handbook of Prompt Gamma Activation Analysis with Neutron Beams*. Berlin: Springer, pp. 1–30.

Révay, Zs., Belgya, T., Kasztovszky, Zs., Weil, J. L. & Molnár, G. L. (2004). Cold neutron PGAA facility at Budapest. *Nuclear Instruments and Methods in Physics Research, Section B* **213**, 385–388.

Robertson, A. H. F. (2002). Overview of the genesis and emplacement of Mesozoic ophiolites in the Eastern Mediterranean Tethyan region. *Lithos* **65**, 1–67.

Robertson, A. & Shallo, M. (2000). Mesozoic–Tertiary tectonic evolution of Albania in its regional Eastern Mediterranean context. *Tectonophysics* **316**, 197–254.

Robertson, A. H. F., Clift, P. D., Degnan, P. & Jones, G. (1991). Paleoceanography of the Eastern Mediterranean Neotethys. *Palaeogeography, Palaeoclimatology, Palaeoecology* **87**, 289–343.

Roddick, J. C., Cameron, W. E. & Smith, A. G. (1979). Permo-Triassic and Jurassic ^{40}Ar–^{39}Ar ages from Greek ophiolites and associated rocks. *Nature* **279**, 788–790.

Rose, E. F., Shimizu, N., Layne, G. D. & Grove, T. L. (2001). Melt production beneath Mt. Shasta from boron data in primitive melt inclusions. *Science* **293**, 281–283.

Rosner, M., Erzinger, J., Franz, G. & Trumbull, R. B. (2003). Slab-derived boron isotope signatures in arc volcanic rocks from the Central Andes and evidence for boron isotope fractionation during progressive slab dehydration. *Geochemistry, Geophysics, Geosystems* **4**, 2002GC000438.

Ross, K. & Elthon, D. (1993). Cumulates from strongly depleted mid-ocean ridge basalt. *Nature* **365**, 826–829.

Ross, J. V. & Zimmerman, J. (1996). Comparison of evolution and tectonic significance of the Pindos and Vourinos ophiolite suites, northern Greece. *Tectonophysics* **256**, 1–15.

Rüpke, L. H., Morgan, J. P., Hort, M. & Connolly, J. A. D. (2002). Are the regional variations in Central American arc lavas due to differing basalt versus peridotitic slab sources of fluids? *Geology* **30**, 1035–1038.

Ryan, J. G. (2002). Trace-element systematics of beryllium in terrestrial materials. In: Grew, E. S. (ed.). *Beryllium—Mineralogy, Petrology and Geochemistry. Mineralogical Society of America, Reviews in Mineralogy and Geochemistry* **50**, 121–145.

Saccani, E. & Photiades, A. (2004). Mid-ocean ridge and supra-subduction affinities in the Pindos ophiolites (Greece): implications for magma genesis in forearc setting. *Lithos* **73**, 229–253.

Salters, V. J. M. & Stracke, A. (2004). Composition of the depleted mantle. *Geochemistry, Geophysics, Geosystems* **5**, 2003GC000597.

Savov, I. P., Ryan, J. G., D'Antonio, M., Kelly, K. & Mattie, P. (2005). Geochemistry of serpentinized peridotites from the Mariana Forearc Conical Seamount, ODP Leg 125: Implications for the elemental recycling at subduction zones. *Geochemistry, Geophysics, Geosystems* **6**, 2004GC000777.

Scambelluri, M. & Philippot, P. (2004). Volatile and mobile element recycling during subduction of the oceanic lithosphere. Insights from metasediments and serpentinites of the Alps. *Periodico di Mineralogia* **73**, 221–233.

Scambelluri, M., Müntener, O., Ottolini, L., Pettke, T. T. & Vannucci, R. (2004). The fate of B, Cl and Li in the subducted oceanic mantle and in the antigorite breakdown fluids. *Earth and Planetary Science Letters* **222**, 217–234.

Scambelluri, M., Hermann, J., Morten, L. & Rampone, E. (2006). Melt- versus fluid-induced metasomatism in spinel to garnet wedge peridotites (Ulten Zone, Eastern Italian Alps): clues from trace element and Li abundances. *Contributions to Mineralogy and Petrology* **151**, 372–394.

Schmidt, K., Koschinsky-Fritsche, A. & Garbe-Schönberg, D. (2006). Detailed geochemical investigation of hydrothermal fluids from Logatchev field, 15°N, MAR. *Geochimica et Cosmochimica Acta Supplement* **70**, A563.

Searle, M. & Cox, J. (1999). Tectonic setting, origin, and obduction of the Oman ophiolite. *Geological Society of America Bulletin* **111**, 104–122.

Seitz, H.-M. & Woodland, A. B. (2000). The distribution of lithium in peridotitic and pyroxenitic mantle lithologies—an indicator of magmatic and metasomatic processes. *Chemical Geology* **166**, 47–64.

Seitz, M. G. & Hart, S. R. (1973). Uranium and boron distributions in some oceanic ultramafic rocks. *Earth and Planetary Science Letters* **21**, 97–107.

Seyfried, W. E., Jr, & Dibble, W. E., Jr, (1980). Seawater–peridotite interaction at 300°C and 500 bars: implications for the origin of oceanic serpentinites. *Geochimica et Cosmochimica Acta* **44**, 309–321.

Seyfried, W. E., Jr, Janecky, D. R. & Mottl, M. J. (1984). Alteration of the oceanic crust: Implications for geochemical cycles of lithium and boron. *Geochimica et Cosmochimica Acta* **48**, 557–569.

Seyler, M., Toplis, M. J., Lorand, J. P., Luguet, A. & Cannat, M. (2001). Clinopyroxene microtextures reveal incompletely extracted melts in abyssal peridotites. *Geology* **29**, 155–158.

Seyler, M., Lorand, J. P., Dick, H. J. B. & Drouin, M. (2007). Pervasive melt percolation reactions in ultra-depleted refractory harzburgites at the Mid-Atlantic Ridge, 15°20′N: ODP Hole 1274A. *Contributions to Mineralogy and Petrology* **153**, 303–319.

Sharma, A. & Jenkins, D. M. (1999). Hydrothermal synthesis of amphiboles along the tremolite–pargasite join and in the ternary system tremolite–pargasite–cummingtonite. *American Mineralogist* **84**, 1304–1318.

Smith, A. G. (1979). Othris, Pindos and Vourinos Ophiolites and the Pelagonian zone. *Proceedings of the Colloquium on Geology of the Aegean Region* **6**, 1369–1374.

Smith, A. G. & Woodcock, N. H. (1976). Emplacement model for some Tethyan ophiolites. *Geology* **4**, 635–656.

Smith, A. G., Spivack, A. J., Staudigel, H. & Hart, S. R. (1995). The boron isotopic composition of altered oceanic crust. *Chemical Geology* **126**, 119–135.

Sobolev, A. V. & Shimizu, N. (1993). Ultra-depleted primary melt included in an olivine from the Mid-Atlantic Ridge. *Nature* **363**, 151–154.

Sovatzoglou-Skounakis, E. & Economou-Eliopoulos, M. (1997). Fe–Cu–Ni–Co sulfide mineralizations from the Pindos and Veria ophiolite complexes, Greece. *Ofioliti* **22**, 227–230.

Spivack, A. J. & Edmond, J. M. (1987). Boron isotope exchange between seawater and the oceanic crust. *Geochimica et Cosmochimica Acta* **51**, 1033–1043.

Spray, J. G. & Roddick, J. C. (1980). Petrology and ^{40}Ar–^{39}Ar geochronology of some Hellenic sub-ophiolitic metamorphic rocks. *Contributions to Mineralogy and Petrology* **72**, 43–55.

Spray, J. G., Bebien, J., Rex, D. C. & Roddick, J. C. (1984). Age constraints on the igneous and metamorphic evolution of the Hellenic–Dinaric ophiolites. In: Dixon, J. E. & Robertson, A. H. F. (eds) *The Geological Evolution of the Eastern Mediterranean. Geological Society, London, Special Publications* **17**, 619–627.

Stampfli, G. & Borel, G. (2004). The TRANSMED Transects in space and time: constraints on the paleotectonic evolution of the Mediterranean domain. In: Cavazza, W., Roure, F. M. & Spakman, W. *et al.* (eds) *The TRANSMED Atlas—The Mediterranean Region from Crust to Mantle*. Berlin: Springer, pp. 53–80.

Stampfli, G., Mosar, J., de Bono, A. & Vavasis, I. (1998). Late Paleozoic, early Mesozoic plate tectonics of the western Tethys. *Bulletin of the Geological Society of Greece* **32**, 113–120.

Sturm, M. E., Klein, E. M., Karsten, J. L. & Karson, J. A. (2000). Evidence for subduction-related contamination of the mantle beneath the Southern Chile Ridge: Implications for ambiguous ophiolite compositions. In: Dilek, Y., Moores, E. M., Elthon, D. & Nicolas, A. (eds) *Ophiolites and Oceanic Crust: New Insights from Field Studies and Ocean Drilling Program. Geological Society of America, Special Papers* **349**, 13–20.

Takahashi, E., Uto, K. & Schilling, J.-G. (1987). Primary magma compositions and Mg/Fe ratios of their mantle residues along Mid Atlantic Ridge 29° N to 73° N. *Technical Report of ISEI, Okayama University* **9**, 1–4.

Tatsumi, Y. (1989). Migration of fluid phases and genesis of basalt magma at subduction zones. *Journal of Geophysical Research* **94**, 4697–4707.

Tenthorey, E. & Hermann, J. (2004). Composition of fluids during serpentinite breakdown in subduction zones: Evidence for limited boron mobility. *Geology* **32**, 865–868.

Thompson, G. & Melson, W. G. (1970). Boron contents of serpentinites and metabasalts in the oceanic crust: implications for the boron cycle in the oceans. *Earth and Planetary Science Letters* **8**, 61–65.

Thuizat, R., Whitechurch, H., Montigny, R. & Juteau, T. (1981). K–Ar dating of some intra-ophiolite metamorphic soles from the East Mediterranean: New evidence for oceanic thrusting before obduction. *Earth and Planetary Science Letters* **52**, 302–310.

Tomascak, P. B., Widom, E., Benton, L. D., Goldstein, S. L. & Ryan, J. G. (2002). The control of lithium budgets in island arcs. *Earth and Planetary Science Letters* **196**, 227–238.

Vils, F., Pelletier, L., Kalt, A., Müntener, O. & Ludwig, T. (2008). The lithium, boron and beryllium content of serpentinized peridotites from ODP leg 209 (sites 1272A and 1274A): implications for lithium and boron budgets of oceanic lithosphere. 2008.08.005. *Geochimica et Cosmochimica Acta* **72**, 5475–5504.

Wagner, C. & Deloule, E. (2004). Li and δ^7Li behaviour in mantle metasomatic processes. *Geochemica et Cosmochemica Acta Supplement* **68**, A49.

Wallin, E. T. & Metcalf, R. V. (1998). Supra-subduction zone ophiolite formed in an extensional forearc: Trinity terrane, Klamath Mountains, California. *Journal of Geology* **106**, 591–608.

Wei, W., Kastner, M., Deyhle, A. & Spivack, A. J. (2005). Geochemical cycling of fluorine, chlorine, bromine, and boron and implications for fluid–rock reactions in Mariana forearc, South Chamorro Seamount, ODP Leg 195. In: Peters, L. L. (ed.) *Proceedings of the Ocean Drilling Program, Scientific Results, 195.* College Station, TX: Ocean Drilling Program, pp. 1–23.

Wicks, F. J. & Whittaker, E. J. W. (1977). Serpentine textures and serpentinization. *Canadian Mineralogist* **15**, 459–488.

Woodland, A. B., Seitz, H.-M. & Yaxley, G. M. (2004). Varying behaviour of Li in metasomatised spinel peridotite xenoliths from western Victoria, Australia. *Lithos* **75**, 55–66.

You, C. F., Butterfield, D. A., Spivack, A. J., Gieskes, J. M., Gamo, T. & Campbell, A. J. (1994). Boron and halide systematics in submarine hydrothermal systems: effects of phase separation and sedimentary contributions. *Earth and Planetary Science Letters* **123**, 227–238.

You, C. F., Chan, L. H., Spivack, A. J. & Gieskes, J. M. (1995*a*). Lithium, boron, and their isotopes in sediments and pore waters of Ocean Drilling Program Site 808, Nankai Trough: implications for fluid expulsion in accretionary prisms. *Geology* **23**, 37–40.

You, C.-F., Spivack, A. J., Gieskes, J. M., Rosenbauer, R. & Bischoff, J. L. (1995*b*). Experimental study of boron geochemistry: Implications for fluid processes in subduction zones. *Geochimica et Cosmochimica Acta* **59**, 2435–2442.

Zanetti, A., D'Antonio, M., Spadea, P., Raffone, N., Vannucci, R. & Brugeir, O. (2006). Petrogenesis of mantle peridotites from the Izu–Bonin–Mariana (IBM) forearc. *Ofioliti* **31** (2), 189–206.

Zhou, M.-F., Robinson, P. T., Malpas, J. & Li, Z. (1996). Podiform chromitites in the Luobusa ophiolite (Southern Tibet): implications for melt–rock interaction and chromite segregation in the upper mantle. *Journal of Petrology* **37**, 3–21.